HARVARD UNIVERSITY
Graduate School of Arts and Sciences

DISSERTATION ACCEPTANCE CERTIFICATE

The undersigned, appointed by the

Division of Medical Sciences

Program in Neuroscience

have examined a dissertation entitled

Functional Development and Plasticity of Parvalbumin Cells in Visual Cortex: Role of Thalamocortical Input

presented by Kathleen Beth Quast

candidate for the degree of Doctor of Philosophy and hereby certify that it is worthy of acceptance.

Signature: _____

Typed Name: Dr. Richard Born

Signature: _____

Typed Name: Dr. Carole Landisman

Signature: _____

Typed Name: Dr. Rafael Yuste

_____

Dr. Richard Born, Program Head

Date: September 17, 2012

_____

Dr. David Lopes Cardozo, Director of Graduate Studies

Functional Development and Plasticity of Parvalbumin Cells in Visual Cortex: Role of Thalamocortical Input

A dissertation presented

by

Kathleen Beth Quast

to

The Division of Medical Sciences

in partial fulfillment of the requirements
for the degree of
Doctor of Philosophy
in the subject of
Neurobiology

Harvard University
Cambridge, Massachusetts
September 2012

Functional Development and Plasticity of Parvalbumin Cells in Visual Cortex: Role of Thalamocortical Input

Abstract

Unlike principal excitatory neurons, cortical interneurons comprise a diverse group of distinct subtypes. They can be classified by their morphology, molecular content, developmental origins, electrophysiological properties and specific connectivity patterns. The parvalbumin-positive (PV^+), large basket interneuron has been implicated in two cortical functions: 1) the control and shaping of the excitatory response, and 2) the initiation of critical periods for plasticity. Disruptions in both phenomena have been implicated in the etiology of cognitive developmental disorders. Careful characterization of PV^+ cell function and plasticity in response to their primary afferent, the thalamo-cortical synapse, is needed to directly relate their vital contribution at a synapse-specific or network level to whole animal behavior. Here, I used electrophysiological, anatomical and molecular genetic techniques in a novel slice preparation to elucidate PV^+ circuit development and plasticity in mouse visual cortex.

I found that GFP-positive PV^+ cells in layer 4 undergo a rapid maturation after eye opening just prior to onset of the critical period. This development occurs across a number of intrinsic physiological properties that shape their precise, fast spiking. I further optimized and characterized a visual thalamocortical slice to examine the primary afferent input onto both pyramidal and PV^+ cells. Thalamic input onto PV^+ cells

is larger, faster and again matures ahead of the critical period. Both the intrinsic and synaptic properties of PV^+ cells are then maintained by a secreted homeoprotein, Otx2 (Sugiyama et al, 2008), which is mediated by an extracellular glycosaminoglycan recognition.

Since the plasticity of fast-spiking, inhibitory neurons is dramatically distinct from their neighboring pyramidal neurons *in vivo* (Yazaki-Sugiyama et al. 2009), I directly examined the plasticity of thalamocortical synapses *in vitro*. After brief monocular deprivation, thalamic input specifically onto PV^+ cells is reduced while remaining unaltered in pyramidal cells. Deprivations prior to critical period onset or in GAD65 knockout mice neither produce a shift of visual responsiveness *in vivo* (Hensch et al, 1998) nor reduce thalamocortical input onto PV^+ cells. These results directly confirm that PV^+ cells are uniquely sensitive to visual experience, which may drive further rewiring of the surrounding excitatory cortical network.

Table of Contents

Table of Abbreviations

ACSF	**Artificial Cerebral-Spinal Fluid**
EPSC	**Excitatory Post-Synaptic Current**
FS	**Fast Spiking**
LGN	**Lateral Geniculate Nucleus**
LTD	**Long-Term Depression**
LTP	**Long-Term Potentiation**
LTMD	**Long-Term Monocular Deprivation**
MD	**Monocular Deprivation**
mEPSC	**miniature Excitatory Post-Synaptic Current**
MGE	**Medial Ganglionic Eminence**
RK	**Argenine-Lysine**
PNN	**Peri-Neuronal Nets**
PV	**Parvalbumin**
STDP	**Spike-Timing Dependent Plasticity**
STMD	**Short-Term Monocular Deprivation**
TC	**Thalamocortical**
V1	**Primary Visual Cortex**
V2	**Secondary Visual Cortex**
VSDI	**Voltage-Sensitive Dye Imaging**
WT	**WildType**

Acknowledgments

I would like to thank all of my mentors past and present for inspiring and teaching me. My thesis committee for their invaluable advice. The entire Hensch lab for their companionship and support. And Dr. Takao Hensch who's breadth and depth of knowledge, inspiration and support have made this work possible.

I would like to express my extreme gratitude to my entire family but notably my parents Laura and Dave, for I could not have done this without their unending love and support.

This work is dedicated to "my boys": Adam and Jamie. They are my inspiration and fun. Thank you for the love, support and encouragement.

Chapter 1

Introduction

Parvalbumin Positive Interneurons

Parvalbumin positive (PV^+) cells are a subtype of GABAergic inhibitory interneurons that can be primarily characterized by fast-spiking electrophysiological properties and the expression of a calcium-binding protein, parvalbumin. PV^+ cells are born in the medial ganglionic eminence (MGE). They can be found throughout the brain, including hippocampus, thalamus and cortex. In mice, PV^+ cells are first born on embryonic day E13.5 (Butt et al. 2005). PV expression in mouse visual cortex begins near postnatal day P12 in layer 5 and matures in an inside-out laminar progression, maturing around P21 (del Rio et al., 1994; Gonchar et al. 2007). PV^+ cells also arise in somatosensory and other cortical regions, but appear and mature at slightly younger ages and in a region specific manner (del Rio et al. 1994).

PV^+ Cell Anatomy

PV^+ cells represent the largest class of inhibitory interneuron and make up 40-50% of the GABA cell population in the cortex, which in turn, make up approximately 20% of neurons in the brain (Gonchar et al., 2007). In the cortex, the two primary types of PV^+ cells are the axon initial segment-targeting chandelier cells and the soma targeting large basket cells (McBain & Fisahn 2001). The localization of inhibitory synapses on the soma or axon initial segment allow the PV^+ cells to control the output of the target cells. The large basket cells have a large, round soma with several

prominent radial dendrites and are more prevalent in the visual cortex. The axons of large basket cells are widely projecting, crossing several columns and even projecting vertically across layers (Markram et al 2004, Packer & Yuste 2011).

With age, PV^+ cells are preferentially enwrapped in chondroitin sulphate proteoglycans that form peri-neuronal nets (PNNs), The nets may buffer the ionic environment surrounding these cells to aid in the rapid transport of cations and support high firing rates (Härtig et al. 1999). PNNs and specifically the chondroitin sulphate side-chains may also act to limit growth and sprouting of impinging thalamic axon terminals by acting as either a physical barrier or through molecular signaling (Galtrey & Fawcett 2007, Miyata et al. 2012, Beurdeley et al 2012).

PV^+ Cell Electrophysiology

Large basket, PV^+ cells are fast-spiking (FS) cells which are characterized by short duration action potentials and respond to a depolarizing current with high frequency, non-adapting action potential trains. They typically do not fire “rebound” action potentials in response to hyperpolarization (Kawaguchi & Kubota 1993; Kawaguchi 1995). PV^+ cells express Kv3.1 channels, a class of inward rectifying K^+ channels that contribute to their fast-spiking characteristics. PV^+ cells undergo maturation of a number of intrinsic physiologic properties that contribute to their precise and rapid firing properties including an experience dependent increase in Kv3.1 channels (Grabert & Wahle 2009), a decrease in input resistance and action potential width and an increase in action potential amplitude and frequency (Plotkin et al., 2005; Doischer et al., 2008).

PV+ cells have fast membrane kinetics and firing rates, and they also express fast AMPA receptors that lack the GluR2 subunit (Geiger et al 1995, Isaac et al. 2007). These AMPA receptor channels are known to have fast kinetics, are calcium permeable and strongly rectifying. In the prefrontal cortex the developmental down-regulation of NMDA receptors are compensated by up-regulation of calcium permeable AMPA receptors (Wang & Gao 2010). Recently it has been discovered that the inputs onto inhibitory neurons are also plastic. An “anti-Hebbian” LTP was discovered in interneurons of the hippocampus: pre- synaptic activation paired with a postsynaptic cell held at or near resting potential potentiates the synapse and is dependent upon postsynaptic calcium influx through calcium-permeable AMPA receptors and is NMDAR independent (Lamsa et al 2007).

At intracortical synapses onto PV+ cells of the somatosensory cortex there is mGluR5 dependent spike timing dependent plasticity (STDP) wherein pairing presynaptic activity with either a preceding or following depolarization causes LTD (Lu et al., 2007). mGluR5-dependent plasticity has also been reported for intracortical excitatory synapses onto PV+ cells in the visual cortex (Sarihi et al., 2008). The rapid rise and decay of the excitatory currents in PV+ cells and possibility of plasticity at these synapses aids the PV+ cells in quickly following and adjusting to changing sensory information.

PV+ Cell Network Function

PV+, fast-spiking cells are connected via gap junctions and inhibitory chemical synapses to form interconnected networks (Galarreta & Hestrin 1999, Galarreta &

Hestrin 2001). They provide fast and strong inhibition to the peri-somatic region of pyramidal cells. The somatic innervation is suited to control the spiking pattern on the target cells. Through feed-forward inhibition there is only a brief window of opportunity, a few milliseconds, for the sensory input to drive the pyramidal cells to spike before inhibition dominates. Thus even slight jitter in the sensory signal onto pyramidal cells may be edited out (Gieger et al 1999, Pinto et al 2000, Atallah et al. 2012).

PV^+ cells play a major role in synchronizing cortical activity. Activation of PV^+ cells alone can drive gamma oscillations (Cardin et al. 2009, Sohal et al. 2009). The fast and precise inhibition provided by the PV^+ cells allows a brief window for excitation of the network that is followed by an interval of strong inhibition. The gap junctions connecting PV^+ cells meanwhile act as a coincidence detector by propagating hyperpolarizing and depolarizing currents, thus amplifying synchronous excitatory input and dampening non-synchronous input (Galaretta & Hestrin, 2001, Bartos et al. 2007).

Critical Periods

Hubel and Wiesel were among the first to find physiologic evidence for developmental time windows when specific brain circuits are more susceptible to experience-dependent changes (Hubel & Wiesel 1963). In their studies of ocular dominance in the cat, they found monocular deprivation (MD) of one eye produced a shift in cortical neuronal response in favor of the open eye only when deprivation occurred during a specific time window, which they termed the critical period (Hubel & Wiesel 1970). Since then it has been found that critical periods exist in many species

including mice and across a variety of brain regions and sensory systems (Hensch, 2004).

Ocular Dominance Critical Period

The ocular dominance critical period remains one of the most studied and refined models of critical period plasticity. Initial characterization of the mouse revealed an ocular dominance critical period that peaks around P26 (Gordon & Stryker, 1996; Antonini et al., 1999) (Figure 1.1). The mouse's visual cortex is primarily monocular, but the lateral region receives input from both eyes representing input from the central 30 degrees of the visual field. Even within binocular cortex, excitatory neuronal responses are normally biased toward the contralateral eye. After MD of the contralateral eye during the critical period, this bias can be shifted so that cells, on average, respond equally well to both eyes. After just two to three days of MD, there is a reduction in cortical responses to stimulation of the deprived eye that causes a shift in ocular dominance. Extending the deprivation for several days more increases the response of the open eye setting up a two stage progression of ocular dominance shift (Frenkel & Bear 2004, Kaneko et al. 2008, Smith et al. 2009), first a Hebbian-like depression in deprived synapses followed by a homeostatic and/or Hebbian potentiation of the non-deprived synapses.

The use of genetically manipulated mice combined with electrophysiological recording *in vivo* and morphological analyses has furthered our understanding of the mechanism and demonstrated the importance of PV^+ cells. Beginning with the discovery that GABA-deficient GAD65 knockout mice do not display a critical period (Hensch et al.

Figure 1.1

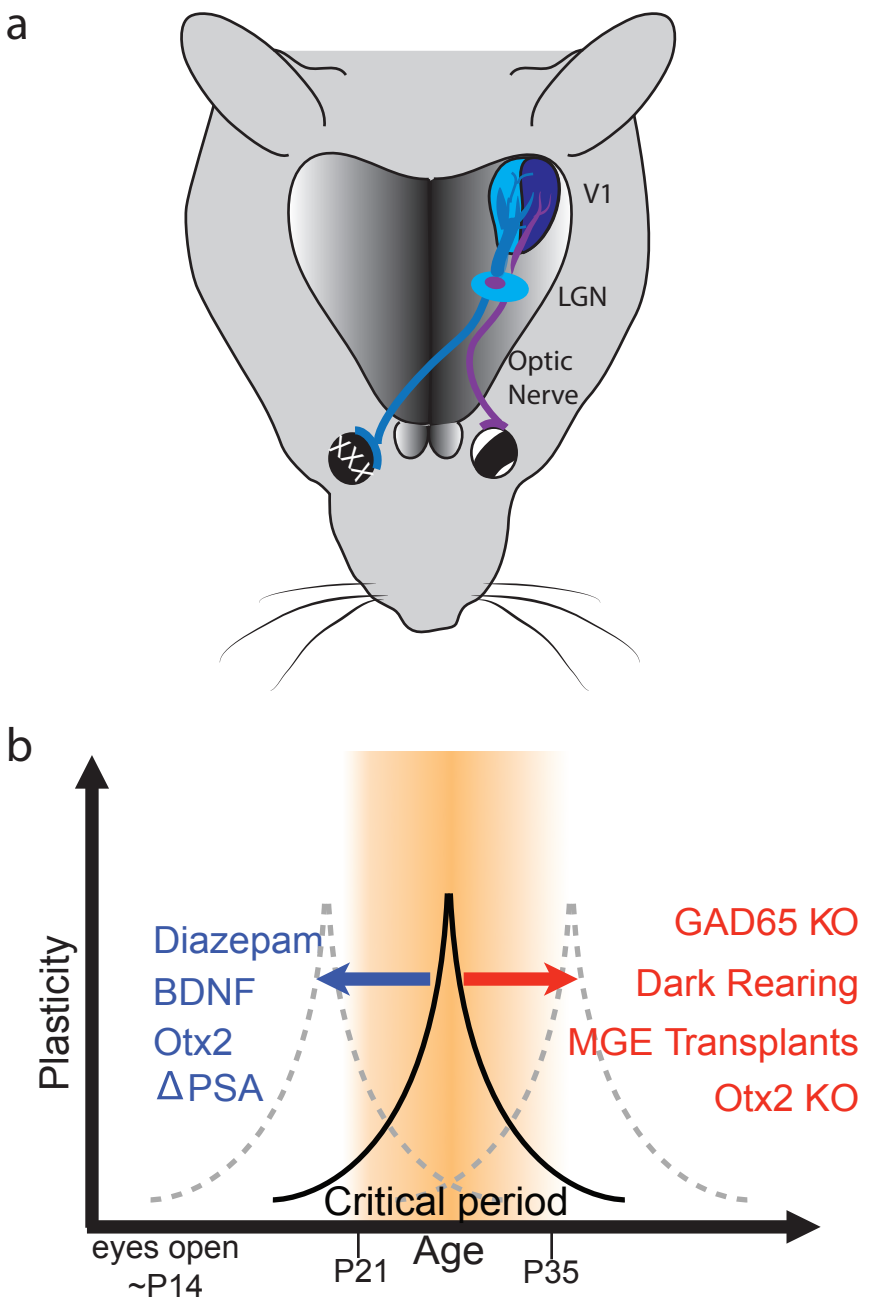

Figure 1.1 - The Critical Period for Ocular Dominance Plasticity in Mice
(**a**) Diagram of mouse visual system depicting eyelid sutures of the right eye and segregation of inputs from each eye in the left hemisphere. (**b**) Critical period for ocular dominance plasticity lasts from P21 to P35 in mice but can be shifted in time through manipulations that generally change the excitatory/inhibitory balance or specifically modulate parvalbumin cell function. (Hensch 2005, Sugiyama et al. 2008, De Cristo et al. 2007, Southwell et al. 2010)

1998) and that this deficit could be rescued at any age with diazepam (Fagiolini & Hensch 2000), the theory emerged that a requisite balance of inhibition to excitation within the cortex allows the initiation and closure of the critical period (Figure 1.1b).

Diazepam is a positive allosteric modulator of $GABA_A$ channels that binds specific subunits to increase the open probability of the channel and increase inhibition. Diazepam administration can prematurely open the critical period of wild-type mice, but targeted point mutation of the α1 subunit prevents diazepam binding as well as its precocious opening of the critical period (Fagiolini et al. 2004). $GABA_A$ receptors containing the α1 subunit are located on the soma and proximal dendrite region of pyramidal cells. PV^+ large basket cells preferentially target this same area, which undergoes an experience-dependent regulation of GABA receptors during the critical period (Katagiri et al. 2007).

The homeoprotein Otx2 has further been found to be an essential transcription factor for the initiation of the ocular dominance critical period, and consistently it is also crucial for the maturation of PV^+ cells (Sugiyama et al. 2008). Conversely, to reactivate ocular dominance plasticity in adult mice, application of chondroitinases to destroy the peri-neuronal nets that predominantly and preferentially surround PV^+ basket cells is effective (Pizzorusso et al. 2002, Beurdeley et al 2012). Taken together, these findings underscore the crucial role PV^+ cells play in visual cortical plasticity.

Other Critical Periods

The study of critical periods is not limited to ocular dominance. Examples of other critical periods include: orientation selectivity in the visual cortex (Fagiolini et al., 2003),

barrel receptive field tuning in somatosensory cortex (O'Leary et al., 1994; Lendvai et al. 2000) and tonotopy in the auditory cortex (de Villers et al., 2007). PV^+ cells have been implicated in the initiation or maintenance of some of these other critical periods. The regular arrangement of sound frequencies in the rodent auditory cortex can be delayed by exposure to pulses of white noise during the second postnatal week (Zhang et al., 2002). This disruption is specific to the bandwidth of the noise and changes not only the tonotopy for the covered frequencies, but also decreases the number of PV^+ cells in that area of auditory cortex (de Villers et al. 2008).

Critical periods are not limited to simple sensory processes either. Language acquisition is an easily recognizable human critical period (Lenneberg 1967, Werker et al. 2009). There are also animal models of critical periods in higher cognitive processes like fear conditioning. In juvenile rats there is a brief window of time where fear conditioning can be reversed, while in adults pairing a neutral stimulus with an aversive stimuli produces a strong, long-lasting effect. Injection of chondroitinase into the amygdala of adult rats, to abolish local peri-neuronal nets, permitted the reversal of the fear conditioning through extinction training. This ability for extinction of the fear training is similar to juvenile rats (Gogolla et al. 2009). Thus, not only are critical periods widespread, but there may be universal mechanisms underlying them.

Thalamocortical Axons

The ultimate result of critical period plasticity is the rearrangement of thalamo-cortical fibers and cortical territories. Hubel and Wiesel were the first to correlate the functional plasticity of cortical ocular dominance plasticity to an anatomical change in

Figure 1.2

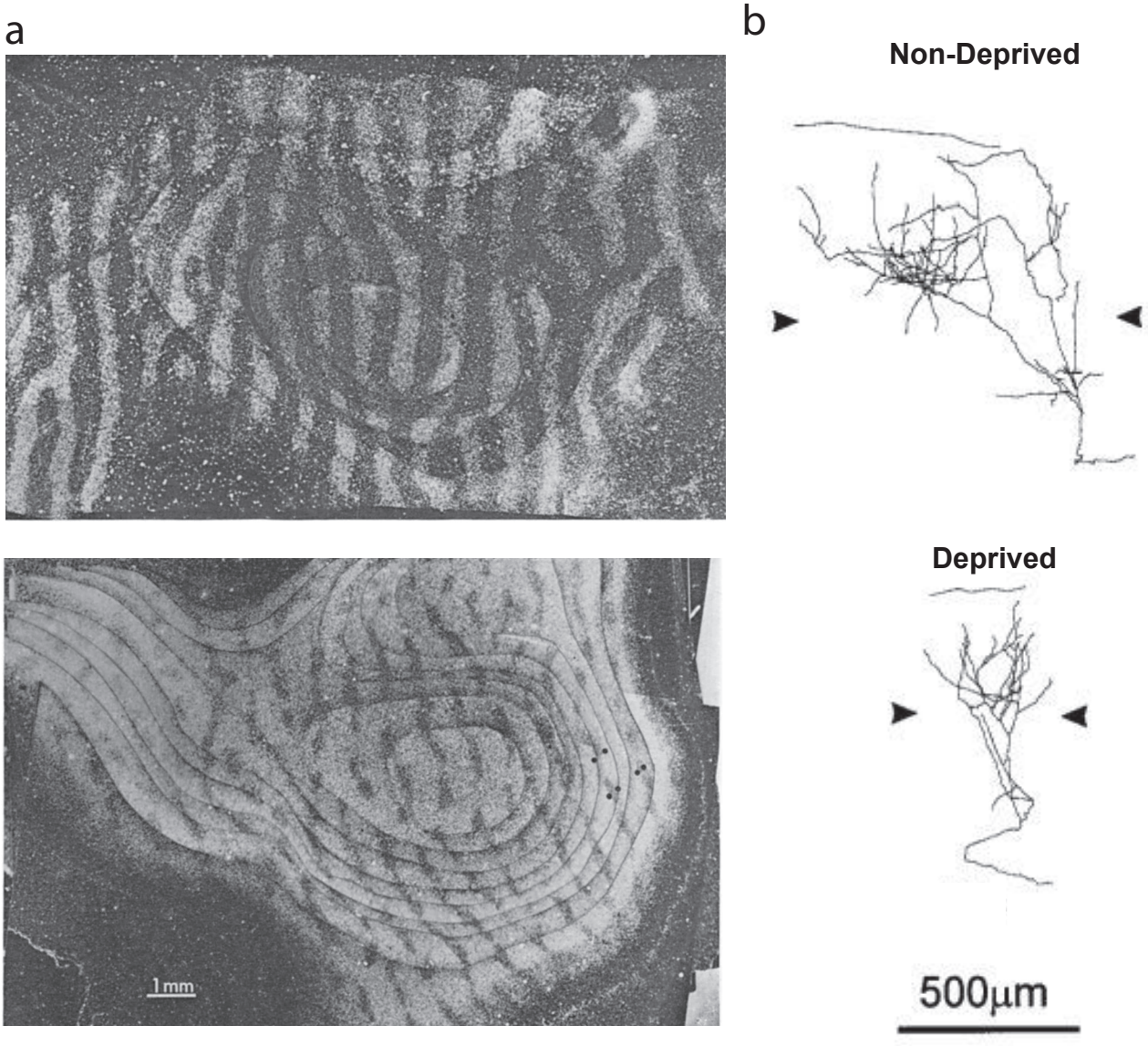

Figure 1.2 - Monocular Deprivation Decreases Thalamocortical Afferents from the Deprived Eye
(**a**) Autoradiograms from Hubel et al. 1977 showing the alternating bands innervated by each eye in a normal monkey (top) and a deprived monkey (bottom). In the deprived animal thalamocortical territory (dark bands) has been reduced in favor of the open eye (light bands). (**b**) Individual thalamocortical axons in mouse cortex also display a reduction in branching and cortical territory from the deprived eye (bottom) compared to the non-deprived eye (top). From Antonini et al. 1999.

the thalamocortical fibers (Hubel & Weisel 1977, Shatz & Stryker 1978). Eye injections with the transneuronal tracer ^{3}H-amino acid reveals the cortical territory innervated by that eye (Figure 1.1 a). In cat or monkeys, thalamocortical afferents from each eye form alternating bands. Long term MD causes a rearrangement of thalamocortical fibers and a shift of the bands so that the thalamocortical afferent territory of the deprived eye shrinks in favor of the open eye (Hubel et al. 1977). Thalamocortical anatomical reorganization is present in the mouse visual cortex as well (Figure 1.1 b). Afferent fibers from the deprived eye decrease or arrest their arborization and expansion after extended deprivation (Antonini et al. 1999).

Critical Period Permissive Factors and Brakes: Otx2

In addition to permissive factors, or conditions that allow for the opening and initiation of critical periods, there are also brakes that close critical periods and prevent further plasticity (Figure 1.2). Many of the permissive factors increase GABA signaling, often targeting PV^{+} cell signaling (Hensch 2005). Several critical period brakes have been discovered that are suspected to act through a variety of mechanisms (Bavelier et al. 2010). Myelination and Nogo receptor activation limit plasticity possibly due to structural limitations (McGee et al. 2005). Similarly peri-neuronal nets may act as a structural brake: not allowing axon rearrangement (Pizzorusso et al. 2006). A decrease in cholinergic signalling has also been implicated as a brake (Morishita et al. 2010). Lynx1 expression increases after the peak of the critical period and acts to decrease cholinergic neurotransmission and inhibit plasiticity. Disruption of any of these brakes can reinstate adult plasticity.

Figure 1.3

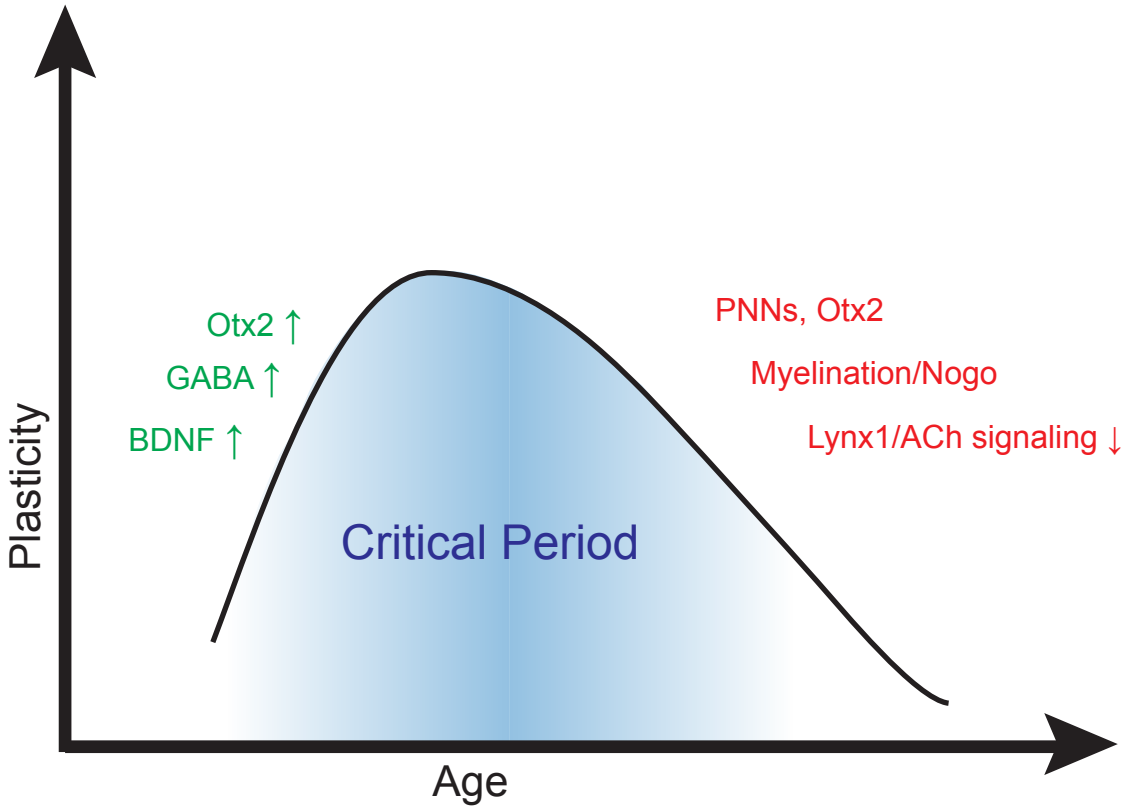

Figure 1.3 - Biological Factors Controlling Critical Periods
Increases in GABA, BDNF and Otx2 is necessary to initiate the critical period. Artificially increasing any these (i.e. Diazepam) or decreasing (dark rearing) can temporally shift the initiation of the critical period. There are also molecules and processes that limit plasticity. Artificially removing any of these brakes reopens plasticity. (PNNs = peri-neuronal nets, ACh = acetylcholine).

Otx2 is a transcription factor that may act as both a permissive factor and a brake. Otx2 is a homeoprotein that is not transcribed by PV^+ cells but through targeted transfer. PV^+ cells acquire Otx2 protein beginning just ahead of the critical period and increasing until adulthood (Beurdeley et al 2012). There seems to be a lower threshold for Otx2 expression to initiate the critical period as infusion can prematurely open the critical period (Sugiyama et al. 2008) yet there also appears to be an upper threshold of expression above which plasticity is restricted. By disrupting Otx2 transfer to PV^+ cells in the adult animal, ocular dominance plasticity can be reinstated (Beurdeley et al. 2012, Miyata et al. 2012). This is similar to the model of GABA control of the critical periods (Feldman 2000, Heimel et al. 2011, Spolidoro et al. 2009). Otx2 and PV^+ cell maturation may be the mechanism that ties it all together.

PV^+ Cell Dysfunction

The importance of PV^+ cells and inhibitory neurons stretches beyond cortical signal processing and control of critical periods. Inhibitory neurons and PV^+ cells specifically have been implicated in a number of cognitive diseases. Specific deficits in PV^+ signaling has been prominently studied in schizophrenia (Lewis et al. 2005). Gamma oscillations, which have been shown to be driven by PV^+ cells are altered in patients with schizophrenia (Tallon-Baudry et al. 1998, Spencer et al. 2003, Behrendt 2003). Consistently, post-mortem studies of diseased brains display lower levels of the major isoform of glutamate decarboxylase (GAD 67), as well as lower $GABA_A$ receptor α1 subunit in pyramidal neurons postsynaptic to PV^+ cells (Hashimoto et al. 2003, Curley et al 2011). Recently the importance of inhibitory cells has been implicated in

the developmental disorder autism and the closely related Retts syndrome (Dhossche et al. 2005, LeBlanc & Fagiolini 2011). PV^+ staining is reduced in several different mouse models of autism (Gogolla et al. 2009b) and targeted deletion of Mecp2, the gene behind the developmental disorder Retts syndrome, in only inhibitory neurons, phenocopies many of the behavioral deficits of the global deletion (Chao et al. 2010).

In this thesis, I have endeavored to study the function and development in terms of laminar migration, intrinsic electrophysiology, synaptic input and experience-driven plasticity of PV^+ cells. Greater understanding of this critical cell type and fundamental synaptic innervation will aid understanding of cortical processing, critical periods and even cognitive function.

Chapter 2

Materials and Methods

Animals and Rearing Conditions:

All experimental procedures were carried out according to Harvard University animal care and use guidelines. C57BL/6 mice (Charles River), PV-GFP mice (Meyer et al. 2002), GAD65 KO mice (Asada et al. 1996), Fos-GFP mice (Barth et al. 2004), Fezf2 KO (Molyneaux et al. 2005) mice or MeCP2 KO (Guy et al. 2001) mice were used for all experiments during specific windows of postnatal development (Figure 2.1). Experiments were performed either during the peak of the critical period for ocular dominance plasticity (postnatal days 24-27 (P24-27)), before the critical period (P16-18), shortly after eye opening (P14) or after the peak of the critical period (P40-50) (Gordon & Stryker 1996) (Figure 2.1 a). Animals were maintained on a 12 hr light/dark cycle with access to food and water ad libitum.

Monocular Deprivation and Injections

For monocular deprivation (MD) eyelid margins were trimmed by iris scissors and eyes sutured shut under isoflurane anesthesia (Gordon & Stryker 1996). Sutures were checked daily to make sure the eyes remained closed. Eyes were closed around P22 and experiments were performed after a brief three to four day MD (short-term monocular deprivation, STMD) or a long-term MD (LTMD) after 21+days (Figure 2.1 b). All recordings and experiments were performed contralateral to the deprived eye.

Figure 2.1

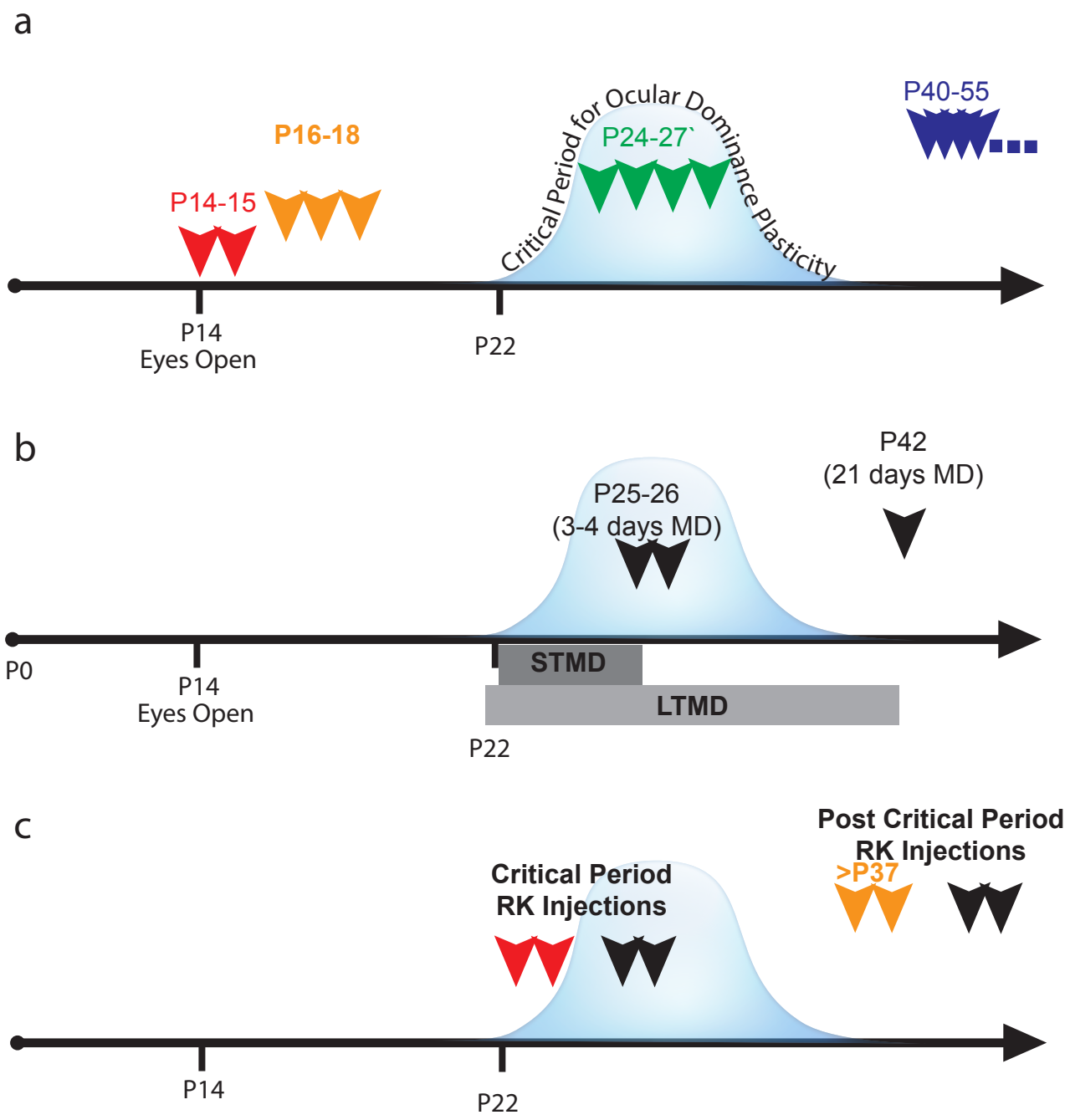

Figure 2.1 - Experimental Time-lines
(**a**) Visual Cortex developmental time-line and recording time periods. Colored arrows indicate electrophysiology recording days. (**b**) Experimental time-line for short term 3-4 days MD and LTMD. (**c**) Experimental time-line for RK injections either during the critical period (red) or after the critical period (orange).

Cortical infusion of either peptide or saline was performed on mice anesthetized with 2% isoflurane plus O_2. Body temperature was maintained through a heating pad. Two small holes were made through the skull: (2.0 mm lateral to the midline, 0.5 mm anterior to the lambda point) and (2.0 mm lateral to the midline, 2.0 mm anterior to lambda) to surround V1b but not interfere with thalamocortical fibers. A 28-gauge Hamilton® syringe connected to a motorized microinjector (Narishige) slowly delivered 400nL of the peptide or saline at a depth of 350εm. After injection, the area was cleaned and skin sutured. For injections performed over two days another 400nL was injected into the same holes at the same depth 24 hours after the first surgery. Mice were given Meloxicam (to reduce pain) every 24 hours for two days after the surgery. Cortical infusion of peptides or saline were performed on two consecutive days then electrophysiological slice recordings were performed three to four days after in initial injection (Figure 2.1 c). For experiments during the critical period, injections were given at P21 and P22. For experiments after the critical period two consecutive days of injections were given between the ages of P38-51 and recordings occurred three to four days after the initial injection.

Labeling of the retinogeniculate fibers in the LGN was obtained by eye injections. Mice, anesthetized with 2% isofluorane, were injected with 2 µl of a 2% solution of cholera toxin β subunit conjugated with Alexa 488 (Green) or 594 (Red) (Invitrogen, Carlsbad, CA) using a Hamilton® syringe. After 2 days, mice were deeply anesthetized and sliced according to the visual thalamocortical protocol and slices were placed in 4% paraformaldehyde overnight. The thick thalamocortical section was cryoprotected in

30% sucrose and sub-sectioned to 50 µm on a freezing Vibratome (Leica), maintaining the initial plane.

Slice Preparation

Mice were anesthetized with isoflurane then rapidly decapitated. The brain was removed and placed in an ice cold choline-based cutting solution (in mM: 78.3 NaCl, 23 $NaHCO_3$, 23 glucose, 33.8 choline chloride, 2.3 KCl, 1.1 NaH_2PO_3, 6.4 $MgCl_2$, and 0.45 $CaCl_2$) (Hooks & Chen 2006). Either 300 µm coronal sections or 500 µm thick visual thalamocortical slices were sectioned on a vibratome (Microm HM 650V, Thermo Scientific) using a sapphire blade. The visual thalamocortical slice was previously described by MacLean et al. (2005) and is discussed in detail later in this thesis. Briefly the brain was mounted on a 55° agar mold and one 500 µm thick slice was sectioned ~300 µm after the disjoining of the corpus callosum. Slices were incubated at 35 °C in oxygenated ACSF (125 mM NaCl, 25 mM glucose, 25 mM $NaHCO_3$, 2.5 mM KCl, 2 mM $CaCl_2$, 1.25 mM NaH_2PO_4 and 1 mM $MgCl_2$ (310–320 mOsm) for at least 15 min, before returning to 20–22 °C.

Voltage Sensitive Dye Imaging (VSDI)

The voltage-sensitive dye Di-4-ANEPPS (Invitrogen), dissolved at 0.01 mg/ml in dimethylsulfoxide stock solution, was diluted in ACSF to a final solution of 5 µg/ml Di-4-ANEPPS. Slices were incubated for at least 90 min in the dye before transfer to an ACSF (20–22 °C) recording chamber. Slices were imaged using an Olympus MVX10 microscope with 4x objective. Excitation light from a shuttered 150 W halogen lamp was

Figure 2.2

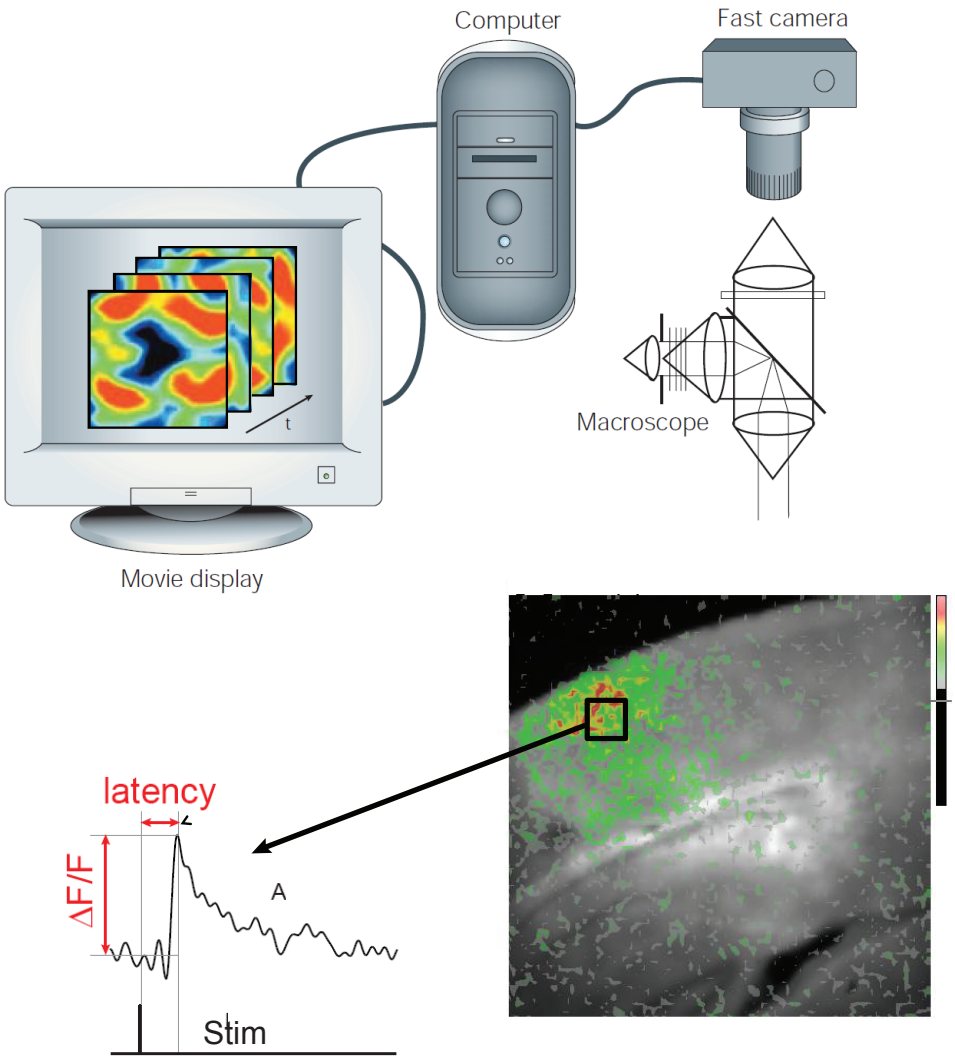

Figure 2.2 - VSDI Setup
Diagram of VSDI setup from Grinvald & Hildesheim 2004 and Rinaldi-Barkat et al 2011. A fast CCD camera connected to a computer allows for ms frame rate of a large field (psuedocolor frame). Using MiCam software and custom Igor analysis regions of interest are integrated and processed.

band-pass filtered (515 and 535 nm) and reflected toward the sample by a 570-nm dichroic mirror (Figure 2-2). Emitted fluorescence, reflecting a change in potential across neuronal membranes (Grinvald, A. & Hildesheim 2004, Ferezou et al. 2006, Homma et al. 2009) was long-pass filtered (590 nm) and imaged using a MiCam Ultima CMOS-based camera (SciMedia). A 1 ms stimulating pulse was controlled by a programmable pulse generator (MiCam Ultima software, SciMedia) linked to a constant current stimulus isolation unit (Iso-Flex, A.M.P.I.) and delivered using a bipolar glass stimulating electrode filled with ACSF. Fluorescent changes for a single stimulation trial were collected at 1 ms frame rate for 512 ms and averaged across ten sweeps.

Regions of interest containing 5 × 5 pixels covering 125 × 125 μm were spatially integrated using MiCam Ultima analysis software. For coronal slices, the upper region was located on beam with the stimulation site 200 μm below the pia and the lower region was located 300 μm above the white matter. Individual time course traces were subsequently exported to Igor Pro (WaveMetrics) for custom analysis (Barakat et al. 2011). Fluorescence change was normalized to resting fluorescence (∆F/F0). Response amplitude was defined as maximum fluorescence change (∆F/F) per trial at a given region of interest. Variations in daily preparation were normalized by slice; all signals were divided by the change in fluorescence measured in the upper region at a stimulating strength of 0.1 mA.

Acute Slice Electrophysiology

Prior to recording, slices equilibrated for at least 1 hr in oxygenated ACSF before being transferred to a submersion chamber for room temperature recording. Layer 4

pyramidal or PV^+ cells were targeted by shape (for pyramidal cell) or GFP expression (PV cells) using a combination of infrared-Nomarski DIC optics and fluorescent microscopy (Eclipse FNI, 40X immersion objective, Nikon). Recordings were obtained on an Axon MultiClamp 700B amplifier and digitized at 10 kHz (Axon Digidata 1440A). Recording electrodes (2-4MΩ) were fabricated from borosilicate glass microcapillaries (outer diameter, 1.5 mm) with a micropipette puller (DMZ Universal Puller).

For whole-cell voltage-clamp recordings the internal solution contained (in mM) 120 Cs-methanesulfonate, 6 CsCl, 2 $MgCl_2$, 0.05 $CaCl_2$, 20 HEPES, 0.02 EGTA, 10 phosphocreatine di(Na) salt, 4 Mg-ATP, 0.4 Na3-GTP, 0.15% biocytin, and 1 lidocaine derivative QX-314 (pH 7.2 with CsOH, 290–300 mOsm). Access resistances were maintained at less than 25 MΩ throughout the experiments. For voltage clamp recordings no more than 3 cells were recorded from each animal and at least 4 animals were tested per group. Thalamocortical excitatory post-synaptic currents (EPSCs) were recorded in the presence of 10μM bicuculline. and were stimulated by a bipolar glass stimulating electrode filled with ACSF placed in the LGN or the fiber bundle exiting the LGN. Incremental stimulus intensities were delivered at 0.05 Hz until an evoked EPSC was discernible from failures (Hooks and Chen 2008) and a consistent connection was present. Typically 8-10 repetitions at a minimal stimulating intensity were average for quantification. If there was an obvious difference in amplitude between the first detected currents with failures and incrementally higher stimulus that produced no failures, that synapse was not recorded. AMPA current measurements were obtained at a holding potential of -70 mV and NMDA current measurements were obtained at a holding potential of +40 mV and measured after the time-course of the AMPA current as

Figure 2.3

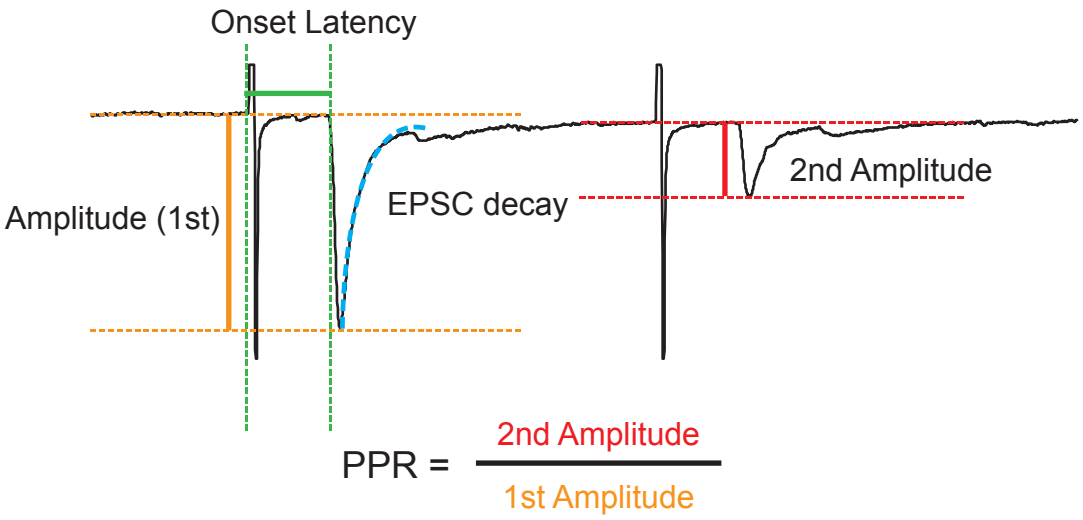

Figure 2.3 - Measurement Parameters of Evoked EPSC Recordings
Analysis of single fiber input using Axon's Clampfit program.

measured at -70 mV. Thalamocortical inputs were differentiated from di-synaptic intracortical inputs on a basis of onset delay (<9 ms), low jitter and by differences in short term plasticity (Gil et al. 1999, Beierlein et al. 2003).

Analysis of voltage-clamp electrophysiological data was performed using pClamp10 (Molecular Devices). EPSC amplitude was measured as the maximum change of the averaged current 4-15 ms after stimulation (Figure 2.3). Onset delay is defined as the time between stimulation and 10% of the maximum amplitude. EPSC decay time constants were measured from single exponential fits of a single average minimal EPSC. Two stimulus pulses 40 ms apart were used to examine the paired-pulse ratio (PPR), an assay for release probability. Here, PPR is defined as the ratio between the average EPSC amplitude evoked by the second stimulus pulse divided by the average EPSC amplitude evoked by the first stimulus pulse (EPSC2/ EPSC1). If the ratio is >1, it represents facilitation, while if the ratio is <1, it represents depression. Jitter was measured using the event detection in the Clampfit software. The value for jitter was defined as the standard deviation for the delay to 10% of the peak as measured for all traces at the single fiber stimulation intensity.

To record AMPA mediated mini EPSCs (mEPSCs), slices were first incubated in ACSF containing 1 μM TTX for 60 minutes prior to recordings. Recordings using the Cs-methanesulfonate internal solution were performed in the presence of TTX (1 μM), APV (50 μM) and bicuculline (20 μM). AMPA mEPSCs were recorded for 10 min, high pass filtered at 2 kHz and analyzed using MiniAnalysis (Synaptosoft).

Whole-cell intrinsic membrane and firing properties of cells were recorded in current-clamp with pipettes containing (in mM): 120 potassium gluconate, 10 KCl, ATP-

MG, 10 phosphocreatine, 0.3 GTP, 10 HEPES and 0.15% biocytin (pH 7.3, 290-300 mOsm). 300 μm thick coronal slices of visual cortex were bathed in oxygenated ACSF during the recordings. For each animal up to 5 cells per cell type were recorded.

Resting potential and compensated input resistance was recorded within seconds of breaking into a cell. Sag calculated as the difference between the negative peak voltage and the steady state voltage of a -100 pA injection. The error for the liquid junction potential was not corrected unless otherwise indicated. Cells with a series resistance of <25 MΩ and <25% change for the duration of the experiment were used for analysis. For most cells the series resistance was <15 MΩ did not change more than 20%.

Analysis of current-clamp electrophysiological data was performed using pClamp10 (Molecular Devices) Single action potential parameters (peak amplitude, half-width and hyperpolarization anti-peak) were measured at threshold and the amplitude of the spikes and after-hyperpolarization potentials were measured relative to the spike threshold. To measure interneuron firing properties, the frequency-current relationship (FI curve) was calculated as the spike frequency when current steps from threshold to 950 pA were applied in increments of 50 pA (0.1 Hz, 1,000 ms). The instantaneous firing rate was calculated as the inverse of the interval between the first and second spikes whereas the average firing rate was calculated from the number of spikes fired after a 1 s current injection. Frequency-intensity curves were calculated as the mean firing frequency of cells that had reached spike threshold. Spike adaptation was calculated as the average of the last two interspike intervals (ISIs) divided by the average of the first two ISIs in response to a depolarizing step that evoked firing rates of ~50 Hz. The

maximal firing rate was determined as the inverse of the shortest ISI for current injections between 500-950 pA.

Post-hoc labeling and morphological characterization of patched cells filled with biocytin was performed when possible. Tissue slices containing biocytin-filled cells were fixed in 4% paraformaldehyde (4°C at least 24 hrs). Slices were washed three times in 0.1 M phosphate-buffered saline (PBS, pH 7.4), incubated with PBS containing Alexa 546 conjugated Streptavidin (Molecular Probes) and 0.25% Triton-X (2-4 hr, room temperature). After washing three times in PBS, slices were mounted and observed under a confocal microscope (Leica) (Katagiri et al., 2007).

Perfusions

Mice were anesthetized with 2.5% isoflurane with O_2. They received an overdose of Nembutal (5mg/ml, i.p.) and were perfused transcardially with 0.9% saline followed by 4% paraformaldehyde (PFA). Brains were post-fixed in PFA for 1.5 hours and then cryoprotected in a 30% sucrose solution overnight.

Puncta Immunofluorescence

40 µm thick sections were cut from perfused brains on a cryostat or freezing microtome (Leica). Every fourth section was collected and washed in phosphate buffered saline (PBS) for 30 minutes followed by 4°C overnight incubation in blocking solution (0.8% Triton X- 100 and 20% bovine serum albumin (BSA) in 0.1 M PBS-Triton). Slices were then transferred to a primary antibody solution in 0.2% Triton X-100 and 5% BSA in 0.1 M PBS-Triton for overnight incubation. Antibodies were used at the

following concentrations, rabbit anti-GFP 1:2000 (ab cam), rabbit anti-PV 1:1000 (Swant), guinea pig anti-VGluT2 1:500 (Synaptic Systems) and mouse anti-Otx2 1:250 (Sugiyama et al. 2008). After three 15 minute washings in PBS-Triton-BSA, sections were incubated overnight in the secondary antibody, goat anti-rabbit IgG Alexa 488, goat anti-rabbit IgG Alexa 596, goat anti-guinea pig 564, goat anti mouse 488 or 633 (Invitrogen), diluted at 1:1000 in PBS-Triton-BSA. Sections were washed three times in PBS-Triton for 30 min prior to being mounted on glass slides.

In order to compare the thalamocortical connectivity onto PV^+ cells, the number of VGluT2 immunoreactive puncta surrounding a PV^+ cell body were estimated using a custom MatLab script. Three to four PV^+ positive cells per section (40 μm thick) were imaged on a Fluoview FV1000TM scanning microscope (Olympus®) at 100x from three sections from each brain, totaling 10 cells per animal. Automatic thresholding within MadLab defined the region of the PV^+ cell. This region was then used to select a 1.25 μm ring around the neuron. The red VGluT2 channel was thresholded to the median intensity plus 4x the standard deviation and all puncta within the ring, larger than 3 pixels (0.123 μm), were automatically counted and analyzed (Figure 2.4).

Mecp2 Staining

Cryosections (40 μm) were incubated with either rabbit anti-PV (Swant, 1:2500 dilution), mouse anti-PV (Swant 1:10000), rabbit anti-NR2A or rabbit anti-NR2B (Frontier Science Co., 1:1000 dilution) and mouse anti-GAD65 (Developmental Studies Hybridoma Bank, 1:1000) followed by fluorescent secondary antibody. NeuroTrace blue fluorescent Nissl (Invitrogen, 1:500 dilution) was added to the primary antibody solution

Figure 2.4

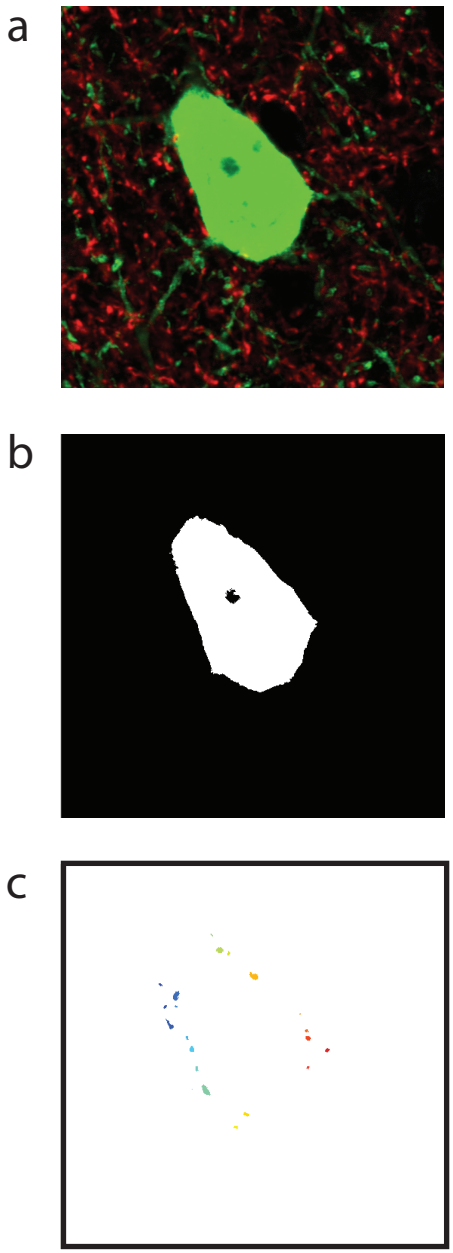

Figure 2.4 - Automatic Analysis of Synaptic Puncta
(**a**) Composite image of PV (green) and VGluT2 (red). (**b**) Automatic thresholding of the green channel to create counting mask. (**c**) The red channel is segmented based on a intensity thresholding (median + 3*stdev). Limited counting of puncta within 1.25µm of PV cell perimeter.

for counter-staining. Sections were analyzed on a laser scanning confocal microscope (Olympus FluoView, FV1000) in multi-channel acquisition mode to avoid fluorescence cross-talk. Quantitative analyses were performed blind on a minimum of three mice per genotype.

Mean pixel intensity (at 20x) of the PV signal in each field (1024x1024) was measured using MacBiophotonics ImageJ software (http://www.macbiophotonics.ca/imagej/). PV^+ cell area (at 100x) was determined in a plane through the center of the nucleus by manually outlining single cell bodies. The number of perisomatic synapses (at 100x) was determined on triple-stained images (PV, GAD65, DAPI). Presynaptic innervation was analyzed using the "particle analysis" function (ImageJ) with 0.05-10 μm^2 as the initial parameters. Pyramidal neurons were identified and traced in the DAPI channel by their typical morphology (triangular cell body). Data were expressed as number of PV-boutons per surface area.

Fos-GFP Single Eye Exposure

MD was performed on the left eye of four Fos-GFP+ mice at P22. The mice were then placed in a dark sound chamber to decrease background Fos expression by decreasing light and sound exposure. After three days the mice were then exposed to a slow strobe light for 90 min. They were then immediately perfused and the brains fixed in paraformaldehyde. Before perfusion the sutures were double checked and 1 mouse was discarded for slight eye opening. After fixation the brains were blocked on the thalamocortical angle and thinly sliced (50 μm). GFP signal was enhanced with rabbit anti:GFP antibody 1:2000 (ab cam). After determining the boundaries for the various

regions, we used ImageJ “particle analysis” function with 0.5-10 μm^2 as the initial parameters to measure the density of Fos labeled cells within each region.

Chapter 3

Laminar Development and Functionality of Parvalbumin Cell Networks

Author Contributions

This chapter contains selections of collaborative work from two papers:

Lodato, S., Rouaux, C.*, Quast, K.B.*, Jantrachotechatchawan, C., Studer, M.I., Hensch, T.K., and Arlotta, P. (2011). Excitatory Projection Neuron Subtypes Control the Distribution of Local Inhibitory Interneurons in the Cerebral Cortex. Neuron 69, 763-779.

Simona Lodato and Caroline Rouaux collected and analyzed the anatomical data (Figure 3.2 & 3.3). Kathleen Quast collected and analyzed the functional data (Figure 3.4 & 3.5). The corresponding results text contains modified excerpts from the paper.

Durand, S.*, Patrizi, A.*, Quast, K.B., Hachigian, L., Pavlyuk, R., Saxena, A., Carninci, P., Hensch, T.K., and Fagiolini, M. (2012). NMDA Receptor Regulation Prevents Regression of Visual Cortical Function in the Absence of Mecp2. Neuron *76*, 1078-1090.

Annarita Patrizi and Lea Hachigian collected and analyzed the anatomical data (Figure 3.6 a-c). Kathleen Quast collected and analyzed the functional data (Figure 3.6 d-f).

* equal contribution

Introduction

Although all inhibitory neurons were originally identified and collectively categorized by Ramón y Cajal as locally projecting, “short axon cells” based strictly on their morphology, they represent a diverse group. The emphasis on classifying inhibitory cells based on their axon projection remains relevant as it largely determines the cell’s

output, but inhibitory cells have further been grouped and sub-grouped based on molecular, functional characteristics and synaptic properties (Petilla Interneuron Nomenclature Group, 2008). These groupings prove useful not only as a framework to study and discuss groups of neurons, but also since specific interneuron subtypes have been implicated in the etiology of a variety of diseases from schizophrenia to autism (Marín 2012, Baroncelli et al. 2011).

The parvalbumin positive (PV^+), fast spiking, large basket cells are an intriguing subtype of cells, not only because of their role in controlling the cortical output of excitatory cells (Atallah et al. 2012), but because of the implications in critical periods (Hensch 2005) and developmental disorders (Gogolla et al. 2010, Pizzarelli & Cherubini 2011). These cells are classified by their innervation of the soma and proximal dendrite of target neurons (Freund, 2003). Among their archetypical characteristics are their fast kinetics, including their intrinsic firing (high-frequency repetitive firing, brief spike half-width and fast membrane time constants) and their synaptic outputs and receptors (Jonas et al., 2004). They innervate postsynaptic targets close to the site of action potential initiation: the soma, proximal dendrite or axon initial segment (Figure 3.1 b).

As a result they have been shown to provide strong inhibitory control over postsynaptic cell firing and provide feedforward inhibition and hence precise control or “gain” of neuronal output (Galarreta & Hestrin 2001b, Pouille & Scanziani, 2001, Beierlein et al. 2003, Atallah et al. 2012). Moreover, as PV^+ basket cells are interconnected through both gap junctions and reciprocal connections (Gibson et al. 1999, Galarreta & Hestrin 1999), and since their axons traverse multiple cortical columns, contacting a vast number postsynaptic cells, this interneuron subtype has the

Figure 3.1

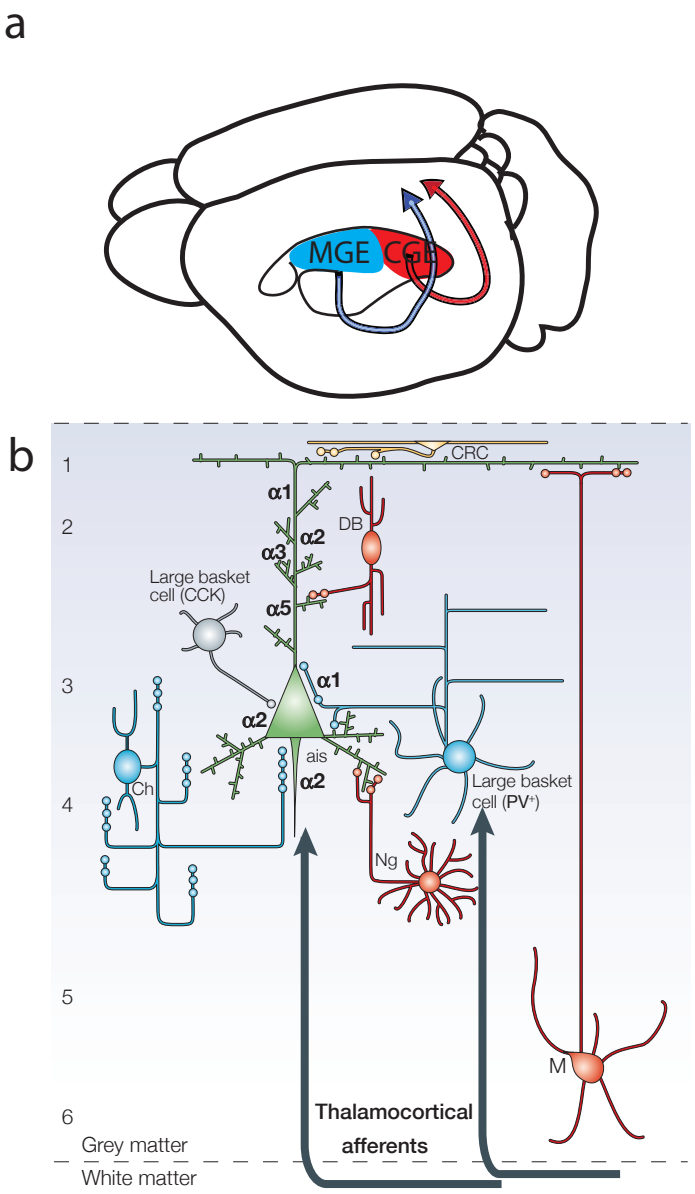

Figure 3.1 - Embryonic Sources and Subtypes of Interneurons
(**a**) Diagram of origins of interneurons. PV+ cells, (along with a few other subtypes) originate in the MGE (red) while other subtypes originate in the CGE. Interneurons undergo tangential migration (arrows) to arrive at the correct cortical area before undergoing radial migration (not shown) to arrive at the correct laminar position. (**b**) Differential laminar positioning and targeting of the post-synaptic cells of a subset of interneurons. (Adapted from Hensch 2005). CCK, cholecystokinin expressing; Ch, chandelier cell; CRC, Cajal–Retzius cell; DB, double bouquet cell; M, Martinotti neuron; Ng, neurogliaform neuron; PV+, parvalbumin

capacity to synchronize the firing of large groups of neurons (Beierlein et al. 2000, Pouille & Scanziani 2001, Cardin et al. 2009).

Excitatory cortical neurons are born in the ventricular and sub-ventricular zones of the developing brain, near their final destination (Kwan et al. 2012). They differentiate in the subplate then migrate a relatively short distance to their final laminar position in an inside out manner where layer 5 and 6 neurons are differentiated and positioned before the upper layer neurons. Unlike the excitatory neurons, inhibitory interneurons are born in distal parts of the brain either the medial or caudal ganglionic eminences (MGE or CGE) (Xu et al. 2004, Wonders and Anderson 2006). After differentiation from the progenitor cells, inhibitory neurons migrate tangentially to the correct cortical area (Figure 3.1 a) before they shift and migrate radially to the correct laminar position. Different subtypes of interneurons are born in the different regions. For example all the PV^+ cells are born in the MGE then migrate throughout the cortex. Like the excitatory cells, inhibitory cells show an inside out pattern of generation. Early-born interneurons of the MGE end up in deep layers, while late-born interneurons occupy superficial layers of the mature cortex (Miyoshi et al. 2007).

A combination of molecular guidance cues and intrinsic cell-autonomous factors are required for the correct tangential and radial positioning of the interneurons (Batista-Brito & Fishell 2009, Miyoshi & Fishell 2011). However, since inhibitory interneurons and excitatory neurons that are synchronously generated, pair-up preferentially (Fairén et al. 1986) and the excitatory neurons arrive at their destination first, it is likely that cell-cell signaling is required, but the exact mechanisms are not fully understood. It is known that when the entire laminar circuitry of the cortex is disrupted such as in *reeler* mice,

the interneuron distribution is abnormal (Hevner et al. 2004). We asked what the effect of a substitution of a single subtype of excitatory neurons, the subcerebral projection neurons with callosally projecting neurons (Chen et al. 2005, Molyneaux et al. 2005), would have on interneuron radial migration. The overall cortical density and thickness is unchanged in these mice, so changes in interneuron lamination should be strictly due to missing cell-cell interactions.

Results

Abnormal Laminar Distribution of Inhibitory Neurons in Fezf2$^{-/-}$ Mice

Fezf2 is a transcription factor expressed in cortical progenitor neurons and is essential for the differentiation of layer 5 subcerebral projection neurons (Molyneaux et al. 2005). Fezf2$^{-/-}$ mice lack corticospinal neurons and instead have an expanded number of callosally projecting neurons. The overall cortical thickness is unchanged and the number of GABAergic interneurons is also unchanged (Figure 3.2 a-c). However the distribution of the GAD 67-positive interneurons was shifted to more superficial layers of the cortex (Figure 3.2 d-r). To quantify this, we divided the cortex into ten bins of equal size spanning the cortical thickness and calculated the percent of interneurons in each bin. Bins with reduced interneurons corresponded to layer 5 and the upper or superficial layers (2-4) had an increased percentage of interneurons in the Fezf2$^{-/-}$ mice.

Despite the fact that cortical interneurons are heterogeneous and it is not currently possible to precisely associate specific interneuron subtypes with strict layer locations, it is known that early-born cells such as PV^{+} and somatostatin expressing interneurons preferentially populate the deep layers of the cortex (Butt et al., 2005;

Figure 3.2

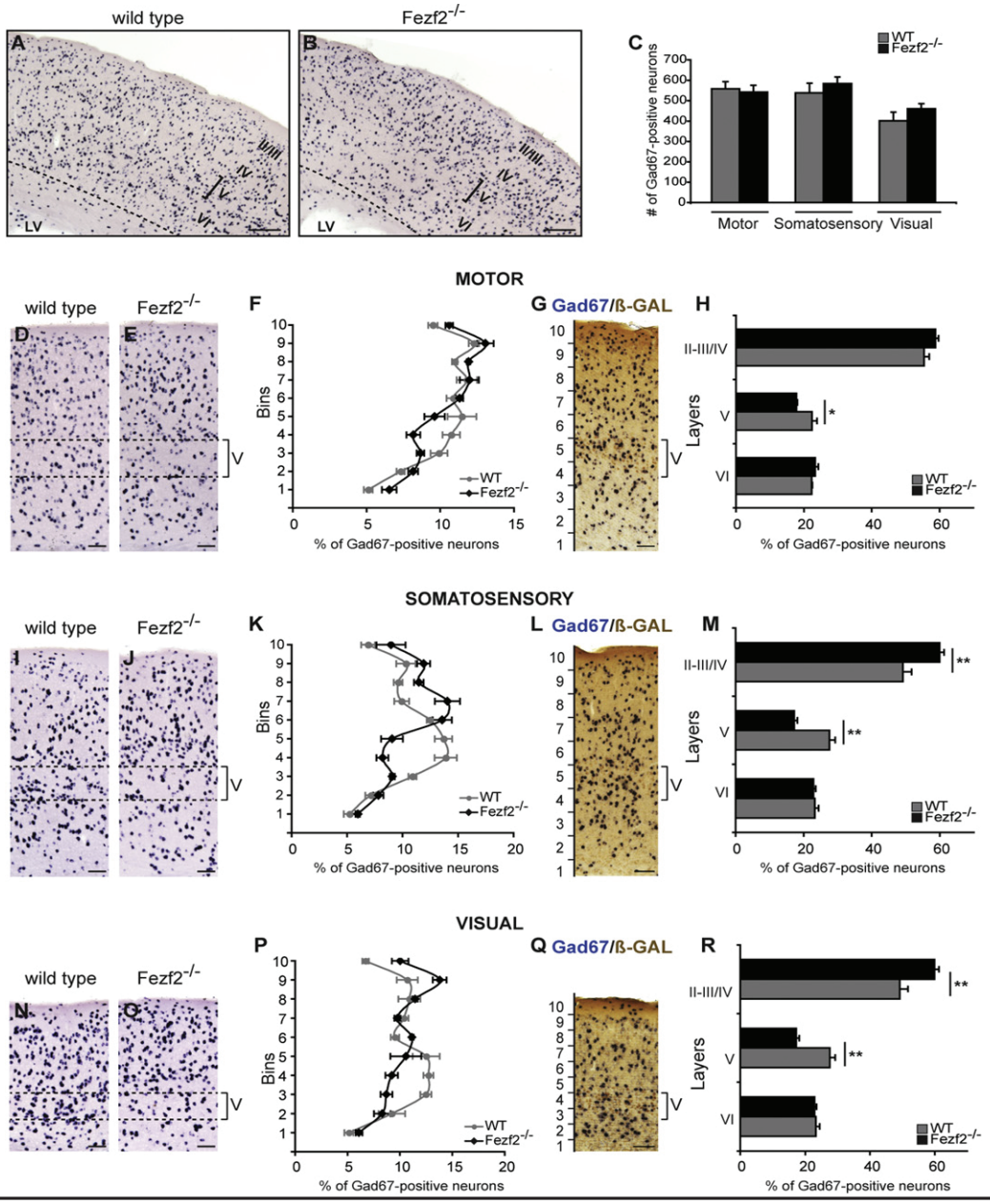

Figure 3.2 - The Fezf2^{-}/_ Cortex Has Abnormal Radial Distribution of GABAergic Interneurons (**A, B**) In situ hybridization for Gad67 in wild-type (**A**) and Fezf2^{-}/- (**B**) cortex at P28 shows reduced numbers of interneurons in layer V and increased numbers in superficial layers of the Fezf2^{-}/- cortex.(**C**) Total number of Gad67 interneurons is unchanged between wild-type and Fezf2^{-}/- cortex.(**D–R**) Quantification of the layer distribution of Gad67 interneurons across motor (**D–H**), somatosensory (**I–M**), and visual (**N–R**) cortex. (**D, E, I, J, N, O**) Representative sections of wild-type and Fezf2^{-}/- cortex. (**F, K, P**) Unbiased binned distribution of Gad67 interneuron percentages shows decreased percentages in deep bins and increased percentages in superficial bins of the mutant. (**G, L, Q**) b-galactosidase immunocytochemistry in Fezf2^{+}/- heterozygote mice demonstrates that layer V corresponds to bins 4–5 (in motor and somatosensory cortex) and bins 3–4 (in visual cortex). (**H, M, R**) Quantification of interneurons within layers demonstrates a specific reduction in interneuron percentages in mutant layer V across all cortical areas and an increase in interneuron percentages in layers II/III-IV. All results are expressed as the mean ± SEM. *p < 0.01; **p < 0.005, t test. LV, lateral ventricle. Scale bars represent 500 mm (**A, B**) and 200 mm (**D, E, G, I, J, L, N, O, Q**). For quantification of interneurons, anatomically matched sections were processed to detect Gad67 (n = 3 Fezf2^{-}/-; n = 3 wild- type, eight to ten hemispheres per area, for each mouse at P28)

Figure 3.3

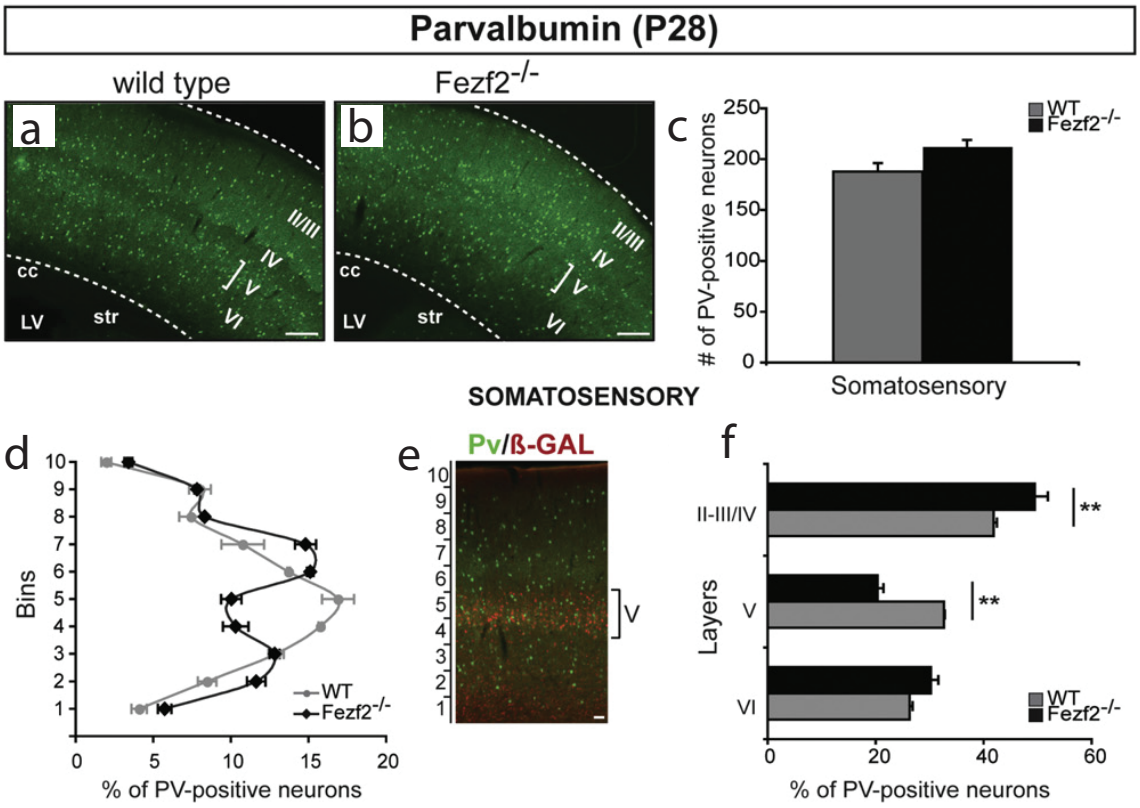

Figure 3.3 - PV Interneuron Subtypes Are Reduced in Layer V and Increased in Superficial Layers of the Fezf2^{-}/– Cortex

(**a, b**) In situ hybridization for PV in wild-type and Fezf2^{-}/- somatosensory cortex at P28 show reduction of both interneuron populations in layer V and increase in superficial layers. (**c**) Total number of PV interneurons is unchanged between wild-type and Fezf2^{-}/- cortex. (**d**) Unbiased binned distribution of PV interneuron percentages shows decreased numbers in deep bins and increased numbers in superficial bins of the mutant. (**e**) b-galactosidase immunocytochemistry in Fezf2^{+}/- heterozygote mice highlights layer V in bins 4–5. (**f**) Quantification of PV interneurons within layers demonstrates a reduction in the percentages of interneuronal subpopulations in mutant layer V and an increase in layers II/III–IV. All results are expressed as the mean ± SEM. **p < 0.005, t test. LV, lateral ventricle; str, striatum; cc, corpus callosum. Scale bars represent 500 mm (a,b) and 100 mm (e). For quantification of interneurons, anatomically matched sections were processed to detect PV, (n = 3 Fezf2^{-}/-; n = 3 wild- type, eight to ten hemispheres per area, for each mouse at P28). Boxes of 300 pixels in width and spanning the thickness of the cortex were superim- posed at matched locations on each section and divided into ten equally sized bins. Interneurons were quantified in each bin, and bin-distribution was defined as the percentage of interneurons in each bin relative to the total number of interneurons.

Cobos et al., 2006; Fogarty et al., 2007), while mostly late-born, calretinin expressing interneurons are present in higher numbers in the superficial layers (Miyoshi et al. 2011, Nery et al. 2002; Xu et al., 2004). The overall number of PV^{+} neurons was unchanged, but again the distribution was shifted to the upper layers (Figure 3.4). Calretinin expressing interneurons were not affected (Lodato et al. 2011). Thus, the absence of subcerebral projection neurons exerts selective control over interneuronal populations that normally occupy the same deep layers of the cortex.

$Fezf2^{-/-}$ Mice Exhibit Unbalanced Cortical Activity due to Defective GABAergic Inhibition

To determine whether the observed changes in interneuron distribution result in unbalanced cortical activity and physiology, we used voltage-sensitive dye imaging (VSDI) (Grinvald & Hildesheim 2004) to examine spatiotemporal dynamics of functional connections in the $Fezf2^{-/-}$ mice. VSDI is uniquely suited to this question as it provides a readout of the entire laminar structure of a cortical slice. We tested the local excitatory-inhibitory circuit of the visual cortex. The spread of activity through coronal slices of the visual cortex in response to a current pulse delivered to the white matter was quantified. The stimulating electrode was placed within the white matter tract in the middle of V1, consistently targeting the base of the triangle of the white matter as it condenses. As expected, wild-type and heterozygous $Fezf2^{+/-}$ mice exhibited a strong response that propagated rapidly to the upper layers "on beam" with the stimulating electrode, spreading only weakly along the deep layers even at threshold stimulating strengths

Figure 3.4

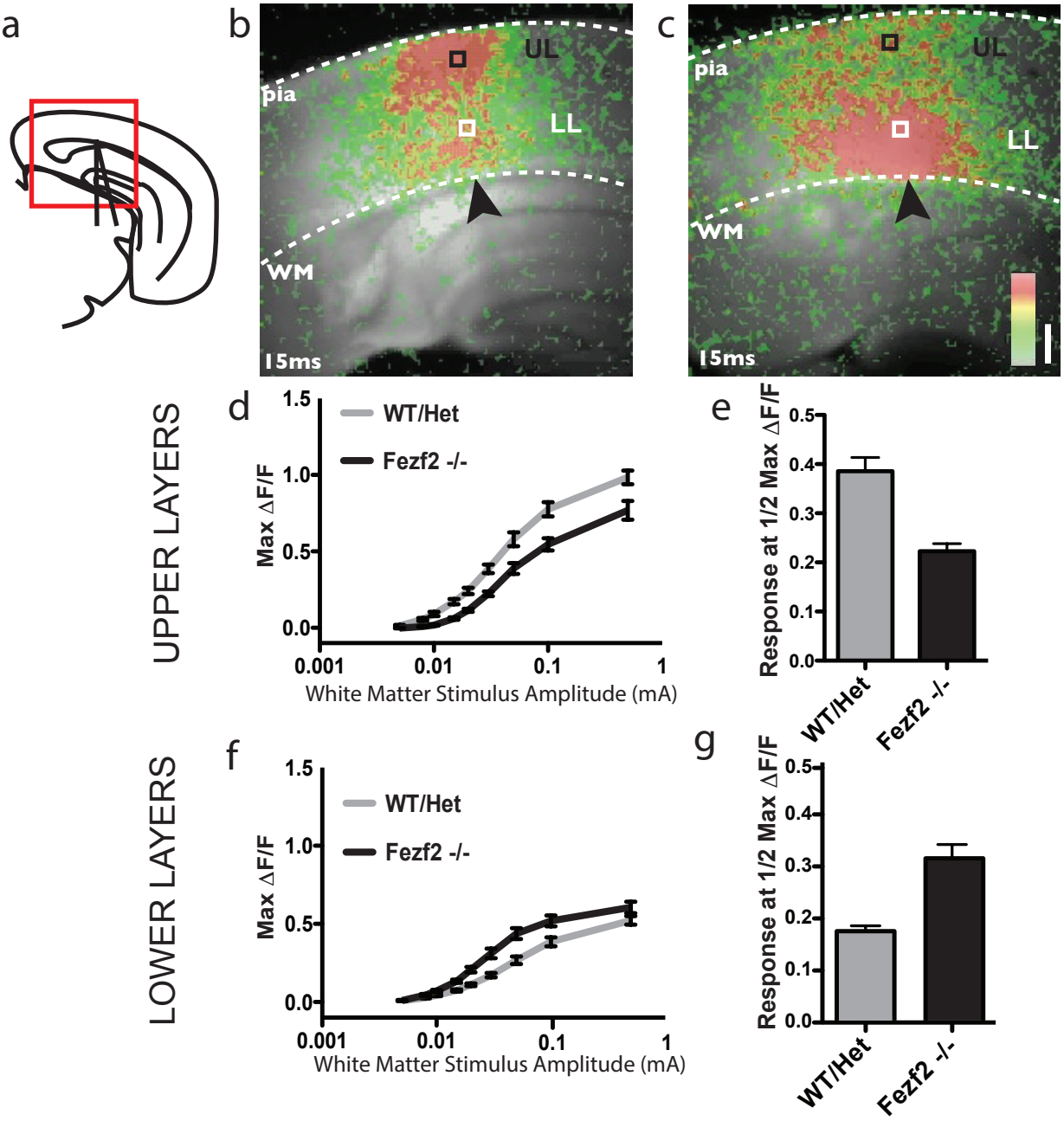

Figure 3.4 - Spread of Neuronal Activity Is Restricted to the Deep Layers in Fezf2−/− Cortex
(**a**) Schematic of recording area (red box) indicating the position of the stimulating electrode in the white matter (WM).(**b,c**) Pseudocolor peak response frames from VSDI movies of wild-type (**b**) and Fezf2^{-}/− (**c**) slices 15 ms after the stimulus (arrowhead) stimulating at half maximal response, showing that wild-type mice exhibit a strong stimulus response that propagates rapidly to the upper layers (**b**), whereas the response in Fezf2^{-}/− slices rarely reaches the upper layers, remaining largely confined to the lower layers (**c**). Black and white squares indicate quantified regions of interest in the upper (UL) and lower layers (LL), respectively. Scale bars represent 250 μm.(**d,f**) Stimulus response curve in the regions of interest for upper (**d**) and lower (**f**) layers.(**e,g**) Response at half max. All results are expressed as the mean ± SEM. *** $p < 0.001$, t test. 1-2 slices per animal n=16 WT/Het, n=11 Fezf2^{-}/-

(Figure 3.4 b). In contrast, the response in Fezf2$^{-/-}$ slices at threshold rarely reached the upper layers and remained largely confined to the lower layers (Figure 3.4c).

Maximum fluorescence intensity was quantified within two 125 x 125 mm^2 regions on-beam with the stimulating electrode, one in upper layers (Figures 3.4 b,c; black box) and one in lower layers (Figures 3.4 b,c; white box). Input-output curves revealed an increase in upper-layer response with increasing stimulus intensity; however, the response failed to reach wild-type levels in the upper layers of Fezf2$^{-/-}$ mice across all stimuli (Figure 3.4 d). Conversely, lower layer responses were consistently stronger in Fezf2 $^{-/-}$ mice compared to wild-type (Figure 3.4 f). These differences were significant for both upper and lower layers at half-maximal stimulation (Figures 3.4 e,g).

These findings are consistent with a shifting of PV$^+$ and other inhibitory neurons to the upper layers. The inhibitory neurons act like a functional ”gate” to prevent the spread of the excitatory signal. Notably, the microcircuit architecture for PV$^+$ interneurons, and probably neocortical inhibition in general, is an unspecific, densely homogenous matrix covering all nearby pyramidal cells (Packer & Yuste 2011). The physiological imbalance of excitation across cortical layers in Fezf2 $^{-/-}$ cortex may be explained by abnormal excitatory networks, altered inhibitory GABAergic interneurons, or both. To distinguish among these possibilities in the rewired Fezf2 brain, we performed VSDI measurements in the presence of the $GABA_A$ receptor antagonist bicuculline. Strikingly, the laminar differences between genotypes were eliminated under these conditions (Figure 3.5), indicating that the excitatory network scaffold is intact in the Fezf2$^{-/-}$ mutant cortex.

Figure 3.5

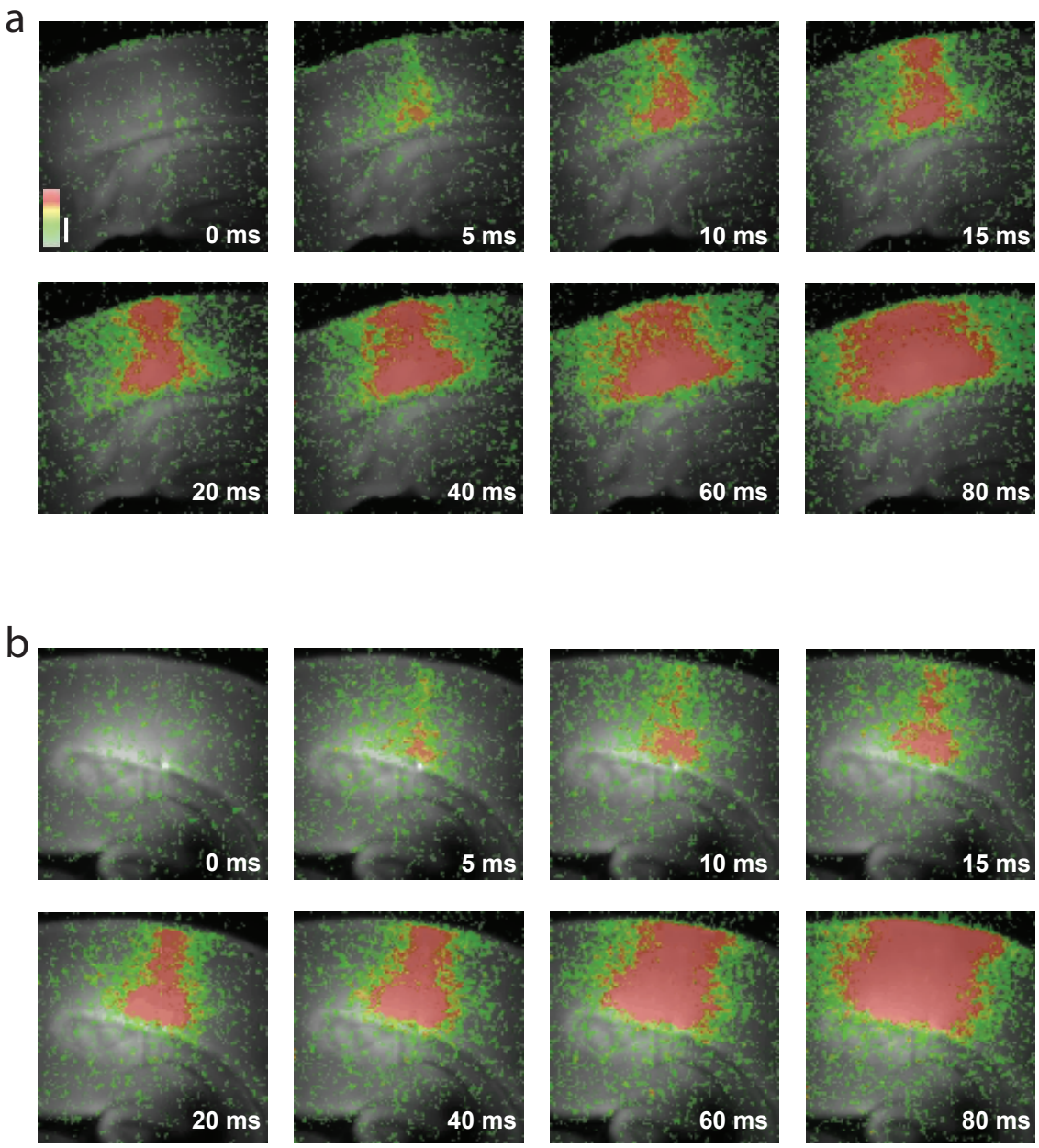

Figure 3.5 - GABA blockade Eliminates Laminar Functional Differences
(**a**,**b**) Snapshots from representative VSDI video of the half maximal stimulation response 10 min after bicuculline application from wildtype (**a**) and Fezf2 (**b**) slices. Frames every 5 ms on the top row and every 20 ms on the bottom row of each. Tested 5 animals per genotype. Scale bar: 250 μm

Taken together, an increased GABAergic tone in the superficial layers of the mutant cortex (without defects in excitatory network function) provides physiological support for our histological findings that interneuron numbers are reduced in layer V and increased in upper layers II/III-IV of the Fezf2$^{-/-}$ cortex which causes signal propagation defects in the knockout mice.

Mecp2

Having established a protocol for testing for laminar inhibitory dysfunction, we asked if we could also detect more subtle inhibitory impairment. Mutations in Mecp2, a transcriptional regulator, causes Rett syndrome and other developmental disorders (Chahrour & Zoghbi 2007). Mecp2 is a critical regulator of inhibitory neurons, as selective deletion of Mecp2 in GABAergic neurons alone recapitulates many of the cognitive deficits of the global deletion and the disorder (Chao et al. 2010). We have found that Mecp2 loss causes a sharp regression in mouse visual acuity after an initial normal development. We have found early changes in the cortical PV circuitry that accounts for this visual deficit.

We used high resolution confocal microscopy to study the GABAergic, and specifically PV^{+} synapses, of the visual circuit. We found that there was an increase in the number of PV^{+} puncta around the soma of pyramidal cells (Figure 3.6 a,b). This PV^{+} cell hyper-connectivity was present and maintained throughout development and into adulthood (Figure 3.6 c). The hyper-connectivity of PV^{+} neurons results in a progressive compensation in functional PV^{+} synapses. Although the GAD65 content was normal in Mecp2 KO mice right after eye opening (P15), which coincides with the onset of PV^{+}

Figure 3.6

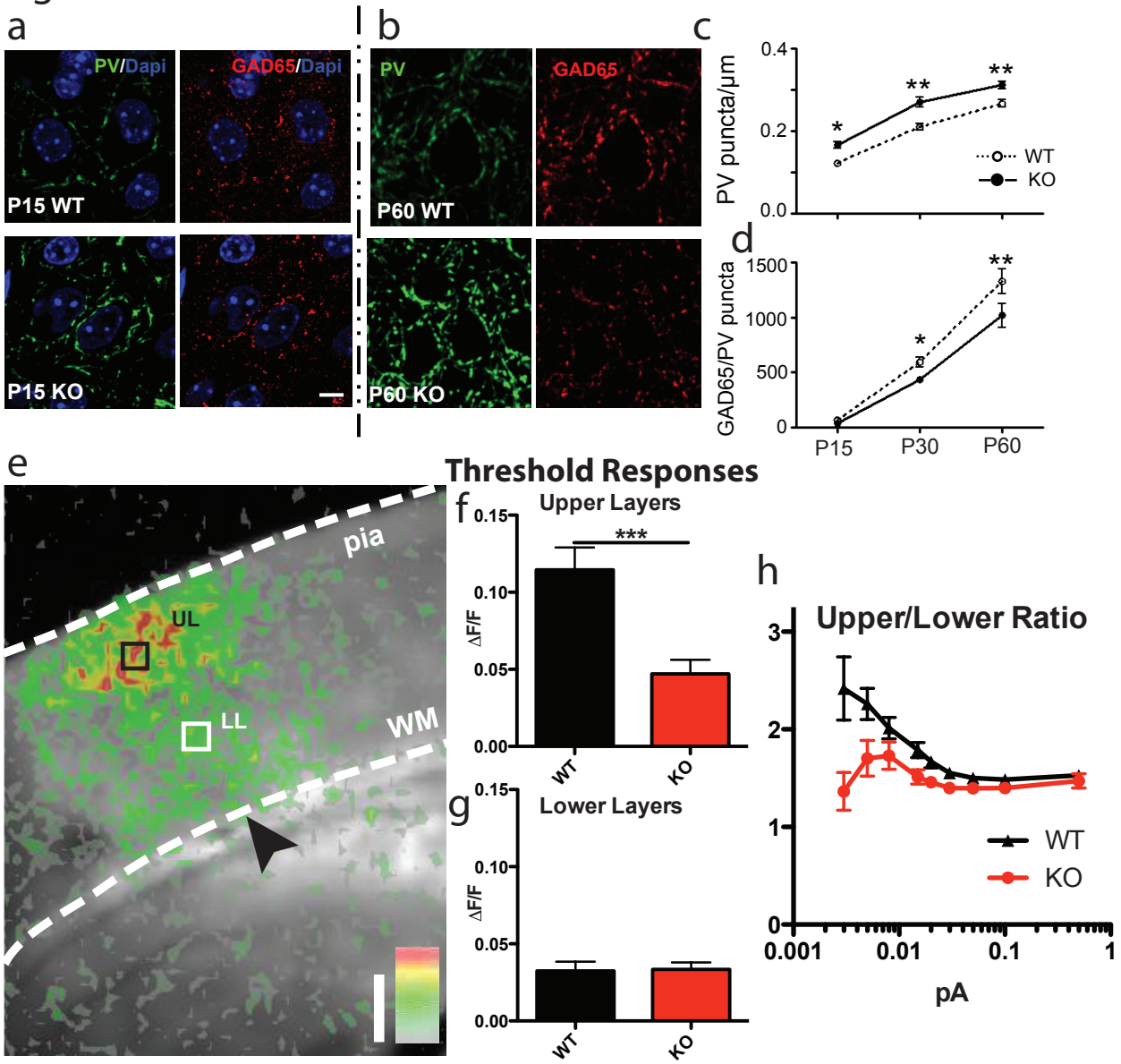

Figure 3.6 - Increased PV Expression causes a Developmental Decrease in GABA signaling and Impaired Circuit Function at P25 in Mecp2 KO Mice

(**a,b**) PV-immunofluorescence is elevated already at P15 in Mecp2 KO animals (3 mice each, P<0.01) and this difference persists into adulthood. (**c**) The density of perisomatic PV-boutons upon pyramidal cell somata is significantly increased in the absence of Mecp2 starting already at P15 and throughout life (3-4 mice each, vs. WT; * P<0.01, ** P<0.001, Mann-Whitney test). WT mice also exhibit a significant increase in PV-puncta across development (3-4 mice each, P<0.01).(**d**) The level of GAD65 within PV puncta is significantly decreased only after P30 in Mecp2 KO mice compared to WT (3-4 mice each, vs. WT; * P<0.01, ** P<0.001, Mann-Whitney test).(**e**) Pseudo-color peak response frames from VSDI movies of wild-type slice at half max stimulation 15 ms after the stimulus (arrowhead), showing that wild-type mice exhibit a strong stimulus response that propagates rapidly to the upper layers whereas the response in Mecp2 KO slices did not propagate to the upper layers as strongly, especially near threshold (not shown). Black and white squares indicate quantified regions of interest in the upper (UL) and lower layers (LL), respectively. Scale bars represent 250 µm. (**f, g**) Quantification of threshold response of upper layers (**f**) and lower layers (**g**). Student t test. *** P<0.001 (**h**) Ratio of upper layer response/lower layer response for entire stimulus range. ** 1 way ANOVA. 2 Slices per animal wildtype n=6, KO n=7.

expression in fast-spiking interneurons, the level of GAD65 positive PV^+ puncta was substantially less at P30 and P60 in the KO mice (Figure 3.6 b,d).

VSDI of coronal visual slices confirmed the increased activity of the PV circuit. We found near the lowest (threshold) stimulating currents which evoke a response the upper layer activation in Mecp2 KO mice was lower than wildtype (Figure 3.6 f,g). As PV^+ cells are directly innnervated by thalamocortical fibers (Gibson et al. 1999, Beierlein et al. 2003, Cruikshank et al. 2007), their hyper-connectivity at threshold "gates" the stimulus propagation into upper layers (Atallah et al. 2012). Increasing the stimulating current caused the ratio between upper and lower layer response to approach control levels as the excitatory drive began to recruit (presumably PV^+ cell) inhibition in the wildtype as well (Figure 3.6 h).

Summary

We have found that proper PV^+ neuron positioning and synaptogenesis is critical for maintaing proper signal propagation as well as excitatory/inhibitory balance. Since PV^+ cells target the soma, they act as a gate for the output of the cell. If there is an imbalance in the number of PV^+ synapses in the upper layers, either due to disrupted migration or enhanced synaptogenesis, the output of the excitatory network is altered and the excitatory/inhibitory balance is disrupted. This disruption may lead to seizures, as has been observed in the $Fezf2^{-/-}$ mice, or autism spectrum disorders such as Rett syndrome caused by Mecp2 deletion.

Chapter 4

Optimizing the Visual Thalamocortical Slice

Introduction

The thalamus is the primary source of visual information to the cortex. Visual information arrives first in the photoreceptors of the eye, is transmitted along the retinal ganglion cell axons to the thalamus where the relay cells of the LGN (visual thalamus) then transmit the information to the cortex. Thalamocortical (TC) afferents arborize extensively in layer 4, synapsing onto both excitatory and inhibitory cells and providing the first layer of cortical processing. Thus, it is desirable to isolate this synapse in a reliable acute visual TC slice to functionally dissect its integral role in the visual circuit and sensory processing.

The thalamus sends migrating axons to the visual cortex very early during development. These fibers play an important role in the patterning of the cortex (Huberman 2007). By embryonic day 12 (E12) of the mouse, axons are already migrating out from the thalamus, arrive at the cortical subplate by E15 and terminate in layer 4 by birth (Auladell et al 2000, Molnar & Blakemore 1995). The establishment and refinement of retinotoptic maps is driven by two factors: molecular gradients and coordinated neuronal activity (McLaughlin & O'Leary 2005). Both spontaneous and patterned activity propagated along the TC fibers is necessary for the anatomical and functional refinement of visual circuits and receptive field properties including refinement of ocular dominance columns and binocular receptive fields (Crair et al 1998, Huberman et al 2008).

TC afferents play a critical role not only in cortical specification, but also in cortical plasticity. The rapid functional shift in response favoring the open eye after MD is followed by anatomical rewiring. Much of this rewiring is the reconfiguration of the TC arbors. The cortical territory innervated by thalamic afferents of the deprived eye shrinks in higher mammals. The familiar autoradiographs depicting a shift in ocular dominance "columns" are the physical readout of thalamic terminals in layer 4 (Figure 1.1 a) (Hubel et al. 1977). Although mice lack ocular dominance columns, the anatomical changes apparent in the cat and monkey also occur there. Extended MD in mice causes an initial shift in the *in vivo* functional response and synaptic anatomy (Mataga et al. 2004) followed by an expansion of the TC fibers driven by the open eye and stunted growth of TC fibers serving the deprived eye (Antonini et al. 1999).It is not known what is the exact sequence of synaptic plasticity that precedes the anatomical shift.

Acute TC slice preparations of both somatosensory and auditory cortex have been widely used for well over a decade (Agmon & Connors 1991, Metherate &Cruikshank 1999, Cruikshank et al. 2002). They have provided numerous insights into the nature of TC connections (Rose & Metherate 2005), the properties of cortical neurons targeted by TC afferents (Metherate & Aramakis 1999), differences between intracortical and thalamocortical transmission (Gil et al. 1997, Gil et al. 1999, Lee and Sherman 2008) and mechanisms of synaptic plasticity (Feldman et al. 1999). They have revealed local inhibitory processing and circuit dynamics (Cruikshank et al. 2007, Gabernet et al. 2005), as well as offered a basis for understanding the mechanisms of cortical map plasticity (Barkat et al 2011). In addition, they also provide a basis for comparison across sensory modalities. Individual synaptic properties and plasticity may be uniform

for TC synapses, while others may be modality or developmental stage-specific. With a rich history of study in the visual system, and an increased interest in using the mouse to study visual processing and plasticity, a visual TC slice will serve multiple purposes.

Previous work by McLean et al. (2005) and unpublished work by our lab have provided a basis for a visual TC slice. However, elaboration of the slice protocol to achieve a consistently connected slice at a variety of ages and a careful dissection of the anatomical features of the slice are required before addressing questions about basic functional synaptic connectivity and the role of the TC synapse in development and plasticity of the visual circuit.

Results

Anatomical Connection of the Visual Thalamocortical Slice

The circuitous trajectory of the TC fibers from the LGN to the cortex has been difficult to isolate in an easy slice prep. Previous work by MacLean et al. (2005) and unpublished work by our lab suggested that a pseudo-coronal slice at 55°, at P20, would contain the primary visual cortex (V1), the LGN and the connecting fibers (Figure 4.1 a-c). We designed a mold to create agar wedges onto which we could glue the brain. The agar would position the brain so that the anterior pointed up and angled so the vibratome blade cut at 55° (Figure 4.1 d). The agar wedge would also provide support for the brain and prevent compression of the long TC fibers, should the brain flex during cutting. To confirm the anatomical connections, we made *in* vivo injections of a retrograde tracer into the visual cortex, waited 2 days, then made acute TC slices

Figure 4.1

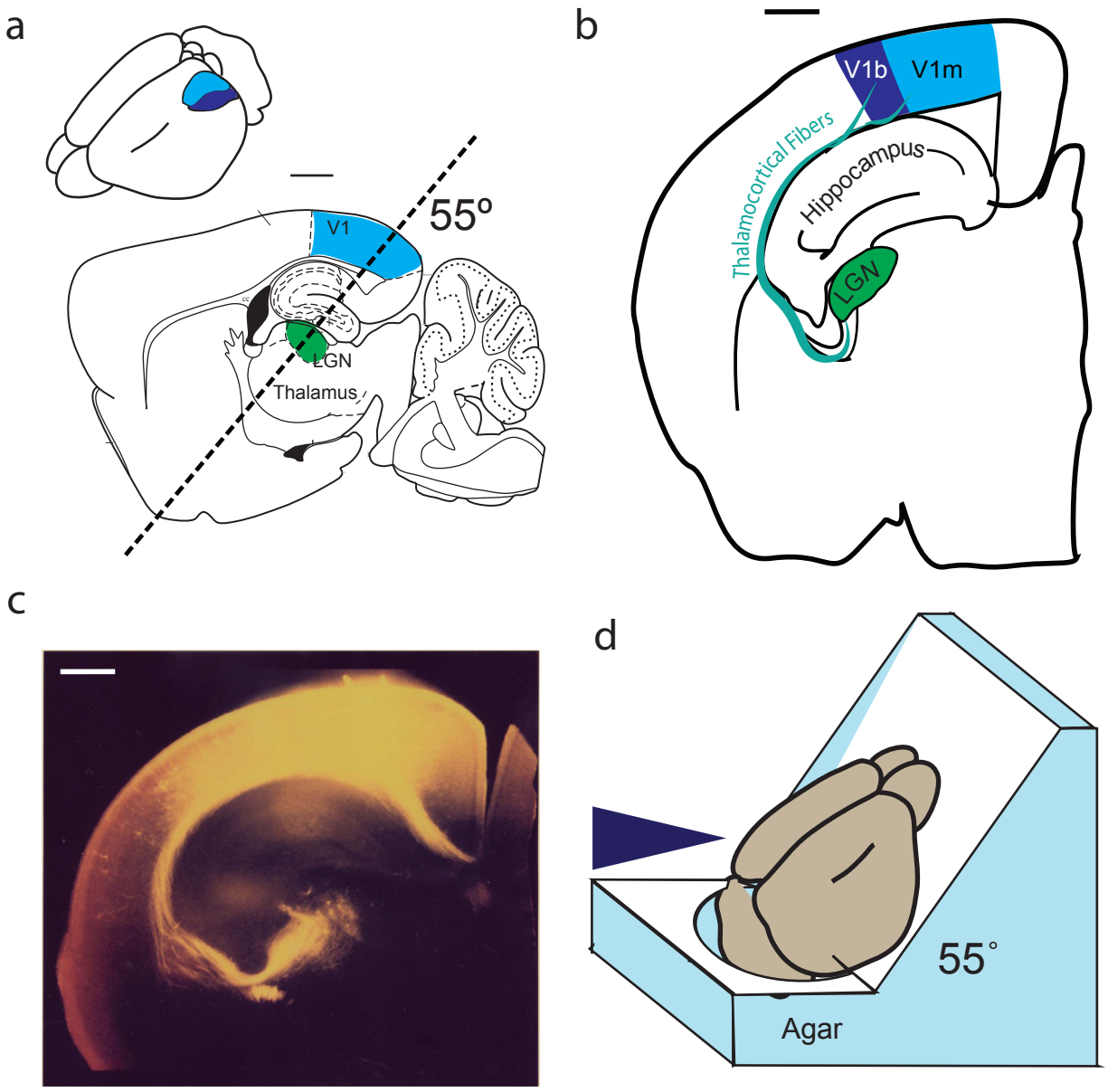

Figure 4.1 Anatomical Connections and Slice Configuration of Visual TC Slice (**a**) Diagram after Paxinos Atlas showing location of LGN and V1 approximately 2mm lateral demonstrating the plane of . Inset shows approximate location of monocular V1 (light blue) and binocular V1 (dark blue) in the 3D mouse brain. (**b**) Diagram of visual TC slice. (**c**) Retrograde tracer injection into V1 demonstrating anatomical connection to LGN within the thalamocortical slice. (**d**) Visual TC Slice set up demonstrating agar mold and cutting angle. Arrowhead represents vibratome blade. Scale bars = 500nm.

using the mold. Visualization of the LGN and fibers as well as the injection site confirmed the connection using the agar to hold the brain at 55° (Figure 2.1 d).

Functional Connection

We next used voltage-sensitive dye imaging (VSDI) and field recordings to confirm the functional connection (Figure 4.2 a). Although we could record AMPA mediated local field potentials (Figure 4.2 b,c) in slices varying from 350-600 μm thick, we needed to optimize the slice thickness and other parameters so that consistently connected slices could be cut every time. Given our previous experience using VSDI to examine local cortical circuitry (Chapter 3), we determined that this technique was ideally suited to view the response of the entire visual cortical area of the slice and thus a single recording location would not miss our survey of “hot spots.” We could then focus on varying the slicing parameters until we found a consistent protocol.

We determined that a 500 μm slice gave consistent connections and would still allow for DIC and fluorescence imaging of single cells. We found, perhaps due to the nature of the TC fibers projecting backwards, that a greater response was found on the posterior/caudal surface of the slice than on the anterior/rostral surface. Moreover, we found that one of the most important parameters was which slice to select, or rather with a slice 500 μm thick, when to begin slicing. We found that there is only one connected slice per hemisphere. Using the disjoining of the corpus callosum or the splaying of the white matter as an anatomical marker (Figure 4.2 d) we determined that a slice beginning ~350 μm after the disjoining to be optimal for a connected slice at P20.

Figure 4.2

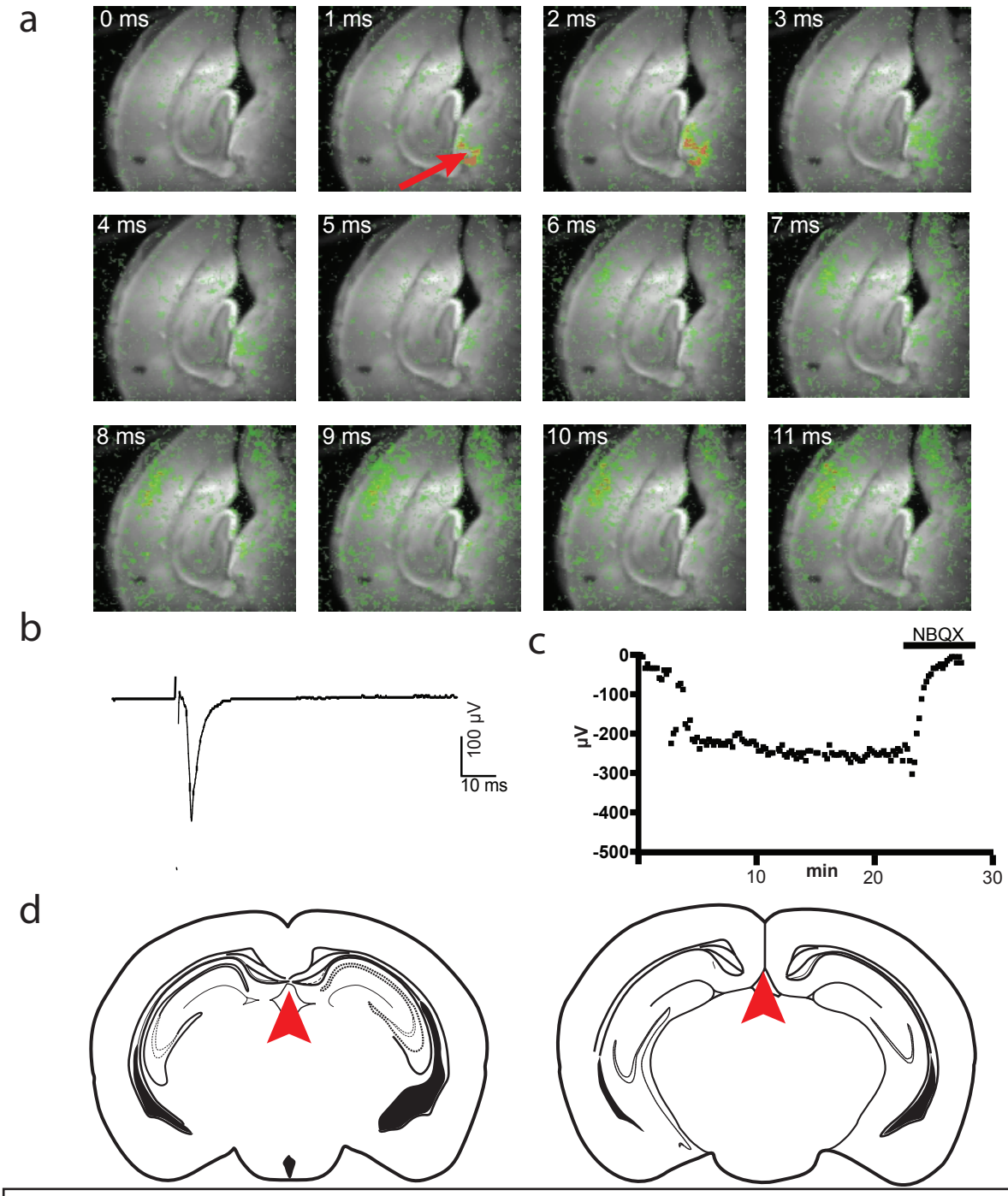

Figure 4.2 - Functional Connection of the Visual TC Slice
(**a**) Snapshots from pseudocolor VSDI movie from 1 ms before stimulation through cortical response, 1 ms between frames. Red arrow in the second frame indicates location and time of stimulus. (**b**) Average layer 4 field recording around half maximal stimulus from a connected TC slice (5-10 min into the experiment). (**c**) Peak amplitude from field recording plotted across entire experiment. (**d**) Diagram of the disjoining of the corpus callosum (red arrowhead) right before (left) and immediately after the separation (~100 µm posterior).

The mouse visual system and the entire brain undergo rapid post-natal development. Eyes do not open until P13-14 and the entire brain grows four-fold larger in the first 4 weeks. Even so, by birth the TC neurons are arborizing within the cortex (Auladell et al. 2000) and the brain has reached almost a mature volume by P14 (Chuang et al., 2011). Thus, only minor adjustments to the slice prep make it possible to record from connected slices from mice aged P14-35. As the myelination of the white matter is weak at early ages, we found that a larger gap (~450 μm) after the apparent disjoining of the corpus callosum is optimal for young mice aged P14-16. We did not attempt younger mice, before eye opening.

In slightly older mice, >P25, simply changing the slice depth did not solve the connectivity issues. Again using VSDI, we slightly varied the cutting angle between 40° and 65° and found that a slightly shallower angle of 50° worked better. This could be achieved by trimming the agar block on the bottom by 5°, slightly tipping the slicing platform or by slightly angling the brain down when glueing. Additionally an interval of ~250 μm after the disjoining of the corpus callosum was optimal in animals >P25. These changes increased the probability of obtaining a connected slice but did not qualitatively change the response. Despite the fact that the slice is symmetric through both hemispheres, occasionally in older animals, only one hemisphere was connected. This could be due to slight twisting during the glueing process, but with meticulous attention and repetition, we could ensure a connected left hemisphere in >90% of the animals aged P16-27. In older animals, perhaps due in part to the decrease in slice viability, the connection rate fell to around 33% in animals P30-35.

Stimulation Location

Cortical VSDI responses could be generated with a bipolar electrode stimulating either within the LGN or the fibers exiting the LGN (Figure 4.4 a). Within the LGN, cortical responses were generated when the electrode was placed in the center or lateral edge. Placing the electrode on the medial edge either did not produce a cortical response or produced weaker responses. Strong stimulating pulses (0.5-1.0 pA) were used to test for connectivity and no obvious changes in VSDI response area were apparent with moderate displacement of the stimulating electrode.

Anatomical Features of the Visual Thalamocortical Slice

The mouse visual system is somewhat simplified; it displays retinotopy yet lacks the hyper-columns present in higher mammals (Hübener, 2003). Although the mouse primary visual cortex predominantly responds to input from the contralateral eye, there is a region of V1 lateral to the monocular zone (V1m) that continues retinotopic space and contains neurons that respond to stimuli presented to both eyes. It is cells within this binocular region (V1b) that undergo a response shift after monocular deprivation during the critical period (Antonini et al. 1999). The mouse LGN is likewise dominated by inputs from the contralateral eye but there is a small area of cells receiving input from the ipsilateral eye. V1b receives input from both the contralateral and ipsilateral regions of the LGN. Thus, there is a simple yet defined ocularity for the mouse visual system.

Figure 4.3

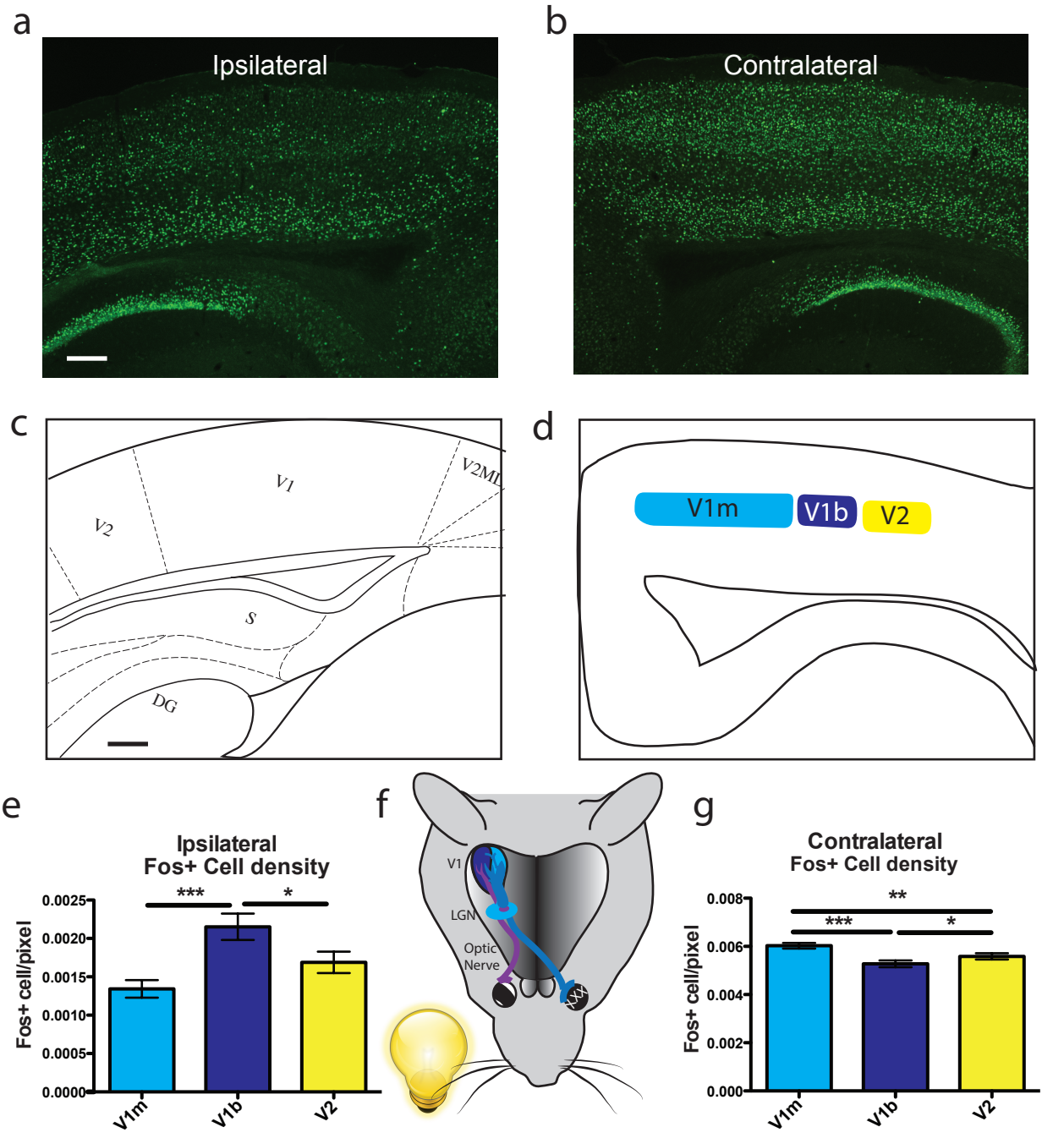

Figure 4.3 - Cortical Anatomy of Visual TC Slice
(**a**) Fos expression in visual cortex after light exposure to the ipsilateral eye. Scale bar 250 μm. (**b**) Fos expression in contralateral cortex. (**c**) Paxinos atlas at Interaural 0.0. Scale bar 250 μm. (**d**) Cortical boundaries of visual TC slice. (**e,f**) Quantification of Fos positive cells from (**e**) ipsilateral and (**g**) contralateral sides (n =9). (f) Diagram of experiment, ipsilateral/contralateral to light exposure. Values are mean ± SEM. Statistics: 1way ANOVA, Tukey post-hoc test. *P<0.05, **P<0.01, ***P<0.001

Although VSDI showed the location in V1 that responded to stimulation of the LGN (Figure 4.2a), we sought to better understand the anatomy and ocularity of the visual TC slice. We assayed Fos expression after light exposure to one eye to locate cortical cells that were excited by light stimuli to that eye, using Fos-EGFP mice. Examining three slices per animal, 200 μm apart and spanning the functionally connected slice, we saw a striking difference between the cortical response of the hemisphere ipsilateral to the open eye and the contralateral side (Figure 4.3 a,b). There is an obvious decrease in layer 4 activation of Fos in the hemisphere ipsilateral to the light exposure. Since the signal is lower in this ipsilateral hemisphere, it is possible to detect a region, slightly larger than 0.5 mm wide with increased Fos expression corresponding to V1b.

After examining the ipsilateral TC slices spanning the functionally connected slice we were able to compile some anatomical guidelines for the boundaries in visual cortex (Figure 4.3 c). Our guidelines align with *"The Mouse Brain…"* atlas (Paxinos and Franklin 2001), specifically the coronal diagrams around Interaural 0.00 (Figure 4.3 d), which corresponds well to the position of layer 4 in our slice when calculating the angle and distance back from the ending of the corpus callosum in the atlas. V1m extends from the horn or peak of the white matter triangle going laterally to the angle where the white matter triangle collapses down to the tract. V1b is located lateral to V1m and is approximately 0.5mm wide, ending at the arch of the hippocampus. V2 and later visual areas are lateral to V1.

Using these guidelines we quantified the density of layer 4 Fos activation in both the ipsilateral hemisphere that we used for establishing the boundaries and the contralateral side, where expression differences are less obvious. Using an automated

Figure 4.4

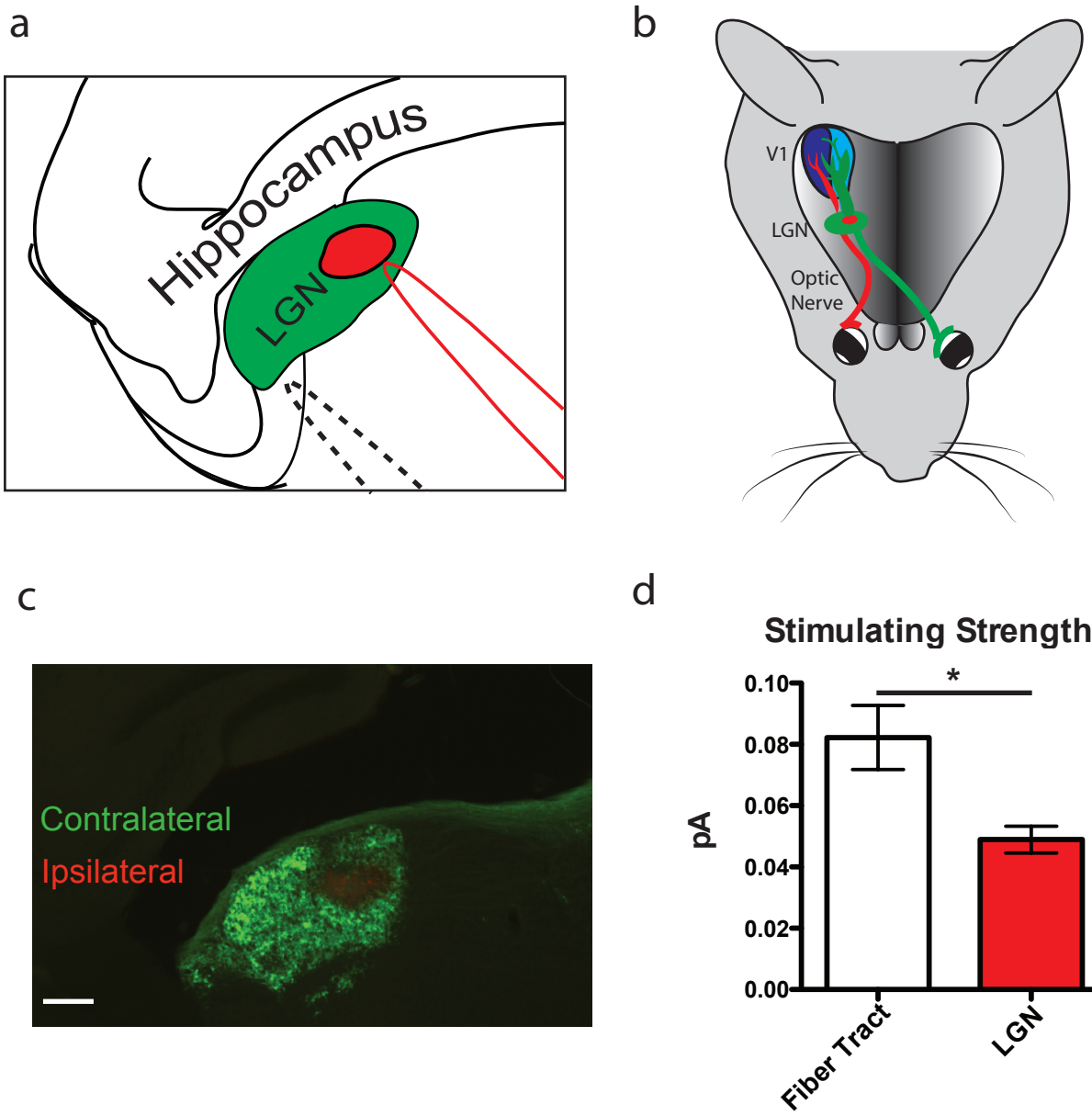

Figure 4.4 - Separated Ipsi and Contralateral Areas and Location in TC slice LGN

(**a**) Diagram of stimulation electrode placement in TC LGN (solid red line) or in fiber bundle (dotted line). (**b**) Diagram of cholera toxin experiment. Right eye injected with red- and left eye injected with green-conjugated cholera toxin. (**c**) Cholera toxin eye injections showing terminals in LGN. Scale bar 250 µm. (**d**) Quantification of initial experiments stimulating either fiber tract or LGN needed to elicit single fiber EPSC. Values are mean ± SEM. Statistics: Mann-Whitney test. * $P<0.05$.

particle count, compared to the corresponding monocular zone, the ipsilateral binocular zone had a significantly higher density of Fos-positive cells (Figure 4.3 e); whereas, the contralateral binocular zone had a significantly lower density (Figure 4.3 f), thus confirming our regions. The small area we labeled V2 had an intermediate density in both hemispheres reflecting either a different proportion of binocular cells, different activation of Fos or known differences in cell density (Antonini et al. 1999).

Although the cortical anatomy of the TC slice was very similar to a coronal slice, we could not be sure that the anatomy of the small LGN would also line up. We found Fos expression in the LGN to be weak so we used eye injected tracers to define the contralateral and ipsilateral regions within the LGN (Figure 4.4 b,c). We found an ipsilateral patch surrounded by the contralateral fibers. This is similar to previously published images of coronal slices (Jaubert-Miazza et al. 2005, Hong & Chen 2011). This patch lies near the medial edge and is within the area of the LGN that produces a robust VSDI cortical response when stimulated at low intensity.

Thalamocortical Synaptic Input onto Individual Cells

Having verified the anatomy and connectivity of the visual TC slice, we sought to examine the synaptic currents elicited by individual TC fibers. We used whole-cell electrophysiology and low stimulating intensities to examine excitatory post-synaptic currents (EPSCs) of single fiber inputs (Hook & Chen 2006) onto cortical cells.
We targeted layer 4 cells within the middle 100 μm of V1b for our recordings. The majority, but not every cell within V1b was connected in each slice (Figure 4.5 a). Specifically targeting cells in V1m elicited an occasional connection, which could

Figure 4.5

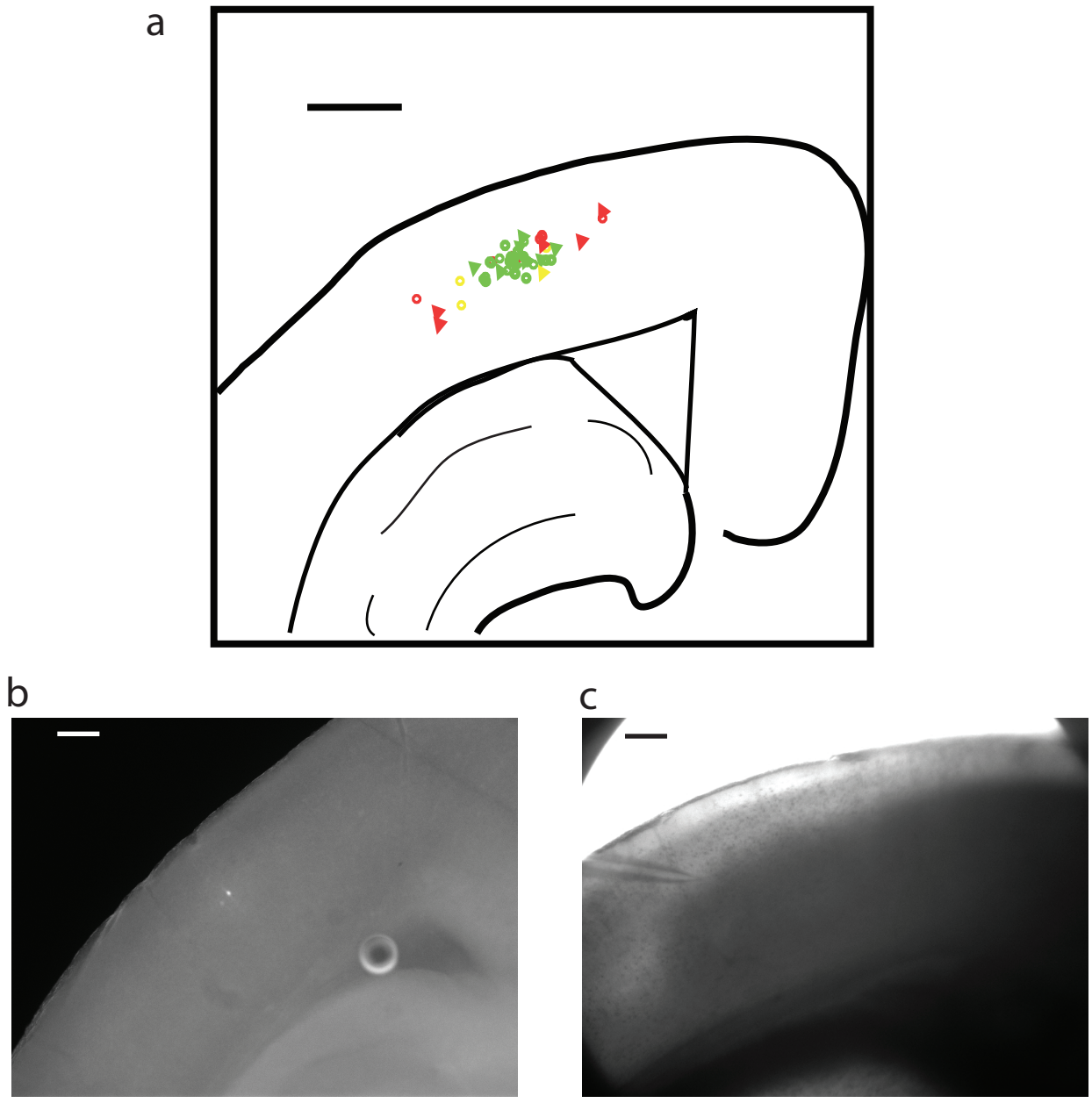

Figure 4.5 - Location of Recorded Cells
(**a**) Diagram of patched cells centered on V1b. Triangles represent pyramidal cells, circles PV GFP positive cells. Green indicates monosynaptic connection, yellow indicates a non-monosynaptic connection and red was not connected. Scale bar 500 µm. (**b**) Biocytin fill of connected cell. Scale bar 250 µm. (**c**) Patch pipette location of connected cell. Scale bar 250 µm.

potentially be improved by moving the stimulating electrode away from the ipsilateral patch in the LGN. Cells in V2 not only had a different laminar structure (Wagor et al. 1980), but they were also not connected in 3 tested cells. Location of recorded cells was confirmed by aligning either the location of the biocytin filled cell after recording and staining or by location of the recording electrode tip (Figure 4.5 b,c).

TC EPSCs in layer 4 of binocular V1 could be elicited by placing the stimulating electrode either within the fiber bundle leaving the LGN or within the LGN adjacent to the medial edge, in or near the patch of fibers coming from the ipsilateral eye (Figure 4.4 a). The stimulating current needed to produce a single fiber EPSC when stimulating the LGN cell bodies was significantly less than that of stimulating the fiber bundle (Figure 4.4 d), reflecting the significant difference in somatic vs. axonal action potential threshold.

We used onset latency, jitter and short term synaptic plasticity to qualify an EPSC as a monosynaptic TC synapse. Like the somatosensory TC synapse (Gil et al. 1999, Beierlein et al. 2003), the visual TC synapse displays paired-pulse depression (Boudreau et al 2005). We used a pair of stimulation pulses 40 ms apart to classify the short term plasticity of the synapse. Poly-synaptic intracortical synapses could occasionally be detected and displayed facilitation (Figure 4.6 a), thus we could discard any synapse showing facilitation.

While the short term plasticity is a quick method for discarding some synapses, we used onset latency and jitter as criteria for a monosynaptic TC synapse. Figure 4.6 c shows a subset of EPSC onset delays from our initial recordings. It displays a bimodal distribution, and from these initial experiments, we established a 9 ms cut off for

Figure 4.6

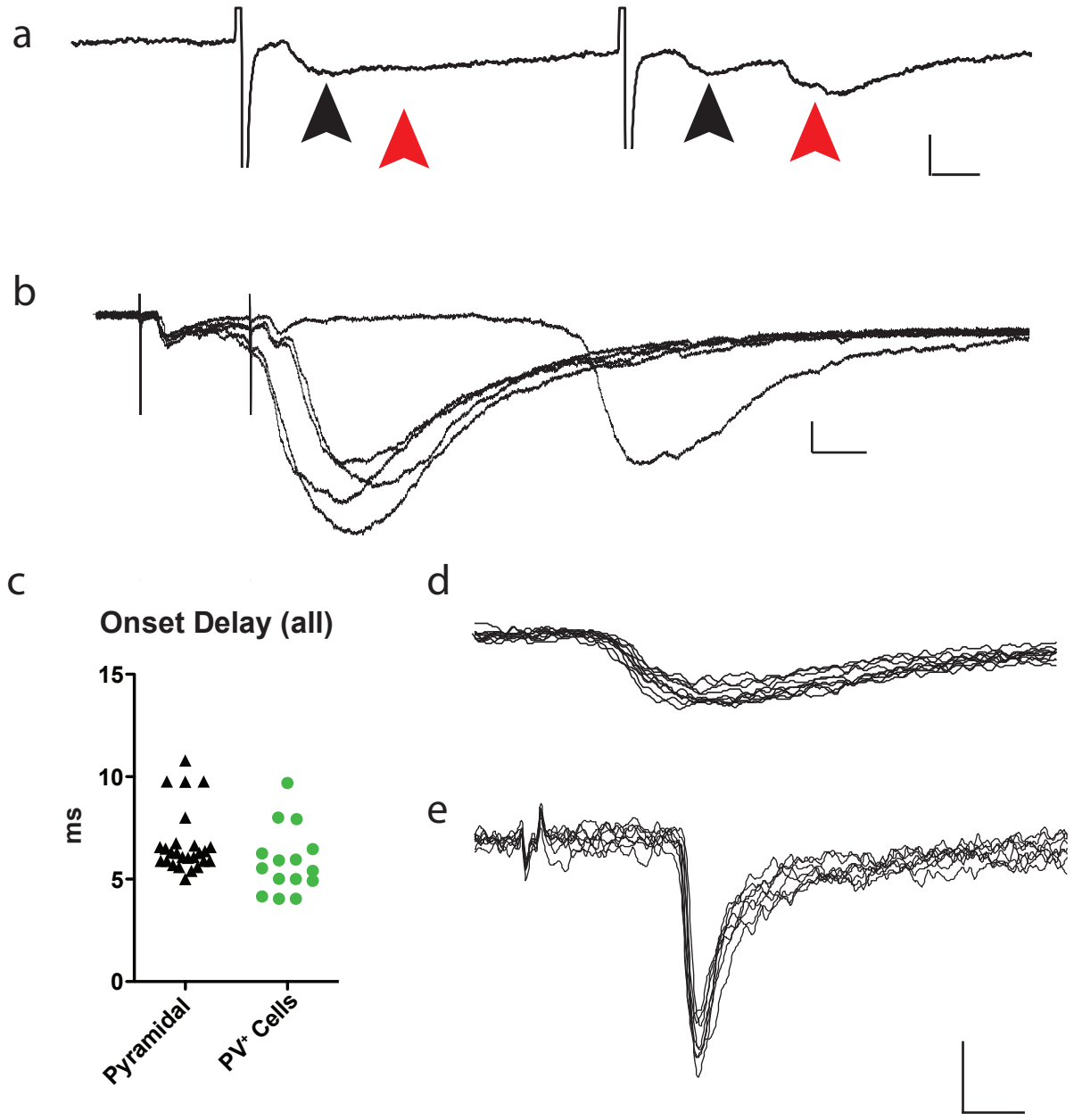

Figure 4.6 - TC Monosynaptic Criteria
(**a**) Single EPSC showing depressing TC current (black arrow head) followed by facilitating intracortical current (red arrow head). Scale bars: 5 ms, 50 pA. (**b**) 5 TC EPSCs showing late, poly-synaptic activity. Stimulus = 0.1pA. (**c**) Subset of single fiber onset delays. (**d**) 10 individual sweeps from layer 4 pyramidal cell with jitter under 0.3 ms. (**e**) 8 individual sweeps from a layer 4 inhibitory neuron with jitter under 0.2 ms. Both d and e are monosynaptic, single-fiber TC EPSCs with low jitter. Scale bars: 1 ms, 50 pA.

recordings at room temperature. If a connection could not be found with an onset delay under 9 ms, that cell was classified as not monosynaptically connected in that slice, and we moved on to the next cell. In addition to being a fast synapse, the TC synapse in other systems has been demonstrated to be precise (Rose & Metherate 2005). We examined individual traces at a single stimulation intensity, measuring the jitter in onset latency (Figure 4.6 d,e). We measured the standard deviation to ~10% of peak and accepted cells with a standard deviation value < 0.5 ms. TC connections in the slice could initiate poly synaptic activity as well, if a clean monosynaptic trace was not isolated from other currents within 3 ms of the TC EPSC peak, that cell was not used for analysis.

We could frequently generate late, poly-synaptic activity within the slice after stimulating the LGN (Figure 4.6 b). The late poly-synaptic activity was more easily detected at high stimulating strengths, but could be ocasionally detected at the single-fiber stimulating strength. The time course of this late poly-synaptic activity occurred 50-250 ms after the first stimulation and was variable. The example in Figure 4.6b is at a single stimulating strength but produces highly variable poly-synaptic activity. The kinetics of this poly-synaptic activity was much slower than the monosynaptic response. Both the rise and decay of the responses were slower. The late poly-synaptic response could be eliminated after blocking AMPA receptors with NBQX. Although we focused and optimized our recording condtions on the monosynaptic single-fiber responses, it would be possible to study other aspects of the fully connected visual TC slice.

Summary

We have established a slicing protocol, verified the anatomy, and determined criteria for a monosynaptic connection in a visual TC slice. The ability to activate and isolate the TC synapse *in vitro* offers 2 major advantages: 1) precise physiological and pharmacological access to the fundamental cortical synapse in a genetically tractable animal model, and 2) the ability to stimulate this input in a more naturalistic or anatomical manner, allowing insight to receptive field construction, cortical connectivity, and plasticity after direct stimulation of the LGN.

Chapter 5

Intrinsic and Synaptic Development of Layer 4 Cells in Visual Cortex

Introduction

Cortical circuits are shaped by balanced excitatory/inhibitory transmission. In layer 4 of visual cortex both the excitatory pyramidal cells and inhibitory parvalbumin positive (PV^+) cells are innervated by the thalamus. Layer 4 receives and performs the initial processing of afferent input before relaying the information on to other cortical layers. Thus, the functional and synaptic development of layer 4 cells is critical for initial sensory cortical development.

GABAergic inhibition in general, and PV^+ neuron differentiation in particular, display delayed development after birth. Although the prototypic PV^+ interneurons from the medial ganglionic eminence are present in the mouse visual cortex by birth, they do not express the calcium binding protein parvalbumin or the voltage-gated potassium channel Kv3.1 until the second post natal week, around eye opening (Gonchar et al. 2007). Both of these molecules are believed to be essential for the interneuron's fast spiking abilities.

In the visual cortex there are a number of determinants for the transition of immature PV^+ cells to fast spiking cells. Dark rearing decreases GABA transmission (Morales et al. 2002) whereas over expression of the growth factor BDNF accelerates the growth and arborization of PV^+ cells in visual cortex (Huang et al. 1999). Postnatal

development enhances the inhibitory transmission and adjusts the excitatory/inhibitory balance that is requisite for the initiation of ocular dominance critical period (Hensch 2004). Inhibition triggers plasticity through α1 containing $GABA_A$ receptors which are targeted by PV^+ cells and these peri-somatic $GABA_A$ receptors are optimally regulated during the critical period (Katagiri et al. 2007).

In addition to the conditions and factors needed for the initial maturation of PV^+ cells, other factors are needed for further maturation and continual maintenance. PV^+ cells are preferentially surrounded by chondroitin sulfate poteoglycan (CSPG) rich perineuronal nets (PNNs). The PNNs are weakly present during the critical period and increase into adulthood. They act as a plasticity brake and to reactivate ocular dominance plasticity in adult mice, application of chondrotinases to destroy the PNNs allows ocular dominance plasticity in adult mice, and reopens the critical period (Pizzorusso et al., 2002).

The homeoprotein Otx2 has been found to be an essential transcription factor for the initiation of the ocular dominance critical period and it is also crucial for the maturation of PV^+ cells (Sugiyama et al., 2008). Targeted knockout of Otx2 from non-GABAergic cells decreases PV expression and PNNs whereas precocious infusion of Otx2 enhances PV expression while prematurely opening and closing the critical period (Sugiyama et al. 2008). Otx2 is not cell-autonomously synthesized but selectively transferred to the PV^+ cells. Even the exogenous infusion of Otx2 is captured by PV^+ cells. This suggests that there is a specific binding site that recognizes PV^+ cells.

Beurdeley et al. (2012) found an RK binding motif in the Otx2 protein that has a high affinity for the the glycosaminoglycan (GAG) side chains of CSPGs. Cortical

infusion of a small peptide mimicking this RK binding motif blocks the transfer of endogenous Otx2 *in vivo* and reopens the ocular dominance critical period. Thus, there is an initial permissive level of Otx2 and/or PV^+ cell maturity that is required for critical period initiation and a critical threshold of Otx2 within PV^+ cells that prevents plasticity. We tested how the level of the transcription factor relates to the functional maturity or input of the PV^+ cells in addition to mapping the intrinsic and synaptic functional maturation of both excitatory and inhibitory layer 4 cells.

Results

TC Synapse onto Pyramidal and PV^+ Cells

Layer 4 cells of visual cortex receive the primary sensory input from the thalamus and are the first step of cortical processing. Both excitatory pyramidal and inhibitory PV^+ cells are strongly innervated by the thalamocortical (TC) synapse (Gibson et al. 1999, Beierlein et al. 2003, Cruikshank et al. 2007). For targeted recordings from PV^+ cells we made use of a transgenic line of mice that expresses green fluorescent protein (GFP) under the parvalbumin promotor (Meyer et al., 2002). We aimed to record basket cells and targeted the large, round or multi-polar fluorescent cells with a minimal membrane capacitance of 35 pF. The excitatory, non-fluorescent pyramidal cells were targeted by their large membrane capacitance (>50 pF) and oblong or tear drop shape.

Previously it had not been possible to functionally isolate this primary synapse, the TC synapse in the visual cortex, but with our visual TC slicing technique we sought to compare this synapse onto layer 4 pyramidal and PV^+ cells of the visual cortex (Figure 5.1). During the peak of the critical period for ocular dominance (P24-27), we

Figure 5.1

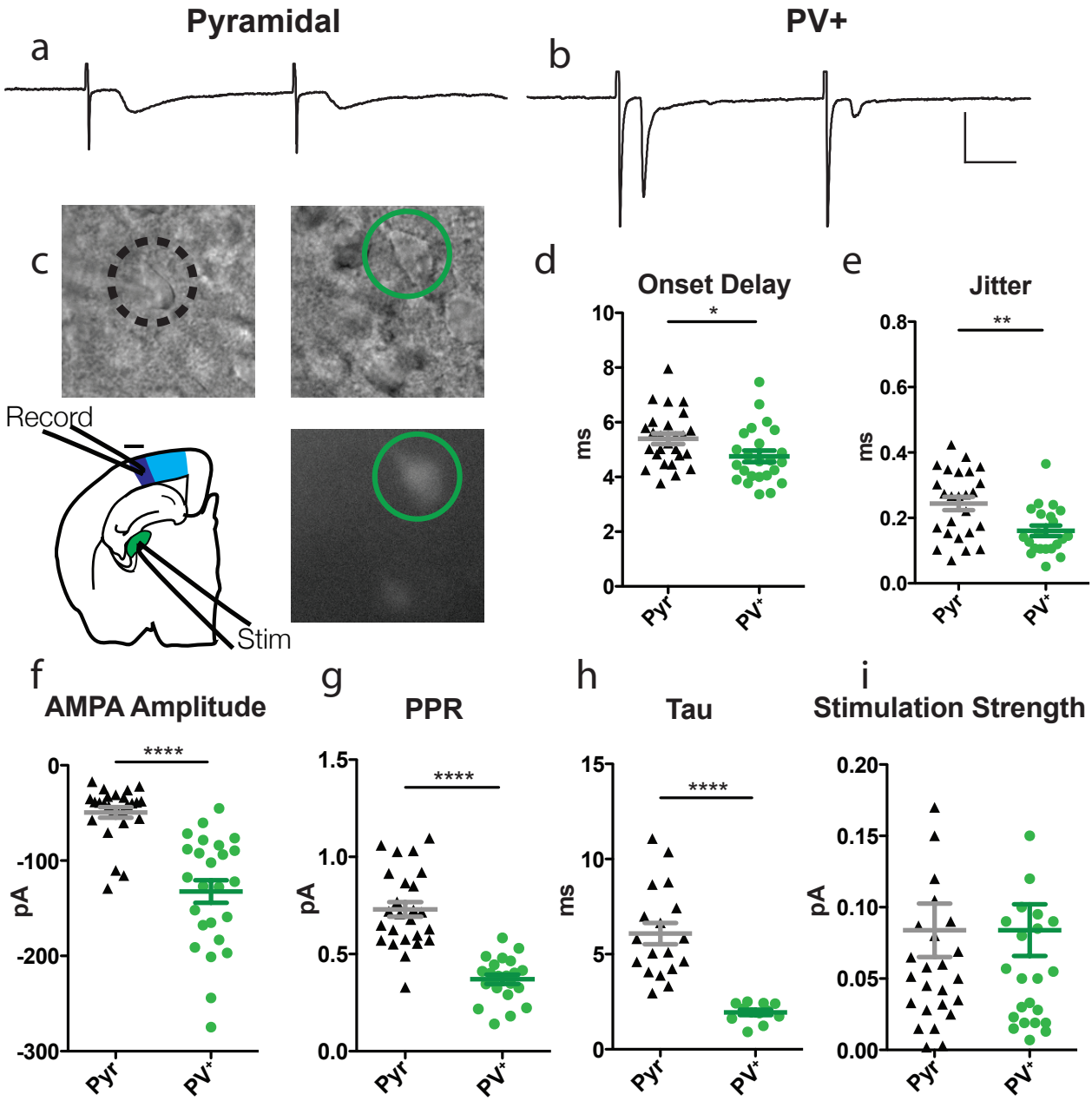

Figure 5.1 - Single fiber TC inputs onto Pyramidal and PV⁺ cells
(**a,b**) Example traces of single fiber TC EPSCs onto (**a**) pyramidal and (**b**) PV⁺ cells. P24-27. ISI 40 ms. Scale bar 10 ms, 50 pA.(**c**) Top IR/DIC pictures of pyramidal cell (left) and PV cell (right). Bottom left diagram of recording and stimulus locations within the TC Slice. Bottom GFP picture of PV⁺ cell. (**d**) TC Synapse onto PV⁺ cells has a quicker onset than onto pyramidal cells. (**e**) Jitter measured as the standard deviation of onset delay measured at ~10% of peak. (**f**) Mean AMPA amplitude is larger in PV cells than pyramidal cells. (**g**) Smaller paired-pulse ratio indicates higher release probability onto PV⁺ cells. (**h**) Decay constant of TC EPSC. (**i**) Stimulation strength of single fiber input. Bars at mean ± SEM. (**d,e**) t test. (**f-h**) Mann Whitney test *P<0.05. **P<0.01 ****P<0.0001

found strong, quick TC currents in both cell types but the connection to PV^+ cells was faster (Figure 5.1d) and had less jitter (Figure 5.1e). We did not find a difference in the amount of current needed to stimulate a single fiber (Figure 5.1i), but the recordings of pyramidal and PV^+ cells were not simultaneous so no conclusions could be drawn from this consistency.

The TC synaptic strength onto the PV^+ cells was much stronger than onto pyramidal cells (Figure 5.1f). The three fold larger single fiber current was accompanied by a smaller paired pulse ratio (PPR) (Figure 5.1g). The synapse onto both cell types displayed short term depression. Short term depression in synapses with a high probability of release occurs because of a decrease in the readily releasable pool of vesicles at the post-synaptic terminal after high frequency stimulation; there are simply fewer vesicles to release after the second stimulation. The small PPR of PV^+ neurons indicated that there is a higher probability of release of the TC fibers onto PV^+ cells over pyramidal cells.

The differences in the decay constant of the EPSCs (Figure 5.1 h) was consistent with the differential expression of AMPA receptor subunits. AMPA subunits of PV^+ cells are known to lack the GluR2 subunit (Jonas et al. 2003, Geiger et al. 1995) whereas pyramidal cells contain GluR2 subunits. AMPA receptors lacking the GluR2 subunit are calcium permeable, inwardly rectifying, and have fast kinetics, resulting in a fast synaptic connection. Thus the differences in the single fiber AMPA mediated EPSCs were due to both pre-synaptic and post-synaptic mechanisms.

Maturation of Intrinsic Properties after Eye Opening

The calcium binding protein parvalbumin is not expressed in the visual cortex until after the onset of vision (del Rio et al. 1994, Gonchar et al. 2007). At P13, while the eyelids are still fused, we have observed no GFP expression in the PV-GFP mice, but within 24 hours of the eyes opening there are numerous layer 4 PV^+ cells. Following this rapid molecular change is an equally rapid maturation of intrinsic membrane properties (Figure 5.2) and firing properties (Figure 5.3). Many intrinsic properties change within three days and reach a plateau within a week, which coincides with the onset of the critical period. The complete list of parameters is detailed in Table 5.1.

Maturation of membrane properties of the cell include a reduction in membrane resistance and membrane time constant. Although the decrease in membrane time constant will require more current to reach threshold, these changes would allow the PV^+ cells to integrate signals quicker and allow more precise response to synaptic inputs. Significant changes in the spike half-width, after hyperpolarization amplitude and duration, input resistance maximal firing rates (1way ANOVA of PV^+ cells across the 4 time periods) are all reflected in the different frequency vs current (FI) curves (Figure 5.3 d). A two-way ANOVA of the FI curves for the PV^+ cells across development indicates a significant difference between the first three time points, but no significance between the critical period (P24-26) and post critical period (P40-55) time points.

Pyramidal cell firing properties also undergo a few changes. Between P14 and P24 the spike half-width decreases ($p<0.001$), and the maximal firing rate increases ($p<0.001$, Mann-Whitney test). These overall shifts of both cell types in intrinsic

Figure 5.2

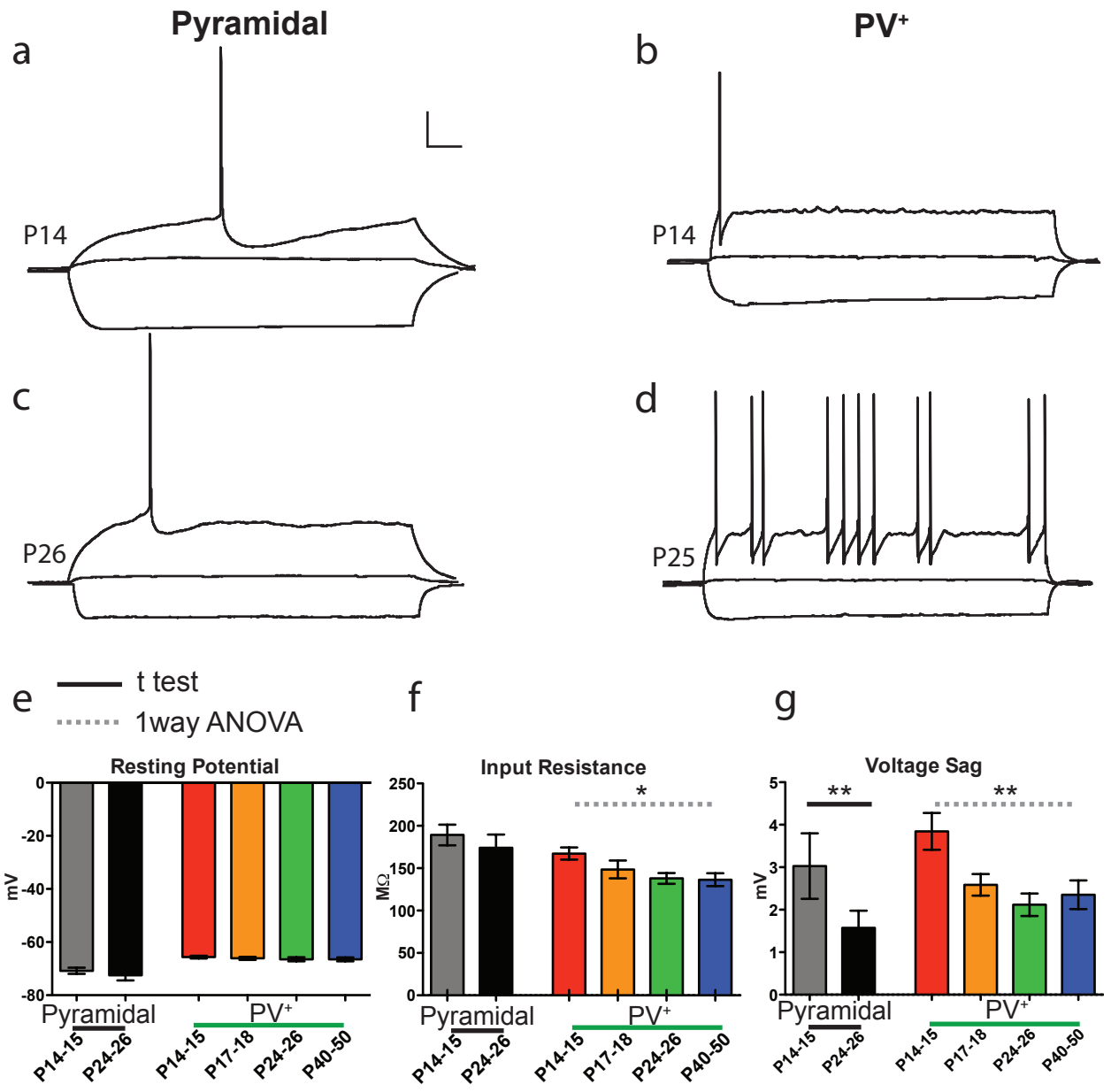

Figure 5.2 - Intrinsic Membrane Properties
(**a-d)** Current steps in example cells of -100 pA, 10 pA and threshold current: (**a**) P14 pyramidal cell, Ithresh = 36 pA. (**b**) P14 PV+ cell, Ithresh = 124 pA. (**c**) P26 pyramidal cell, Ithresh = 60 pA. (**d**) P25 PV+ cell, Ithresh = 136 pA. Scale bar: 100 ms, 10 mV. (**e-g**) Quantification of membrane properties. (**e**) Resting potential measured right after break in. (**f**) Input Resistance. (**g**) Voltage Sag, (difference in peak voltage - steady state). Values are mean ± SEM. Pyramidal P14-15 n=11, P24-26 n:8. PV+ P14-15 n:16, P17-18 n:16, P24-26 n:12, P40-50 n:12. Statistics: t test, 1way ANOVA. *P<0.05. **P<0.01.

Figure 5.3

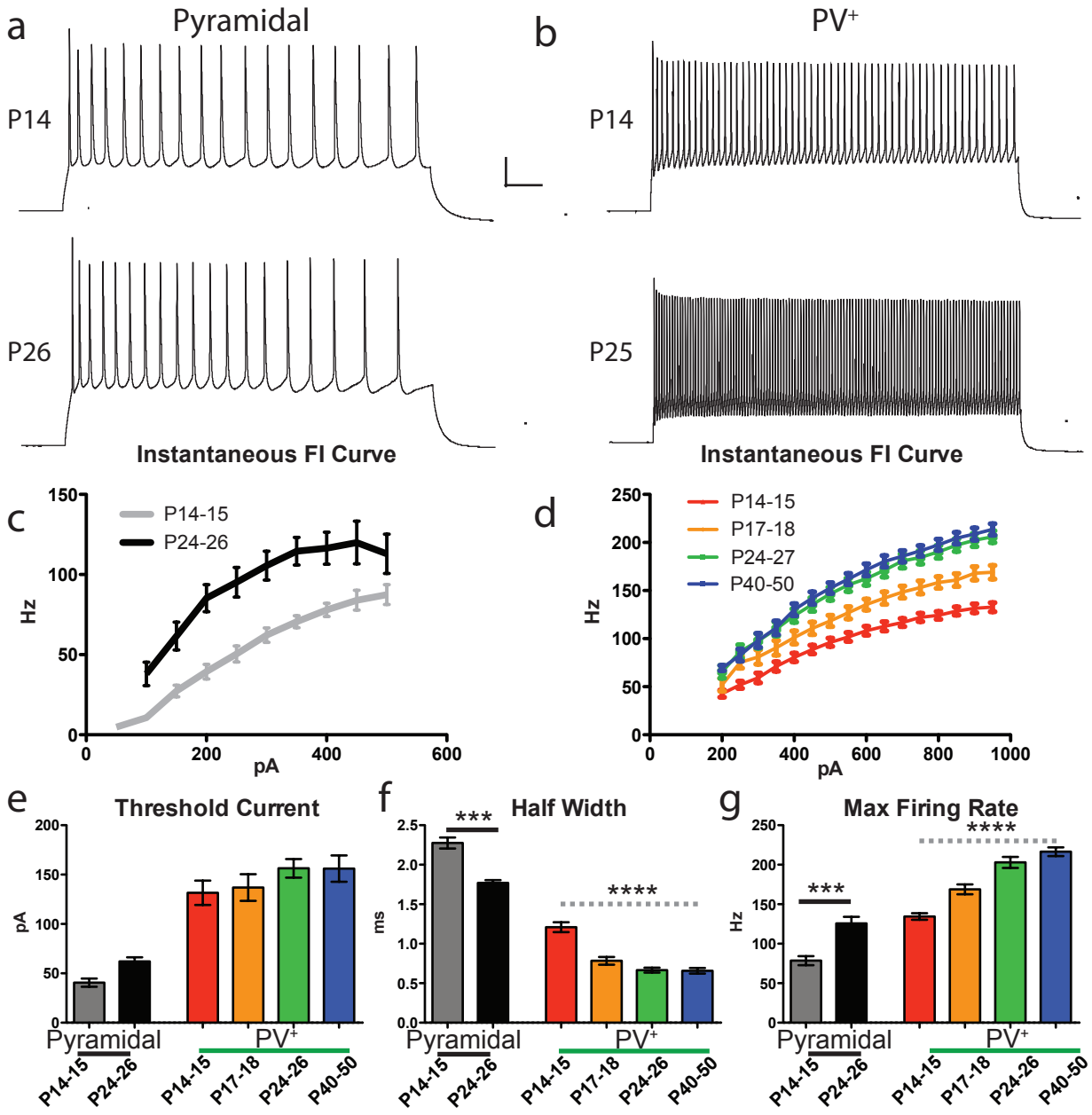

Figure 5.3 Developmental Spiking profile of PV⁺ and Pyramidal Cells
(**a,b**) Example spike trains for the same cells in Figure 5.2. (a) P14 (top) and P26 (bottom) pyramidal cells responses to a 200pA current injection. Scale bar: 100 ms, 10 mV. (**b**) P14 (top) and P25 (bottom) PV⁺ cells responses to a 500pA current injection. (**c,d**) Instantaneous FI curves, plotting the inverse of the 1st 2 spike ISI for pyramidal cells (**c**) and PV⁺ cells (**d**) across development. (**e**) Current required to generate an action potential. (**f**) Half width of action potential at threshold. (**g**) Maximal firing rate: inverse of the shortest ISI for current injections >500pA. Values are mean ± SEM. Pyramidal P14-15 n=11, P24-26 n:8. PV+ P14-15 n:16, P17-18 n:16, P24-26 n:12, P40-50 n:12. Statistics: t test (solid black line), 1way ANOVA (dashed gray line). ***P<0.001. ****P<0.0001.

Table 5.1 - Developmental Intrinsic Membrane and Firing Properties of PV^+ and Pyramidal Cells

Values are means ± SEM. **PV**: PV^+ cells. **Pyr**: Pyramidal cells **Vrest**: Membrane resting potential measured just after breaking into the cell. **Rm**: Membrane input resistance measured just after breaking into the cell. **Cm**: Membrane capacitance measured just after breaking into the cell. **tau**: Decay constant of the membrane, single exponential fit of the membrane response to a -100 pA current injection. **Sag**: Difference between the negative peak voltage and the steady state voltage of a -100 pA injection. **I Thresh**: Current injection required to elicit an action potential. **V Thresh**: Voltage threshold to spike. **Spike Amp**: Amplitude of the action potential from voltage threshold. **After-Hyperpolarization**: Amplitude of the hyperpolarization after the action potential spike measure from threshold voltage. **Time to Hyper Peak**: Time to reach after-hyperpolarization from action potential peak. **Adaptation**: Ratio of the last two interspike intervals (ISIs) divided by the first two ISIs. **Max Firing Rate**: Inverse of the shortest ISI for current injections >500pA.
Statistics: Developmental profile of PV^+ cells (ages P14-15 through P40-55) was analyzed as a 1way ANOVA and significance is listed on the bottom row of the table. Comparing Pyramidal Cells at P14-15 and P24-26 t test, significance for comparison given after the P24-26 value. Both STMD and GAD65 PV+ cells were compared to age-matched P24-26 control values t test. *P<0.05, **P<0.01, ***P<0.001

Table 5.1 continued

	n	Vrest (mV)	Rm (MΩ)	Cm (pF)	tau (ms)	Sag (mV)	I Thresh (pA)	V Thresh (mv)	Spike Amp. (mV)	Spike Half-width (ms)	After Hyper-polariz (mV)	Time to Hyper Peak (ms)	Adapta-tion	Max Firing Rate (Hz)
PV^+ P14-15	16	-65.64 ±0.59	167.3 ±7.2	44.2 ±2.0	20.65 ±1.46	3.85 ±0.43	131.6 ±12.3	-38.98 ±0.85	71.91 ±2.94	1.210 ±0.062	-15.26 ±0.65	5.912 ±0.747	1.16 ±0.05	134.5 ±4.1
PV^+ P17-18	16	-66.13 ±0.58	148.5 ±10.5	39.94 ±1.3	13.31 ±0.74	2.59 ±0.25	136.9 ±13.5	-42.92 ±1.02	81.19 ±1.43	0.784 ±0.048	-17.62 ±0.65	2.426 ±0.199	1.06 ±0.04	168.6 ±6.4
PV^+ P24-26	16	-66.50 ±0.76	137.9 ±6.3	40.5 ±2.0	11.09 ±0.51	2.12 ±0.27	156.4 ±9.4	-41.74 ±1.26	74.65 ±2.67	0.666 ±0.031	-19.39 ±0.56	1.926 ±0.166	1.01 ±0.03	203 ±7.1
PV^+ P40-55	12	-66.50 ±0.76	136.5 ±7.6	40.4 ±2.4	11.29 ±0.58	2.35 ±0.34	156.1 ±4.1	-39.57 ±0.65	73.50 ±3.09	0.658 ±0.035	-18.94 ±0.71	1.961 ±0.152	1.12 ±0.04	216.5 ±5.6
Pyramidal P14-15	11	-70.80 ±1.15	189.2 ±12.2	63.73 ±3.8	26.33 ±2.85	3.03 ±0.77	40.6 ±4.1	-42.95 ±0.78	90.88 ±1.03	2.275 ±0.070	-5.609 ±0.89	12.26 ±0.121	1.52 ±0.24	78.54 ±5.7
Pyramidal P24-26	8	-72.50 ±1.92	174.0 ±15.7	54.29 ±3.4	17.51 ±2.17	1.58 ±0.40**	62.13 ±4.1	-43.61 ±0.97	93.97 ±2.75	1.770 ±0.35***	-6.863 ±0.73	11.84 ±0.083	2.251 ±0.21*	125.7 ±8.2***
PV^+ STMD	7	-66.14 ±0.91	148.3 ±10.78	39.00 ±3.0	11.00 ±0.58	2.096 ±0.49	165.0 ±31.67	-41.87 ±1.20	76.12 ±1.90	0.7115 ±0.042	-21.15 ±0.92	2.085 ±0.140	1.048 ±0.04	186.6 ±7.5
PV^+ $GAD65^{-/-}$ P24-26	6	-65.00 ±1.18	140.3 ±17.27	40.83 ±4.14	11.37 ±0.91	1.780 ±0.34	195.0 ±30.49	-35.64 ±1.31*	66.7 ±3.51	0.7195 ±0.022	-20.39 ±0.85	2.180 ±0.102	1.109 ±0.04	176.2 ±10.6*
1way ANOVA PV^+ cells (Rows 1-4)		ns	*	ns	*	**	ns	ns	ns	****	****	****	ns	****

properties towards more precise and sustainable firing is an indication of not only the maturation of the excitatory/inhibitory circuitry but sensory processing as well.

Developmentally Stable TC Synapse

Witnessing the developmental changes evident in the intrinsic properties we next asked if there were similar synaptic changes by assaying TC input earlier, before the onset of the critical period for ocular dominance plasticity, between P16-18 (Figure 5.4). We checked if there were any specific changes that marked the critical period as different or plastic. The onset delay onto both cell types shortened (Figure 5.4 b). This is likely due to on going myelination of the postnatal brain which increases conduction velocity. Aside from changes in the onset delay, the synapses onto each cell type do not change significantly between before the onset of the critical period and the peak of the critical period. This suggests that the synapses are functionally established before or right around eye opening.

NMDA Mediated Thalamic Transmission

While we focused predominantly on AMPA mediated currents as they predominate synaptic transmission in PV cells and in mature TC transmission (Agmon & O'dowd 1992), we did record a set of NMDA mediated EPSCs by holding the cell at +40 mV and measuring the amplitude after the time course of the AMPA EPSC. We found little to no NMDA TC current onto PV^+ cells either during the critical period or before (Figure 5.5 a,b). We did occasionally notice poly-synaptic NMDA currents at a substantial delay from the onset of the TC EPSCs, suggesting that layer 4 PV^+ cells

Figure 5.4

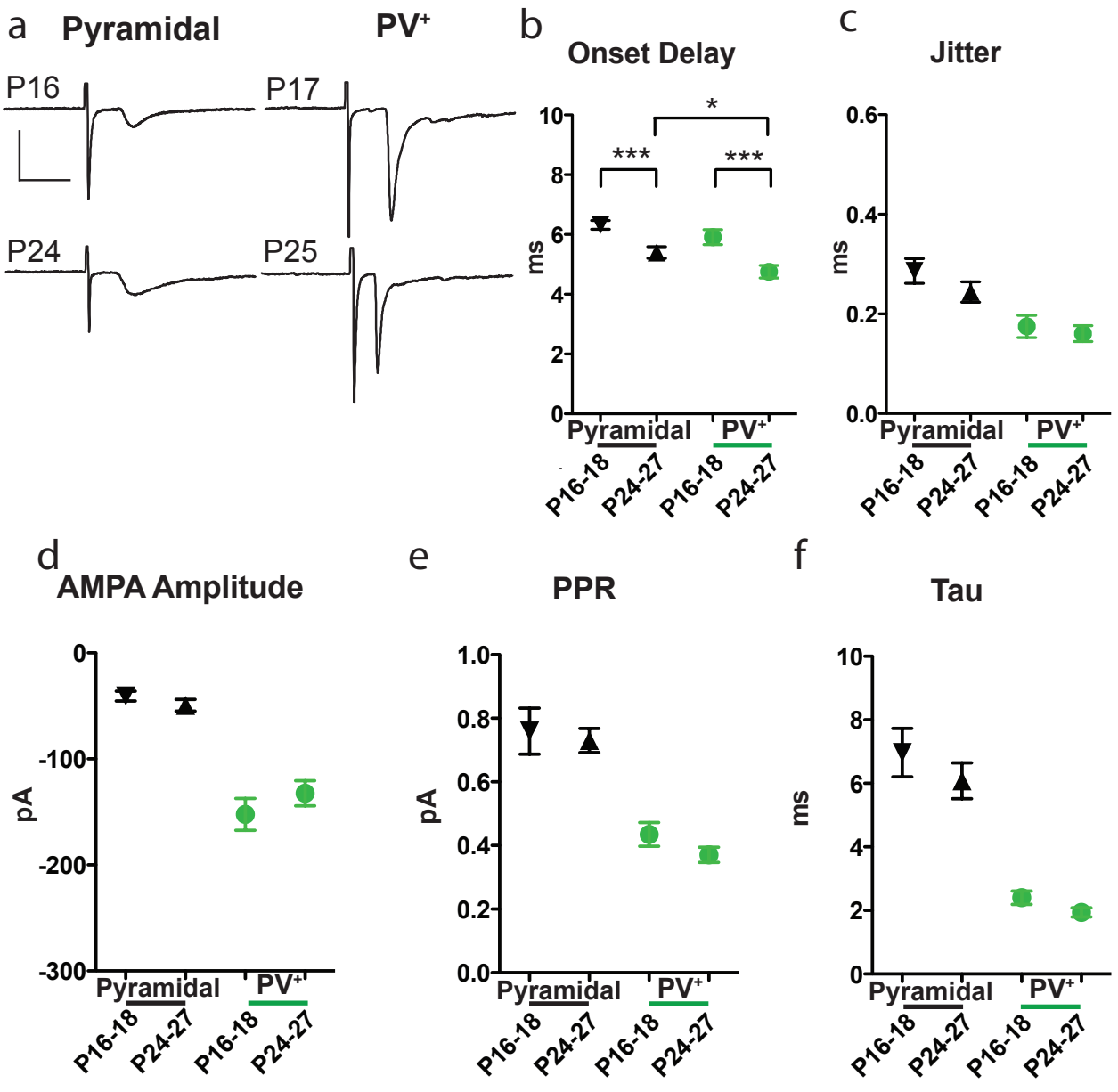

Figure 5.4 - TC Single Fiber AMPA Currents Before & During the Critical Period
(**a**) Example traces of TC AMPA currents for both cell types at a pre-critical period (P16-18) and peak critical period (P24-27) timepoint, ISI 40 ms. Scale bar 10 ms, 50 pA. (**b**) Onset Delay. (**c-f**) Quantification: 1way ANOVA indicates significance, but post-hoc test shows significance between cell types but not between ages within cell type. Values are mean ± SEM. Pyramidal: P16-18 n=22, P24-27 n:26. PV+: P16-18 n:20, P24-27 n:25. *P<0.05. ***P<0.001.

Figure 5.5

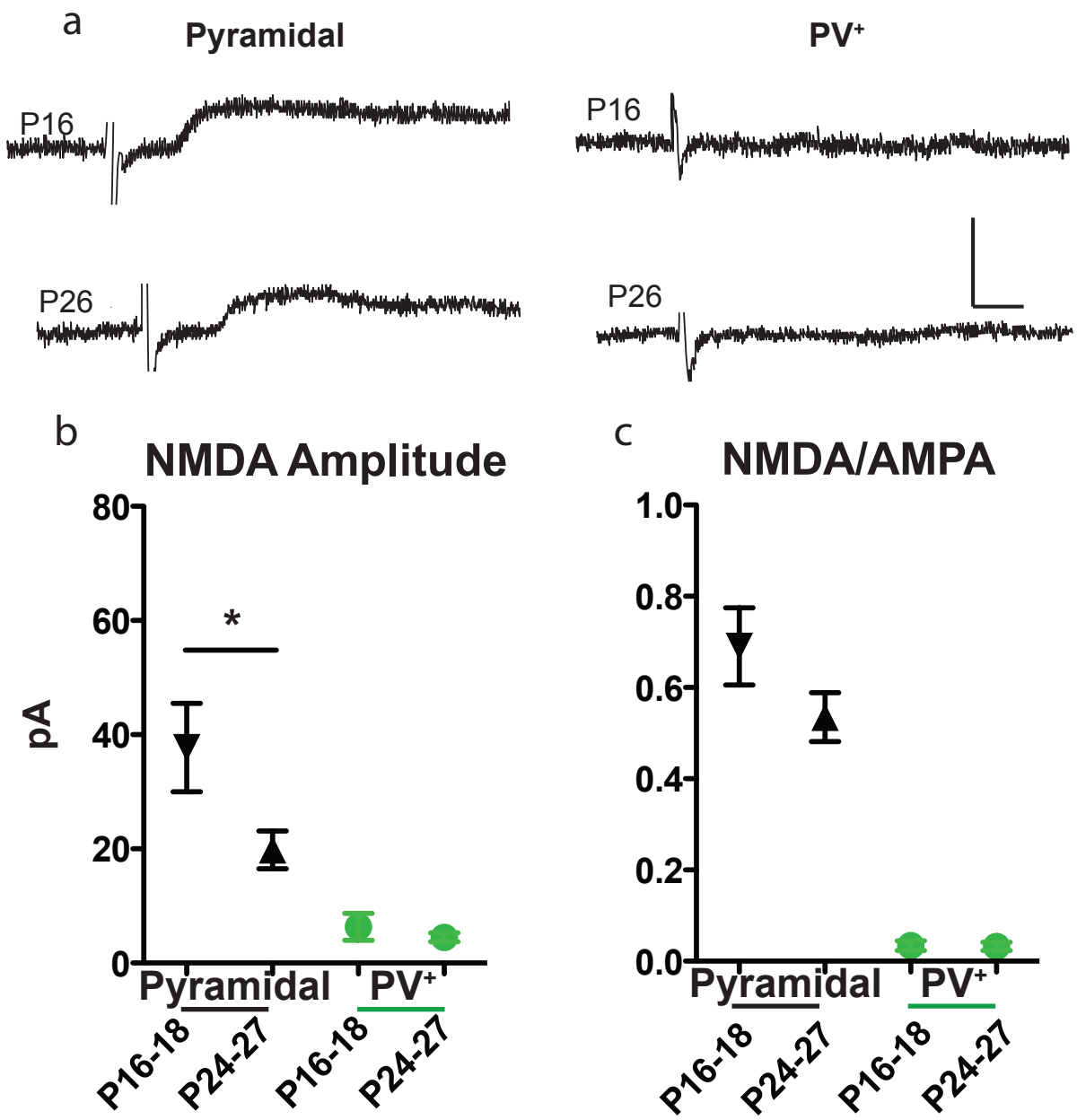

Figure 5.5 - NMDA mediated TC Synaptic Currents
(**a**) Example traces of TC NMDA currents for both cell types at a pre-critical period (P16-18) and peak critical period (P24-27) timepoint, Scale bar 5 ms, 50 pA. (**b**) Pyramidal cells but not PV+ cells display NMDA mediated single fiber TC currents in visual cortex during the pre-critical period and critical period. NMDA currents decrease in pyramidal cells during the critical period. (**c**) The ratio between the NMDA and AMPA demonstrates the dominating AMPA currents in PV+ cells. The ratio does not significantly change for either cell type with development. Values are mean ± SEM. t test. Pyr 16-18 n = 5. Pyr P24-27 n=8. PV P16-18 n=6. PV P24-27 n=6. * P<0.05

contain NMDA receptors, however in visual cortex the TC synapse is dominated by AMPA receptors.

Pyramidal cells exhibited NMDA mediated TC EPSCs (Figure 5.5 a,b). Although the single fiber NMDA component has a smaller amplitude than the AMPA mediated currents (Figure 5.5 c), the NMDA component of the TC synapse displays a maturational decrease. Like in the somatosensory cortex, the NMDA mediated currents on pyramidal cells are more prominent before the maturation of inhibition (Agmon & O'dowd 1992) however unlike somatosensory cortex, we did not see persistent NMDA receptor activation by TC afferents in PV^+ cells (Hull et al. 2009). It is possible that we missed the NMDA mediated currents and that they are present earlier in development, before our pre-critical period recording period. In the pre-frontal cortex, the elimination of NMDA EPSCs is concurrent with the rise in the calcium permeable, GluR2 lacking AMPA receptors (Wang & Gao 2010). The decay constant of the AMPA EPSCs in PV cells is already fast in the pre-critical period (Figure 5.4 f) and does not significantly change during through the critical period.

Otx2

In addition to transmitting sensory information, shaping receptive fields, and being an anatomical manifestation of ocular dominance plasticity (Antonini et al. 1999), the TC axon delivers molecular cues and transcription factors that target PV^+ cells. The homeoprotein Otx2 is not transcribed in the visual cortex; mRNA is detected within the retina, LGN and choroid plexus of the mature mouse brain. Otx2 protein is however

Figure 5.6

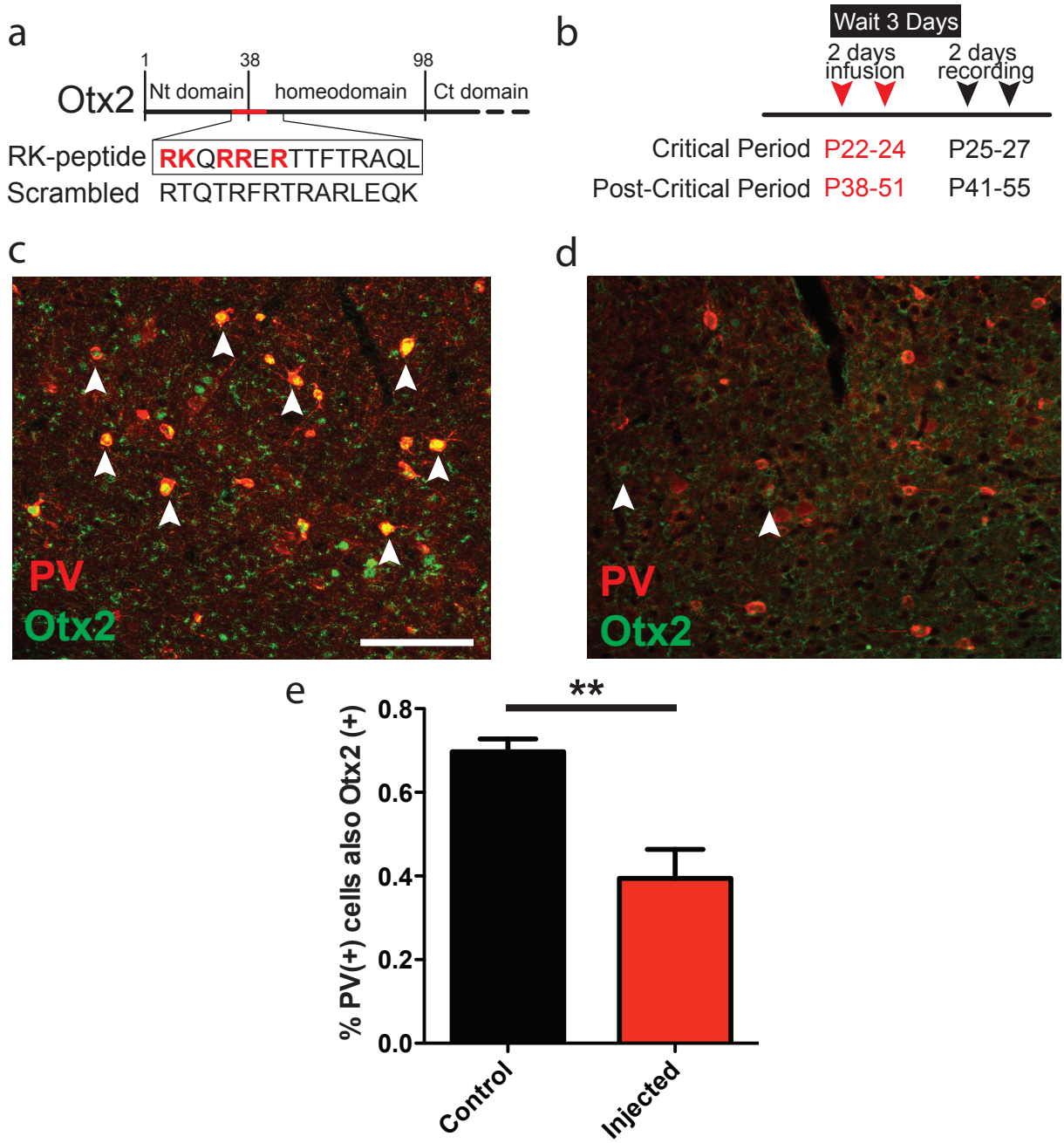

Figure 5.6 - Reduction in Otx2
(**a**) Putative GAG-binding motif (in red) in the Otx2 N-terminal region bears an argenine-lysine (RK) doublet just before the homeodomain. RK peptide and scrambled sequences are indicated. From Beurdeley et al. 2012. (**b**) Experimental timeline for both critical period and post-critical period experiments. (**c,d**) Confocal images (20x) of Otx2 and PV^{+} staining from control (**c**) and injected (**d**) hemispheres of critical period mouse. Arrowheads mark co-localization. Scale bar 100 µm. (**e**) Quantification of 6 slices from 2 animals. Values are mean ± SEM. Statistics: t test. **P<0.01

found in the visual cortex. It is preferentially transferred to the PV^+ cells just before the onset of the critical period (Sugiyama et al. 2008).

We know that Otx2 is important for maintaining the critical period and even parvalbumin expression within inhibitory neurons, but we do not know what is the role of Otx2 within the PV^+ cells. We tested the functional effects of Otx2 removal at two different periods. One during the critical period to see if Otx2 is required for the initial functional maturation of the PV+ cells and one after the closure of the critical period to see if Otx2 is required for maintaining the functional maturity (Figure 5.6 b).

We tested the effect of Otx2 on the developing and mature visual PV^+ cells by blocking Otx2 uptake with targeted injections. Otx2 contains an arginine-lysine (RK) motif that is recognized by the peri-neuronal nets that surround the PV^+ cells and is required for internalization (Beurdeley et al. 2012). By injecting a small peptide (15 amino acids) containing this motif we are able to decrease the Otx2 labeling of PV nuclei specifically near the injection (Figure 5.6). Quantifying the percent of PV^+ cells co-labeled with Otx2 antibody four days after a two-day infusion of RK peptide (Figure 5.6 b) showed a significant decrease in Otx2 positive cells in the injected hemisphere compared to the control, un-injected hemisphere (Figure 5.6 d).

We compared the intrinsic properties of PV^+ cells in visual cortex after receiving either an injection containing the RK peptide or saline alone. We found a number of changes in the membrane and firing properties suggesting that the cells had remained in, or reverted to, an immature state (Table 5.2). There were no changes in the membrane resistance, but the spike half-width and time to after-hyperpolarization peak increased and the maximal firing rate was decreased (Figure 5.7 c-j). The entire FI

Figure 5.7

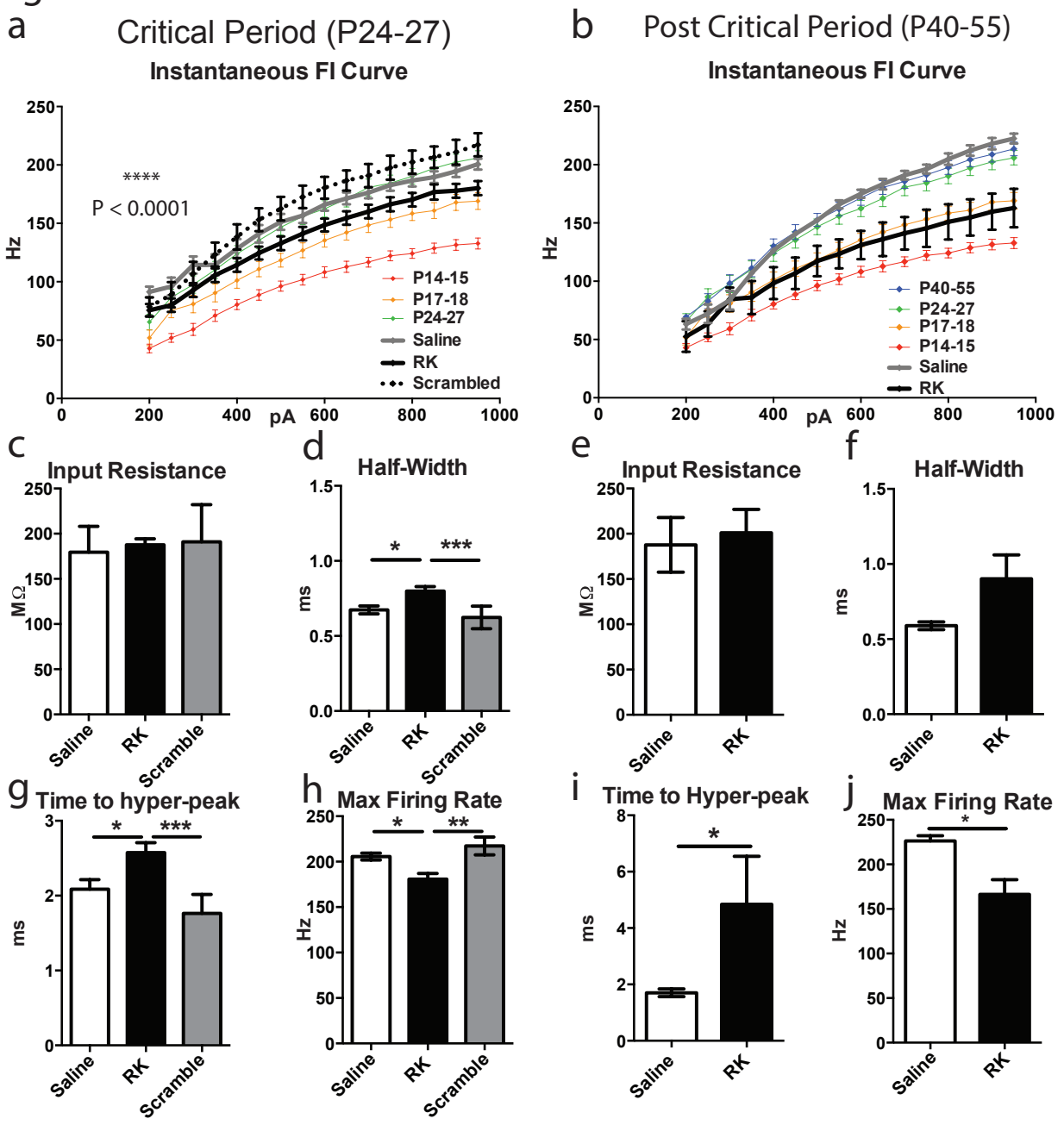

Figure 5.7 - RK Injection Alters PV+ Cell Intrinsic Firing

(**a**) FI Curve of PV⁺ development overlaid with saline, RK or scrambled curves recorded during the critical period (P24-27) with injections 3-4 days before recording. (**b**) FI Curve of PV⁺ development overlaid with saline and RK curves recorded after the critical period (P40-55) with injections 3-4 days before recording. (**c,e**) No Change in the input resistance at either age. (**d**) Half-width of action potentials after RK injections is significantly wider than either saline or scrambled peptide injections during critical period . (**f**) Trend towards wider action potential of RK injections after the critical period. (**g,i**) RK injections increases the time to reach the hyper-polarization peak at both time periods. (**h,j**) Maximal firing rates decreases after RK injections at both time periods. Values are mean ± SEM. Critical Period: saline n: 9, RK n:18, scramble n:10. Post-Critical period: saline n: 4, RK n: 7. Statistics: (a,b) two-way ANOVA (c,d,g,h) 1way ANOVA, Tukey post-hoc test, (e,f,i,j) t Test. *P<0.05 **P<0.01, ***P<0.001.

Table 5.2 - Intrinsic Membrane and Firing Properties of Saline and RK injected PV^+ Neurons During and After the Critical Period

Values are means ± SEM. **Vrest**: Membrane resting potential measured just after breaking into the cell. **Rm**: Membrane input resistance measured just after breaking into the cell. **Sag**: Difference between the negative peak voltage and the steady state voltage of a -100 pA injection. **I Thresh**: Current injection required to elicit an action potential. **V Thresh**: Voltage threshold to spike. **Spike Amp**.: Amplitude of the action potential from voltage threshold. **After-Hyperpolaization**: Amplitude of the hyperpolarization after the action potential spike measure from threshold voltage. **Time to Hyper Peak**: Time to reach after-hyperpolarization from action potential peak. **Adaptation**: Ratio of the last two interspike intervals (ISIs) divided by the first two ISIs. **Max Firing Rate**: Inverse of the shortest ISI for current injections >500pA.
Statistics: Critical period - (Rows 1-3) 1way ANOVA, Tukey post-hoc test between controls and RK; Post-Critical Period - t test *P<0.05, **P<0.01, ***P<0.001

Table 5.2 continued

	n	Vrest (mV)	Rm (MΩ)	Sag (mV)	I Thresh (pA)	V Thresh (mv)	Spike Amp. (mV)	Spike Half-width (ms)	After Hyper-polariz (mV)	Time to Hyper Peak (ms)	Adapta-tion	Max Firing Rate (Hz)
Critical Period Saline	9	-68.89 ±0.63	179.5 ±28.7	2.13 ±0.40	164.2 ±25.2	-42.85 ±1.88	73.79 ±2.30	0.673 ±0.026*	-18.64 ±0.50	2.087 ±0.126*	1.11 ±0.03	203.0 ±4.4*
Critical Period RK	18	-68.28 ±0.68	199.7 ±15.5	1.96 ±0.27	138.5 ±7.6	-42.35 ±0.77	71.76 ±2.62	0.799 ±0.030	-17.55 ±0.97	2.575 ±0.133	1.15 ±0.03	180.7 ±6.3
Critical Period Scrambled	11	-67.18 ±0.96	191.0 ±12.4	2.48 ±0.25	127.1 ±13.8	-42.92 ±1.14	79.73 ±2.01	0.623 ±0.025***	-20.06 ±1.05	1.764 ±0.085**	1.12 ±0.09	217.3 ±9.9**
Post-Critical Period Saline	4	-67.86 ±1.58	187.7 ±30.1	2.51 ±0.56	179.0 ±20.4	-40.88 ±0.50	74.28 ±3.66	0.589 ±0.026	-20.12 ±0.92*	1.703 ±0.137	1.12 ±0.09	226.2 ±6.0*
Post-Critical Period RK	7	-66.25 ±1.32	201.1 ±25.91	1.76 ±0.32	122.0 ±15.6	-46.83 ±1.88	84.34 ±3.07	1.038 ±0.191	-14.10 ±2.17*	4.841 ±1.706	1.58 ±0.24	166.4 ±16.4

curve for RK peptide injections during or after the critical period were most like the pre-critical period state (P17-18) whereas saline injections were unchanged from the age-matched curves (Figure 5.7 a,b). A two-way ANOVA comparing saline and RK injections shows significant decrease in the current-frequency relationship.

To determine if the changes we saw were specific to the blockade of Otx2 transfer and not an immune reaction, we also performed control experiments of injecting a scrambled version of the RK peptide during the critical period (Figure 5.6 a). The scrambled version had the same amino acid composition as the RK peptide and thus maintained the same charge (Beurdeley et al. 2012). However, the scrambled version lacks the RK sugar binding motif and thus did not block Otx2 transfer when tested by Beurdeley et al. 2012. We found no effect of the scrambled peptide on the intrinsic properties of PV^+ cells (Figure 5.7 a,c,d,g,h). This suggests the blockade of the functional maturation is specific to the removal of Otx2 within the PV cells. Further control experiments including testing the scrambled peptide after the critical period and anatomical verification of the specificity of RK peptide for removal of Otx2 with our protocol are underway.

Otx2 Helps Maintain Synaptic Inputs

The synaptic input onto PV^+ cells was also altered by RK peptide injection. We surveyed all of the synaptic input onto the cells by recording spontaneous miniature EPSCs (mEPSCs). Three to four days after RK peptide injection we found a decrease in the frequency of mEPSC events both during (Figure 5.8 b,c) and after the critical period (Figure 5.9 b,c). Otx2 therefore seems necessary for maintaining synaptic inputs.

Figure 5.8

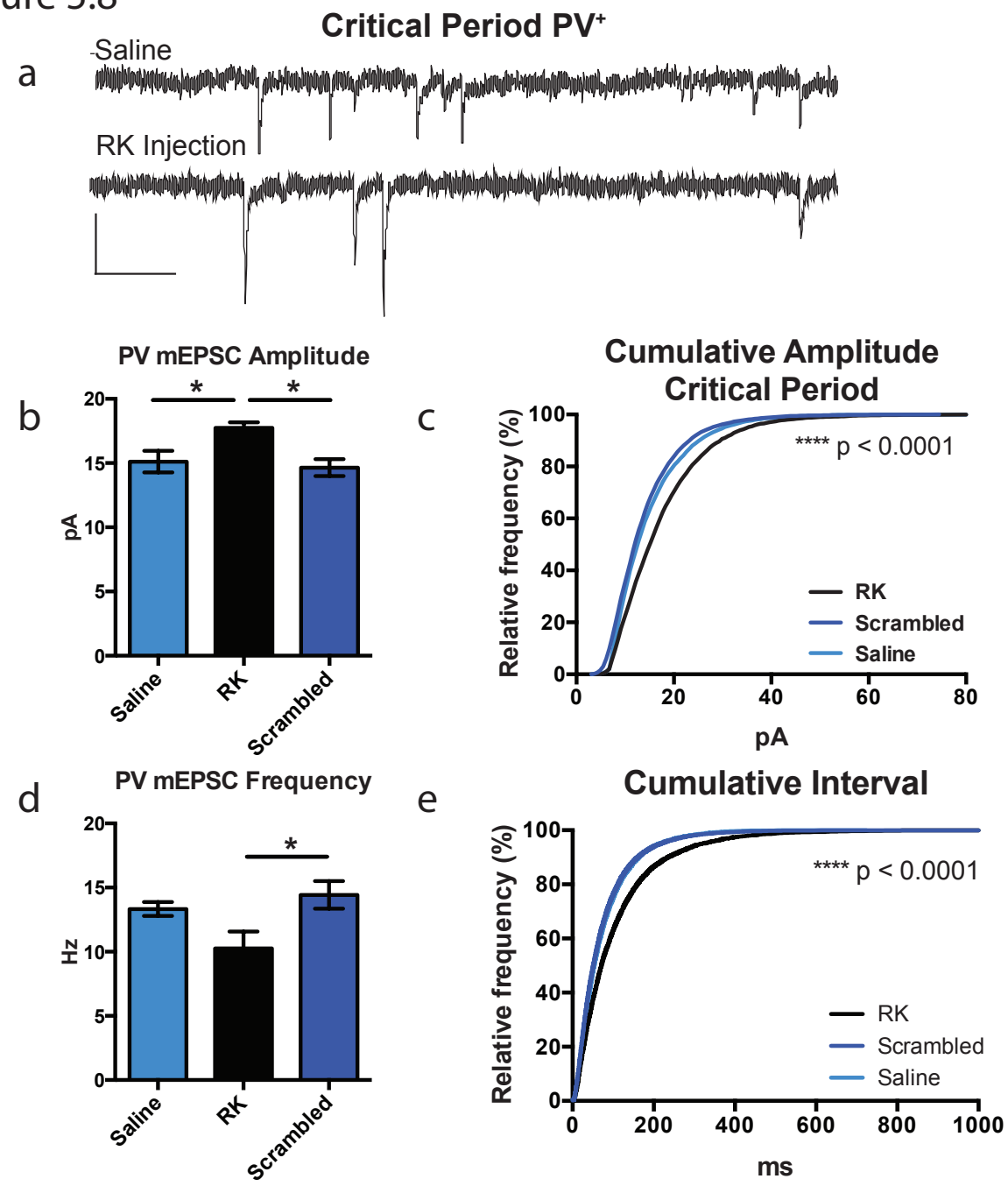

Figure - 5.8 Otx2 Maintains Synaptic inputs onto PV+ Cells during the Critical Period

(**a**) Sample PV+ cell mEPSC trace from saline injected (top) and RK peptide injected (bottom) mice during the critical period, 3 days after first injection. (**b**) Mean frequency of mEPSC events. (**c**) Cumulative inter-event interval from all events (1000-2000 events per cell). (**d**) Mean AMPA mediated mEPSC amplitude. (**e**) Cumulative amplitude from all events. Scale Bar: 20pA, 50 ms. Values are mean ± SEM. Statistics: 1way ANOVA, Tukey post-hoc test. (**b,d**) Mann-Whitney test (**c,e**) Saline n=8, RK n=6, Scrambled n=10. *P<0.05, ****P<0.0001

Figure 5.9

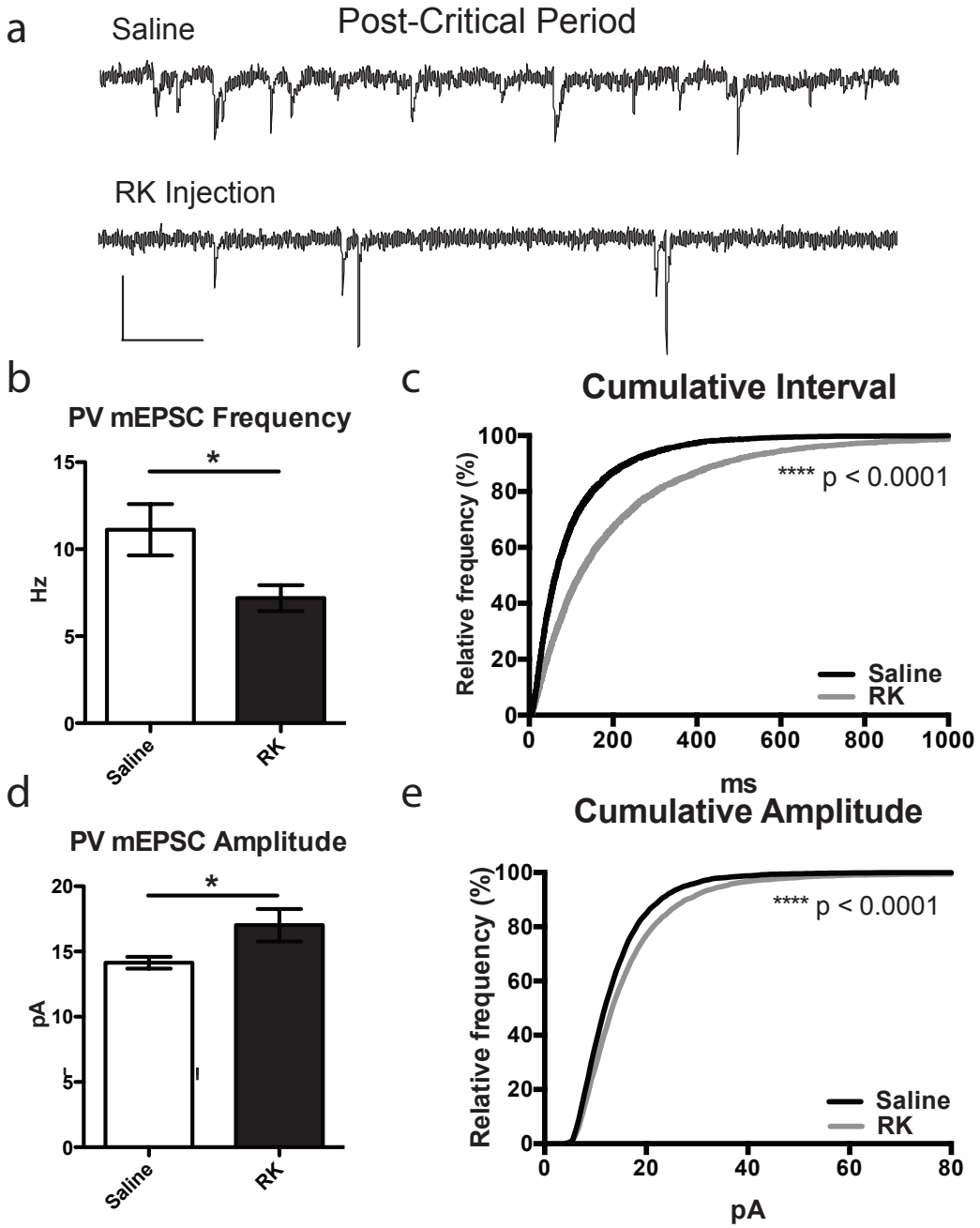

Figure - 5.9 Otx2 Maintains Synaptic inputs onto PV+ Cells after the Critical Period (P40-55)

(**a**) Sample PV+ cell mEPSC trace from saline injected (top) and RK peptide injected (bottom) mice after the critical period, 3 days after first injection. (**b**) Mean frequency of mEPSC events. (**c**) Cumulative inter-event interval from all events (1000-2000 events per cell). (**d**) Mean AMPA mediated mEPSC amplitude. (**e**) Cumulative amplitude from all events. Scale Bar: 20pA, 50 ms. Values are mean ± SEM. Statistics: t test (b,d) Mann-Whitney test (c,e) Saline n=8, RK n=6. *P<0.05, ****P<0.0001

Accompanying the decrease in mEPSC frequency, we found an increase in the amplitude of the mEPSCs (Figure 5.8 d,e & Figure 5.9 d,e). There are two plausible explanations for this increase: either homeostatic scaling mechanisms are in effect to normalize the excitatory drive onto the PV^+ cells, or Otx2 removal eventually disrupts the peri-neuronal nets that selectively surround the PV+ cells (Beurdeley et al. 2012), which would then change the dynamics of the neurotransmitter within the synaptic cleft.

As with the intrinsic properties we saw no changes in the synaptic input onto PV^+ cells after injecting a scrambled version of the RK peptide that does not contain the sugar binding motif and does not block the transfer of Otx2 to the PV^+ cells during the critical period (Figure 5.8). This suggests that the reduced synaptic input is specific to the actions of Otx2 but further experiments and testing post-critical period will also need to be done.

In some cells the change in both the intrinsic and synaptic properties was very dramatic after the critical period. In two cells we saw a marked increase in the mEPSC decay. The larger effect of RK peptide injection after the critical period evident within these cells is perhaps due to functional differences in Otx2 initial expression versus maintenance. Another possibility is the peri-neuronal nets are firmly established after the critical period (Beurdeley et al. 2012) before the RK peptide injection eventually disrupts them and dramatically changes the cell's performance.

Summary

PV^+ cells are traditionally characterized functionally as fast-spiking cells. Layer 4 PV^+ cells displayed the narrow half-width, large after-hyperpolarization and high

maximal firing rates. All of these properties showed significant maturation from just after eye opening to the critical period then plateaued. The fast membrane properties and high firing rates of the PV^+ cells is mirrored by the quick, precise and strong TC input. The TC synapse has faster kinetics and is stronger onto PV^+ cells than pyramidal cells. When combined with the fast intrinsic properties, this would allow the PV^+ cells to provide fast feed forward inhibition.

We have found that the homeoprotein Otx2 is required for both the initial maturation and maintenance of functional mature PV^+ cells. The intrinsic and synaptic maturation of PV^+ cells is maintained in part through Otx2 acquisition and expression. Disruption of Otx2 though RK peptide infusion causes a weakening of the fast spiking capabilities of the PV^+cells and a reduction in synaptic input. It will be interesting to see the effect Otx2 removal has specifically on the TC synapse. This disruption of PV^+ cell function and the concurrent reopening of plasticity underscore the importance of excitatory/inhibitory balance in maintaining cortical circuits.

Since PV^+ cells and Otx2 are both required for the initiation and closure of the critical period, this sets up a two threshold model of Otx2 levels for controlling the critical period (Figure 5.10). An initial level of Otx2 is required for functional maturation of PV^+ cells and the opening of the critical period (Sugiyama et al. 2008). Increasing levels of Otx2 maintains the functional maturation, sets up structural brakes in the form of peri-neuronal nets and limits the critical period (Beurdeley et al. 2012).

Figure 5.10

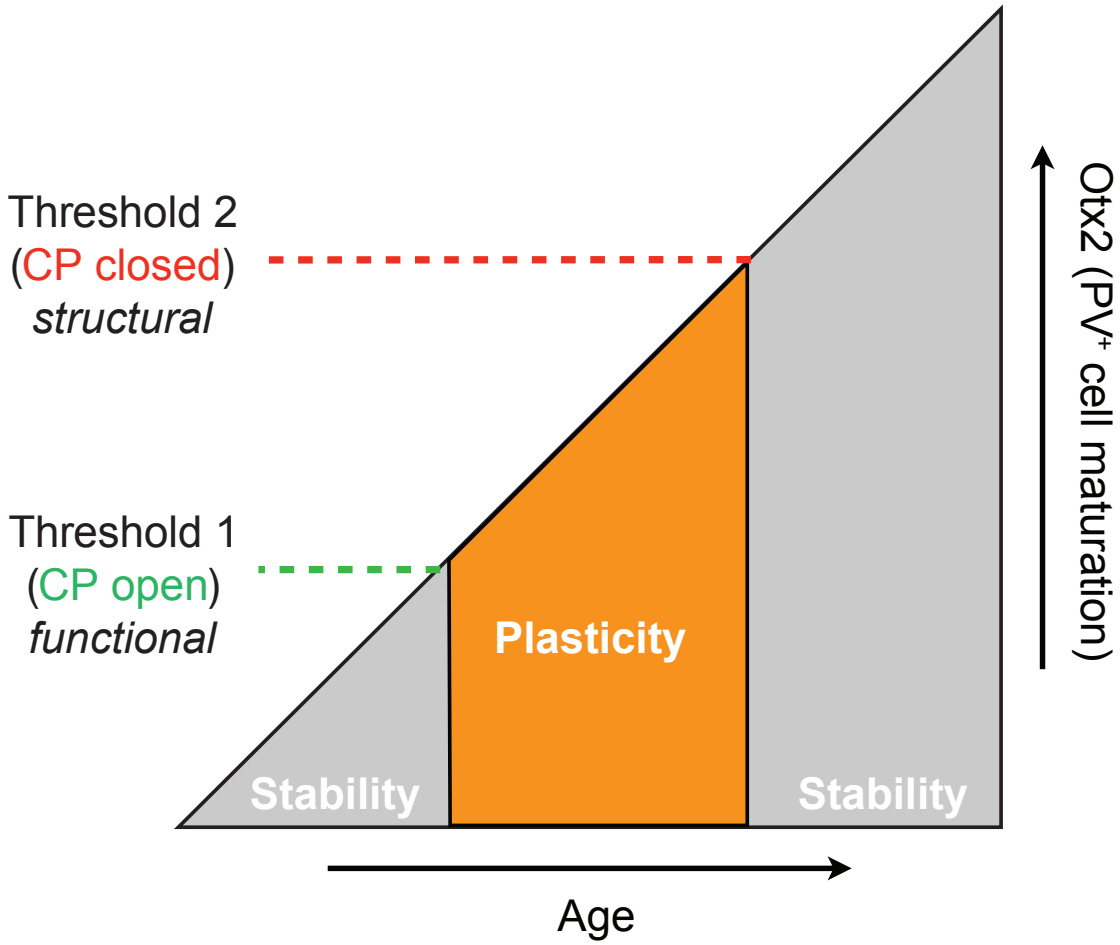

Figure 5.10 - Two Threshold Model of Otx2 Controlling the Critical Period

Chapter 6

Parvalbumin Cell-Specific Thalamocortical Plasticity in Mouse Visual Cortex

Introduction

Specific GABA circuit function is essential for the experience-dependent loss of vision by monocular deprivation (Hensch, 2005). To what extent the balance of local excitation-inhibition in cortical circuits is altered during the shift in visual responsiveness has remained elusive. Equally elusive is how this shift drives downstream plasticity. Thalamocortical (TC) fibers target both excitatory and inhibitory cells, but there is evidence that the input onto PV^+ large basket cells is stronger than that onto excitatory pyramidal cells (Gibson et al. 1999, Beierlein et al. 2003, Cruikshank et al. 2007).

Only recently has it been appreciated that the dynamics of plasticity in fast-spiking, inhibitory neurons is dramatically distinct from their neighboring pyramidal neurons *in vivo* (Gandhi et al. 2008, Yazaki-Sugiyama et al. 2009*)*. After two days of MD, response of PV^+ cells to stimulation through the deprived eye is stronger than the non-deprived eye (Yazaki-Sugiyama et al. 2009). After a longer period of MD, this paradoxical bias switches so that the deprived eye eventually becomes weaker. This two stage response profile is distinctly different from the response of the pyramidal neurons where both short and longer deprivations shifts the response to the non-deprived eye. Inhibitory cells have further been found to have distinct and enhanced plasticity after the end of the critical period when compared to excitatory cells (Kameyama et al. 2010).

The majority of these studies have been performed on layer 2/3 cells due to constraints of optical identification *in vivo*. Maffei et al. (2006) studied changes in intracortical inhibition in monocular V1 layer 4 following three days of MD. Paired recordings showed there is an increase in the inhibitory tone through strengthening of excitatory cell connections onto inhibitory interneurons and vice versa, but no change in the strength of excitatory connections onto other excitatory cells. The strengthening of inhibitory transmission occurs through a novel form of potentiation (LTPi), which was occluded by prior MD. Interestingly if the deprivation occurs before the onset of the critical period, the inhibitory connection from fast-spiking cells to pyramidal cells weakens; thus this switch may regulate the onset of the critical period (Maffei et al. 2004, Maffei et al. 2010).

As it has previously not been possible to truly isolate the functional TC synapse, there have been previous studies that have examined the TC input onto layer 4 cells through alternative methods. Quantifying the number of pre-synaptic release sites onto spines in layer 4 showed a decrease in the number of TC synapses in layer 4 after three days of deprivation, that was normalized after seven days of deprivation presumably due to homeostatic regulation (Coleman et al. 2010). Pharmacological blockade of cortical spiking showed that the sub-threshold visually evoked potentials had shifted towards the open eye after three days of MD (Khibnik et al. 2010). Recent intracellular recordings of pyramidal cells using the pharmacological blockade found a decrease in subthreshold, presumably TC synaptic currents in the monocular zone of V1, after MD (Iurilli et al. 2011).

Traditionally, TC axon rearrangement is thought to be the ultimate outcome of critical period plasticity, however anatomical rearrangement is much too slow to explain the rapid shift of ocular dominance that occurs within days of deprivation. We tested both of the primary post-synaptic cell types, pyramidal and PV^+ cells, of the TC synapse for functional precursors to the anatomical shift and to gain insight on how the response at the first cortical synapse may drive further cortical plasticity.

Results

Monocular Deprivation Decreases Mini EPSCs

We examined layer 4 cells in the binocular region contralateral to the closed eye, after short term monocular deprivation (STMD) during the critical period (3-4 days of MD P22-26, recording P25-27). We examined miniature EPSCs (mEPSCs) in control animals or after STMD in pyramidal cells (Figure 6.1) and PV^+ cells (Figure 6.2). mEPSCs report all synaptic events, both thalamocortical (TC) and intracortical. We found a 12% reduction in the mean amplitude of mEPSCs in pyramidal cells (Figure 6.1 c) and a 20% reduction in the mean amplitude of mEPSCs in PV^+ cells (Figure 6.2 c). The cumulative distribution of amplitude was also shifted towards smaller EPSCs in both cell types (Figures 6.1 d & 6.2 d).

Along with the larger change in mEPSC amplitude, the mean frequency of events was lower only in PV^+ cells (Figure 6.2 e). The cumulative frequency between events was also shifted towards longer intervals in PV^+ cells (Figure 6.2 f). Pyramidal cells displayed neither a change in mean frequency (Figure 6.1 e) or a change in cumulative frequency (Figure 6.1 f). Typically the reduction in amplitude would correlate to a post-

Figure 6.1

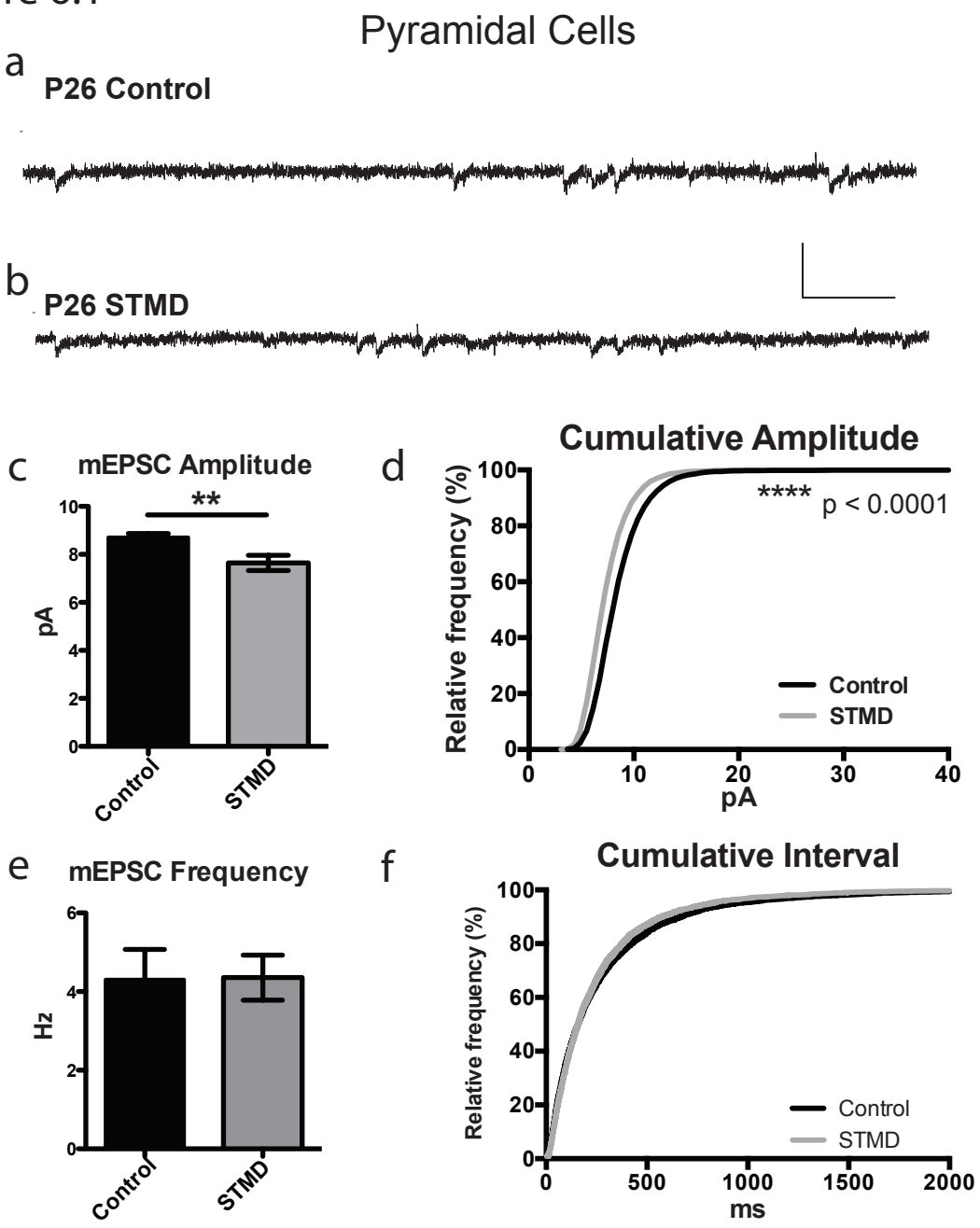

Figure 6.1 - STMD Reduces mEPSC Amplitude but not Frequency in Layer 4 Pyramidal Cells

(**a**) Sample mEPSC trace from control P26 mouse. Scale bars: 100 ms, 20 pA. (**b**) Mini trace from STMD P26 mouse after 3 days of MD. (**c**) Mean amplitude of mEPSCs in pyramidal cells. STMD significantly reduces mEPSC size. (**d**) Cumulative plot of all mEPSC amplitudes (500-1000 events per cell). (**e**) Frequency of mEPSCs in pyramidal cells. STMD has no effect on the frequency. (**f**) Cumulative plot of inter-event interval from all events. Control n=7, MD n=8. Values are mean ± SEM. Statistics: t test (c,e), Mann-Whitney test (d,f) **P<0.01, ****P<0.0001

Figure 6.2

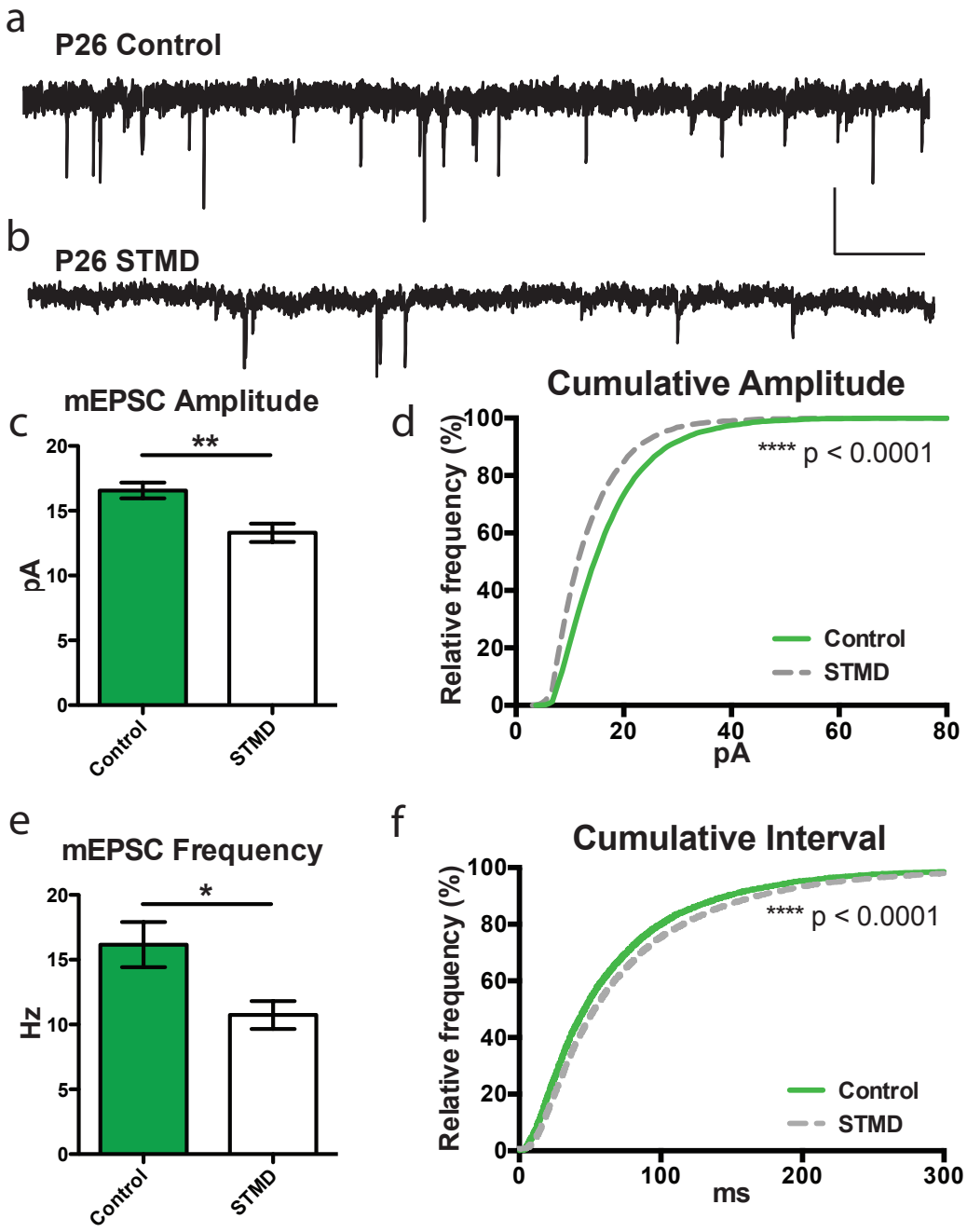

Figure 6.2 - MD Reduces mEPSC Amplitude and Frequency in PV⁺ Cells
(**a**) Mini trace from control P26 mouse. Scale bars: 100 ms, 20 pA. (**b**) Mini trace from STMD P26 mouse after 3 days of MD. (**c**) Mean amplitude of mEPSCs in PV⁺ cells. STMD significantly reduces mEPSC size. (**d**) Cumulative plot of all mEPSC amplitudes (1000-2000 events per cell). (**e**) Frequency of mEPSCs in PV⁺ cells. STMD significantly reduces frequency. (**f**) Cumulative plot of all inter-event intervals. Control n=7, MD n=9. Values are mean ± SEM. Statistics: t test (c,e), Mann-Whitney test (d,f) . *P<0.05. **P<0.01, ****P<0.0001

synaptic reduction in AMPA receptors while the reduction in frequency might indicate a reduction in pre-synaptic release sites or release probability. We next tested specific synapses to dissect the STMD changes and differences between the two cell types.

PV^+ Cell Specific TC Plasticity in Response to MD

Even though mEPSCs report all synaptic events, the strong TC synapses should be prevalent, but not exclusive, as the TC fibers target the proximal dendrites or soma of pyramidal and PV^+ cells (Bannister et al. 2002, Richardson et al. 2009, Bagnall et al. 2011). However, using our TC slicing protocol and stimulating near the ipsilateral patch of the LGN and recording in the binocular zone contralateral to the closed eye, STMD produced a shift in the TC synapse onto the PV^+ cells only.

The functional TC synapse onto pyramidal cells remained unchanged (Figure 6.3). Since mEPSCs report all of the synaptic input, the decrease in the mEPSC amplitude onto pyramidal cells is likely due to intracortical synapses and not the TC synapse. It is also possible that the small change in the mEPSC amplitude was within the error of TC synapse. In PV^+ cells, STMD caused a dramatic reduction in the TC synapse. The 45% reduction in amplitude (Figure 6.3 f) combined with a near doubling of PPR (figure 6.3 g) indicate that the plasticity onto PV^+ cells may be due in part, to pre-synaptic changes in release probability. It is possible that the plasticity of the TC synapse onto PV^+ cells is due to a combination of both pre- and post-synaptic mechanisms.

This plasticity was limited to the critical period. Performing 4 days of MD from P14-P18, before the onset of the critical period, did not produce a reduction in the

Figure 6.3

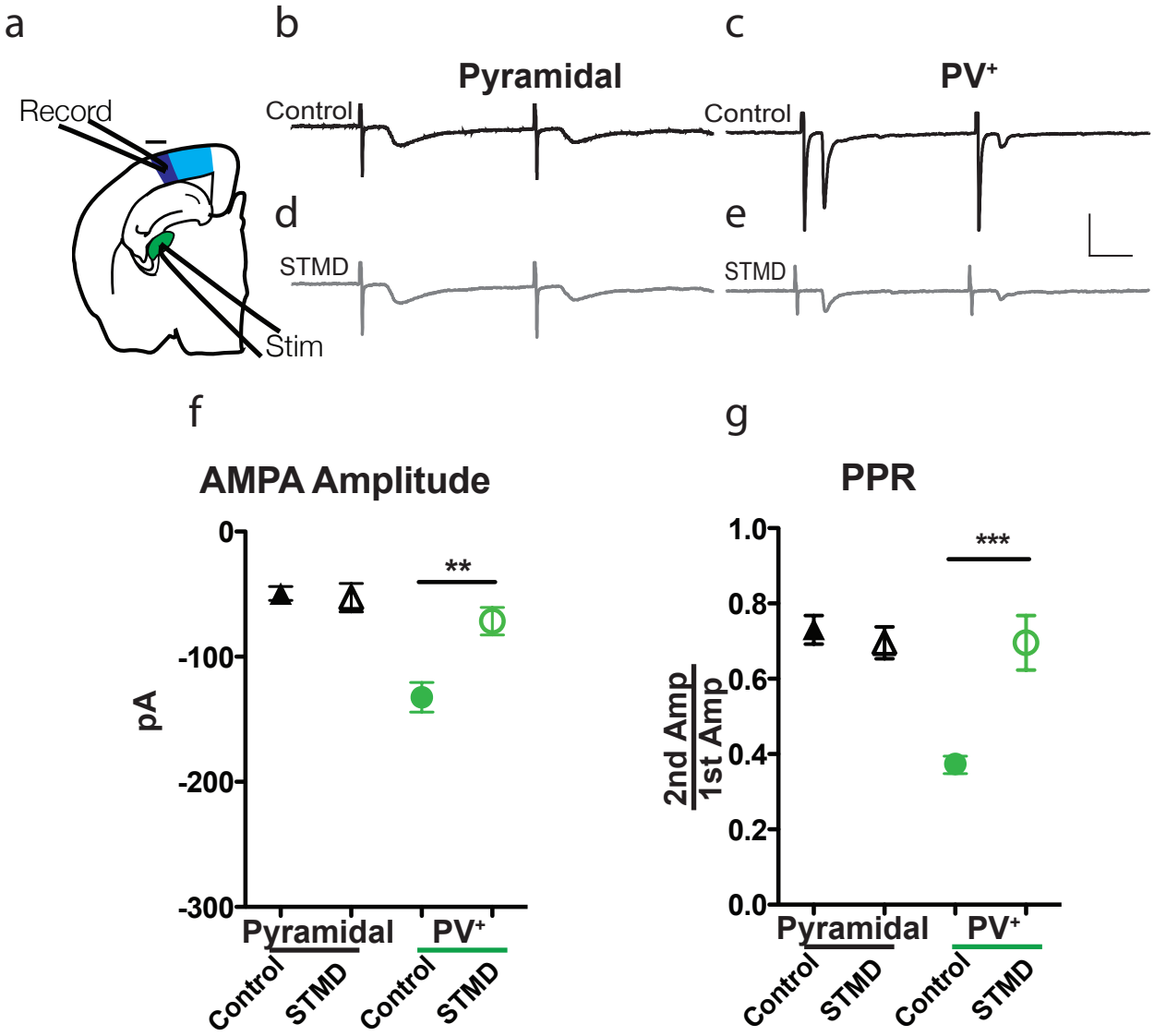

Figure 6.3 - MD Reduces TC Input Specifically onto PV⁺ Cells
(**a**) Diagram of recording and stimulus locations within the TC Slice. (**b-e**) Example traces of TC AMPA currents, ISI 40 ms. Scale bar 10 ms, 50 pA. (**b**) Pyramidal control (P25). (**c**) PV⁺ control (P26). (**d**) Pyramidal STMD (P25). (**e**) PV⁺ STMD (P26). (**f**) AMPA Amplitude. (**g**) Paired pulse ratio. Values are mean ± SEM. Statistics: 1way ANOVA, Tukey post hoc test. Pyramidal Control n = 30, Pyramidal STMD n = 12, PV⁺ Control n = 24, PV⁺ STMD n = 14. **P<0.01. ***P<0.001

Figure 6.4

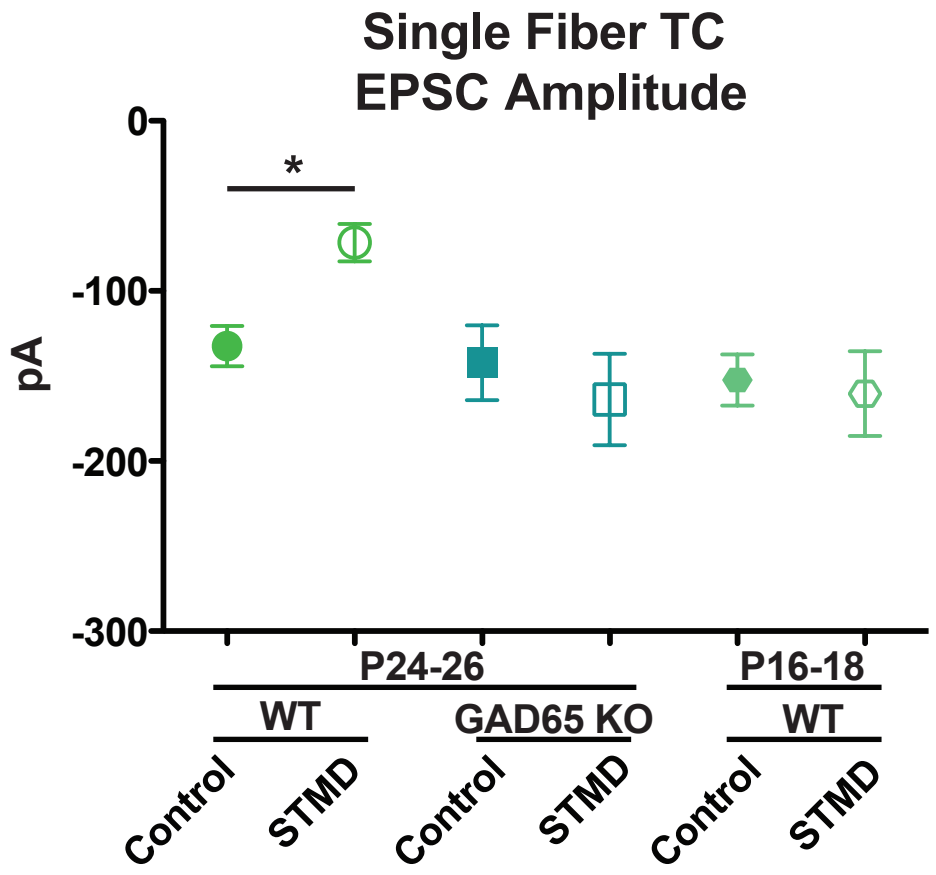

Figure 6.4 - TC Plasticity onto PV+ Cells is Consistent with *In Vivo* Ocular Dominance Plasticity
STMD shifts TC EPSCs onto PV+ cells during the critical period but not before the critical period begins nor in animals with reduced GABA signaling. Values are mean ± SEM. WT Control n = 24, WT STMD n = 14. P16-18 Control n = 22. P16-18 STMD n = 7. GAD65 KO Control n = 5. GAD65 KO STMD n = 5. Statistics: 1way ANOVA, Tukey post-hoc test. *P<0.05

strength of the TC synapse (Figure 6.4). The TC plasticity is consistent with *in* vivo results (Sugiyama et al. 2008). Similarly in animals with decreased GABA signaling, GAD65 KO mice, who do not display an *in vivo* shift in response after MD (Hensch et al. 1998), also did not display a reduction in the TC synapse onto PV^+ cells after MD (Figure 6.5).

We have discovered experience-dependent plasticity in the first cortical synapse, the TC synapse and this plasticity is evident only in PV^+ cells. The TC synaptic plasticity emerges during the critical period for ocular dominance plasticity.

Altered Intrinsic Properties of GAD65 $^{-/-}$ PV^+ Cells

We checked the intrinsic properties of PV^+ cells to see if STMD altered their membrane or firing properties. STMD did not significantly change the intrinsic properties of PV^+ cells (See Table 5.1). Additionally we checked the intrinsic properties of control P24-26 GAD65$^{-/-}$ PV^+ neurons. As neither TC synaptic plasticity nor *in vivo* ocular dominance plasticity occurs in these animals, we wondered if they were significantly altered, perhaps indicating immaturity. We found some changes in the intrinsic firing properties that are consistent with an overall decrease in GABA signaling, but not necessarily immature. The membrane voltage required to reach threshold was significantly increased and the maximal firing rate was decreased (Figure 6.5 b&d) thus the PV+ cells in the GAD65$^{-/-}$ mice will reach threshold and fire less *in vivo.* This indicates that in addition to the decreased synaptic release of GABA, specifically related to the deletion, GAD65$^{-/-}$ PV^+ interneurons display decreased firing which would further decrease the amount of GABA released.

Figure 6.5

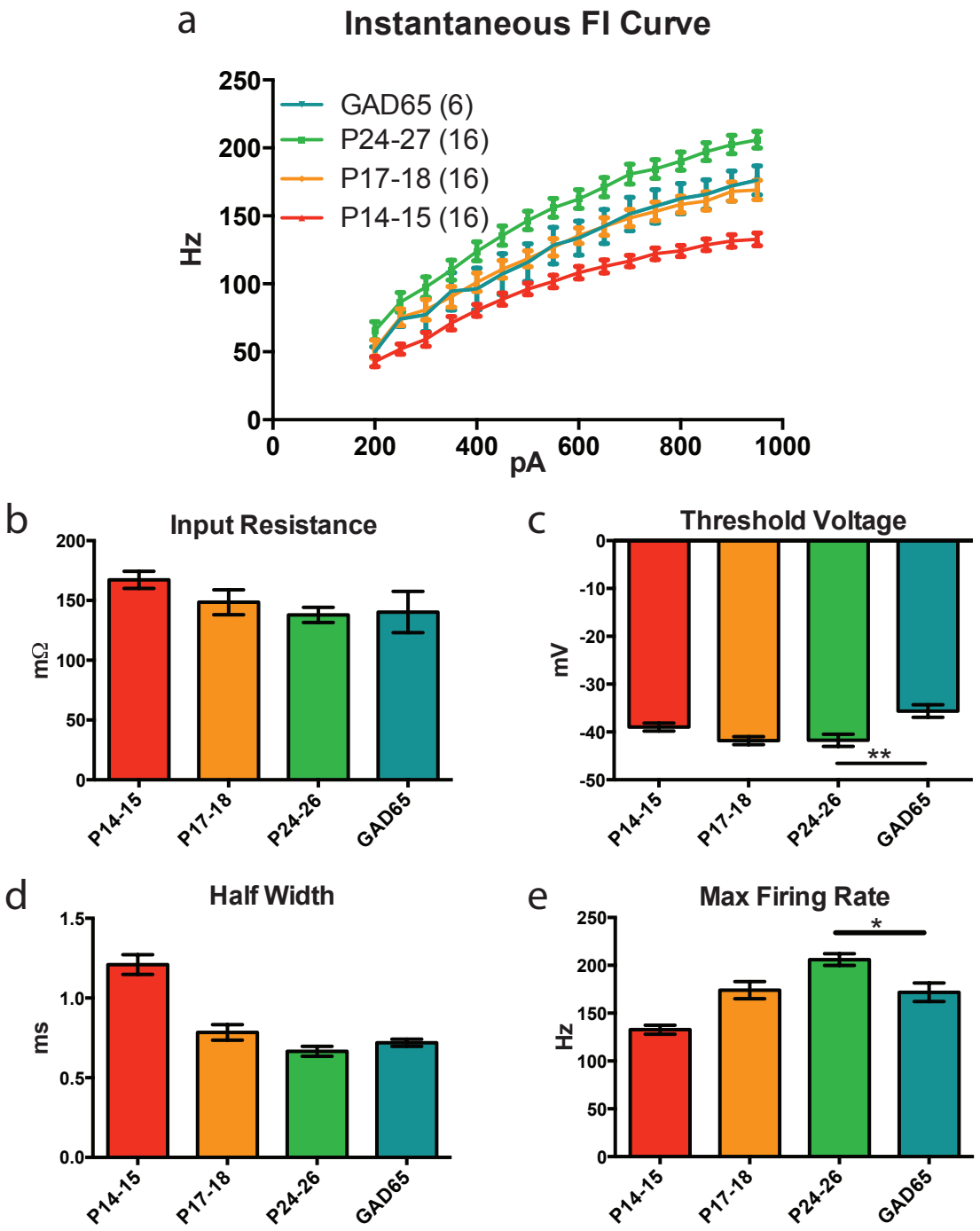

Figure 6.5 - Reduced Firing Rate of GAD 65 -/- PV+ Neurons
(**a**) The FI curve of GAD 65-/- PV+ neurons, age P24-26 (during the critical period) matches the pre-critical period curve and not the age-match curve. (**b**) No change in input resistance (**c**) Increased threshold voltage. (**d**) No significant change in action potential half-width but a significant decrease in (**e**) maximal firing rate. Values are mean ± SEM. Statistics: 1way ANOVA, Tukey Post-hoc test. *P<0.05, **P<0.01

Anatomical Evidence of TC Synapses

Previous findings by Coleman et al. (2010) report that STMD reduces the number of anatomical TC synapses onto spines, indicating pyramidal cells, though they did not specifically look at post-synaptic cell types. We found a functional reduction of the TC synapse onto PV^+ cells only and not pyramidal cells. We also examined the TC synapse from an anatomical rather than a strictly functional aspect. There are two main mammalian isoforms of the vesicular glutamate transporter expressed in the cortex. Vesicular glutamate transporters assist in the packaging of glutamate at excitatory synapses and can be used to label pre-synaptic terminals. VGluT1 is predominantly expressed by cortical neurons whereas VGluT2 is expressed by subcortical neurons and therefore VGluT2 has been used to label TC terminals in the cortex (Nakamura et al. 2007, Coleman et al. 2010). As a measure of anatomical pre-synaptic input, we quantified the number of VGluT2 labeled puncta around PV^+ soma as ~15% of TC inputs onto PV^+ cells may be somatic (Bagnall et al. 2011, Ahmed et al. 1996).

There was a significant decrease in the size but not the number of puncta surrounding PV^+ cells in layer 4 after three days of STMD in both the binocular and monocular zone, contralateral to the deprived eye (Figure 6.6 c,d). Smaller pre-synaptic terminals would be consistent with a reduction in the release probability as may contain fewer vesicles in the readily releasable pool (Murthy et al. 2001). In control animals, the number of puncta in the binocular zone was higher than in the monocular zone, consistent with an increase in TC fibers as they receive input from both eyes in the binocular zone.

Figure 6.6

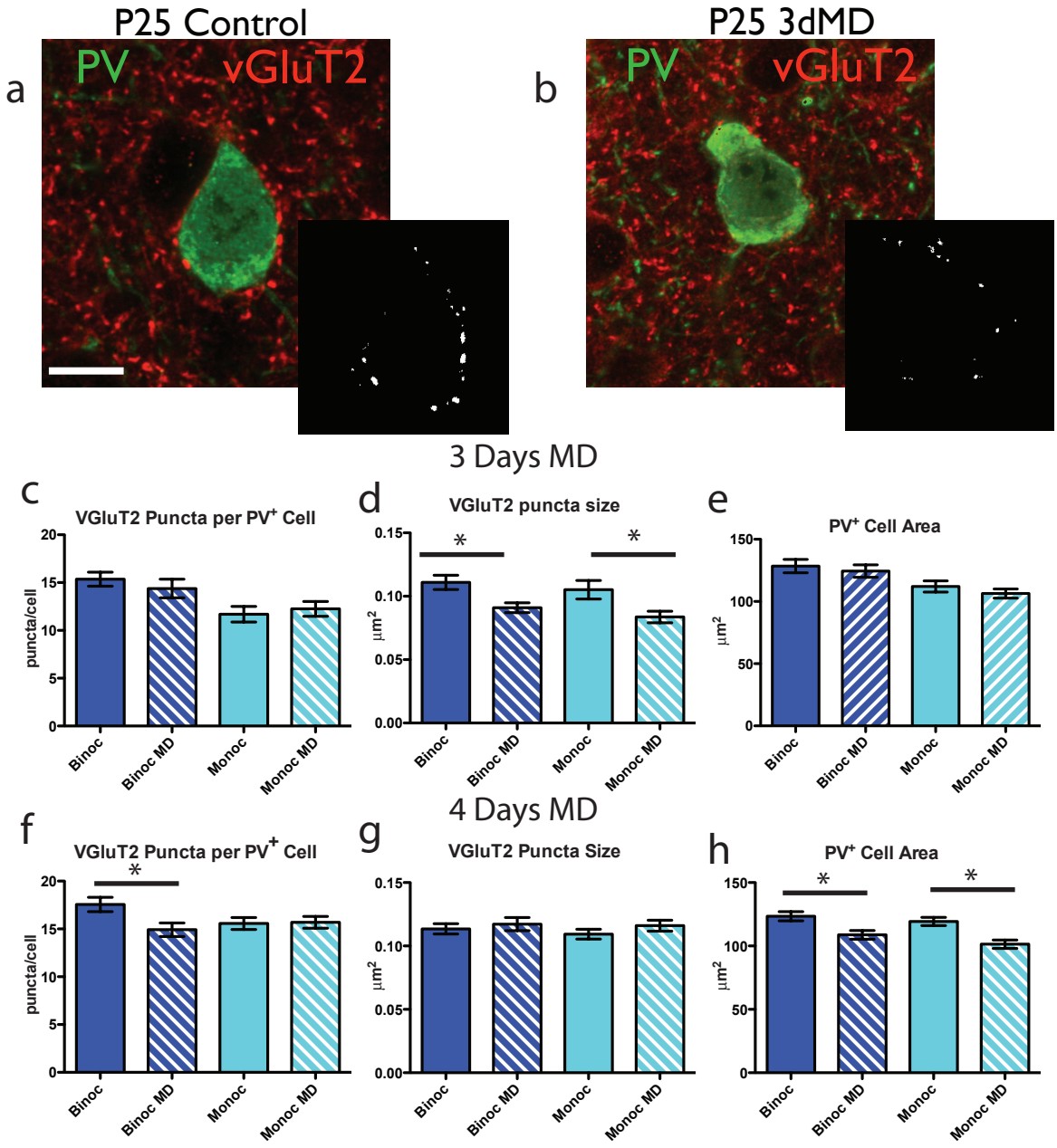

Figure 6.6 - VGluT2 Puncta on PV⁺ Cell Soma after STMD
(**a,b**) PV and VGluT2 staining of PV⁺ cells in control (**a**) and MD (**b**) animals after 3 days MD. Inset images after thresholding. Scale bar 20 µm. (**c-e**) Quantification after 3 days of MD. Number of puncta within 1 µm of the PV+ soma remains unchaged (**c**) but, (**d**) mean VGluT2 puncta size around PV cells is reduced in both binocular and monocular cortex. (**e**) PV⁺ soma area is smaller in V1m than V1b, but no change after MD. 1 way ANOVA**. (**f-h**) Quantification after 4 days of MD. (**f**) 4 days of MD reduces the number of VGluT2 puncta but the size of the puncta is unchanged (**g**). 4 days of MD reduces the size of the PV cells. Values are mean ± SEM. n=4 animals per group, 10 cells for each area per animal. Statistics: 1way ANOVA, Tukey post-hoc test to compare conditions. *P<0.05. **P<0.01. ***P<0.001

Figure 6.7

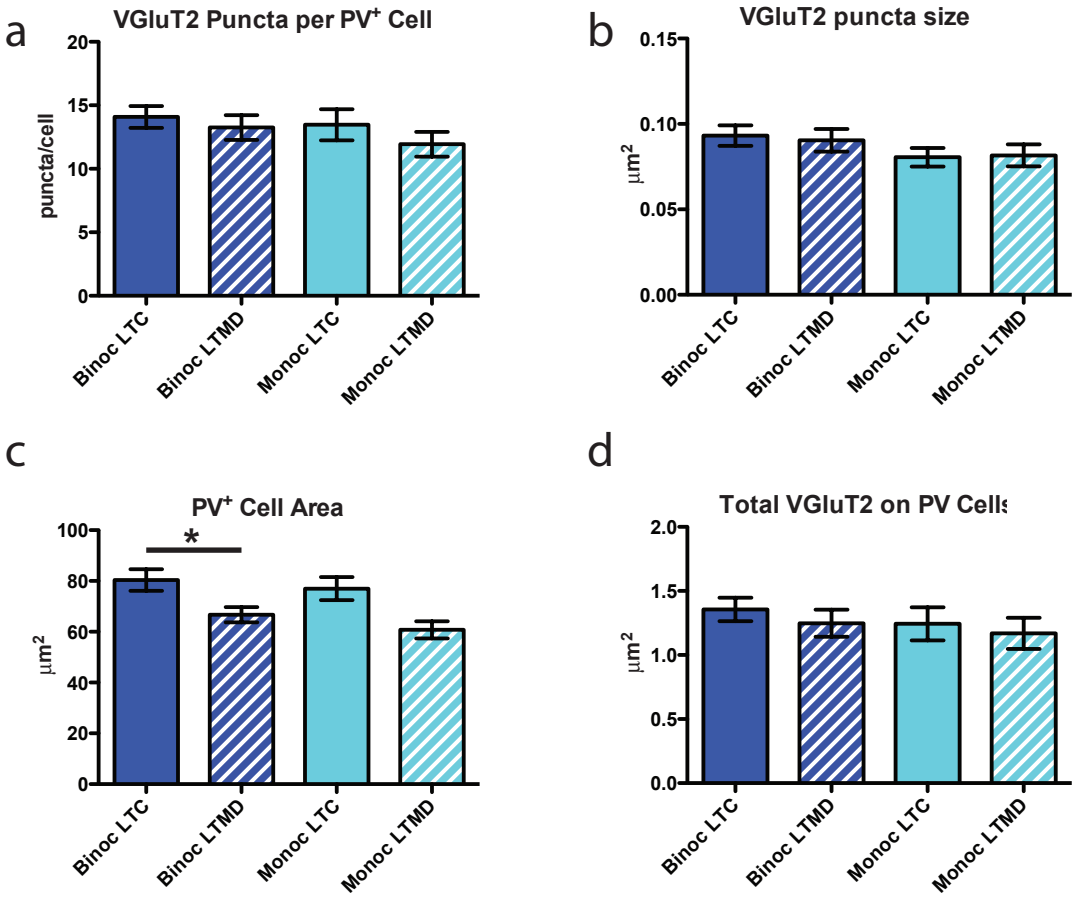

Figure 6.7 - LTMD Reduces PV+Soma Size but VGluT2 Levels have Normalized (**a**) Number of puncta within 1 µm of PV+ soma. (**b**) Mean VGluT2 puncta size around PV+ cells. (**c**) LTMD Reduces the soma size of PV+ neurons *** (**d**) The total amount of VGluT2 area above threshold within 1 µm of the PV+ soma. LTC: Long-term control. Values are mean ± SEM. n=4 animals per group, 10 cells for each area per animal. Statistics: 1way ANOVA, Tukey post-hoc test. *P<0.05, ***P<0.001

One additional day of MD reduced the number of VGluT2 puncta in the binocular zone specifically (Figure 6.6 f) suggesting a competitive mechanism for synapse elimination of weakened synapses. The vGluT2 puncta remaining on PV+ cells in the binocular zone of the deprived animals were the same size as the control cells (Figure 6.6 g), perhaps because the shrunken puncta from the depressed TC fibers had been eliminated. The additional day of deprivation caused a reduction in the size of the PV^+ cell soma (Figure 6.6 h) perhaps due to a reduction in transfer of a homeoprotein Otx2 to PV^+ cells. The non-cell-autonomous expression of Otx2 is necessary for maintaining mature firing properties in the PV cells (See Chapter 5) and may be delivered by thalamocortical axons (Sugiyama et al. 2008).

Extended periods, more than 2 weeks, of monocular deprivation causes large scale reductions in the arborization and length of the TC fibers from the deprived eye (Antonini et al. 1999). However PV^+ cells remain responsive to the deprived eye *in vivo* as assayed by c-Fos expression (Mainardi et al. 2009). Quantification of VGluT2 puncta after 21 days of MD (LTMD) showed a normalization in the number and size of VGluT2 puncta around the PV^+ soma. However the PV^+ soma size remained reduced again possibly due to a reduction in Otx2 expression.

Summary

We found a strikingly distinct plasticity in the functional TC synapse onto pyramidal and PV^+ cells. While both PV^+ and pyramidal cells displayed a decrease in mEPSCs, PV^+ cells exhibited a 45% amplitude reduction of single fiber thalamocortical stimulation while input onto pyramidal cells remained unchanged. The experience-

dependent plasticity of input onto PV+ cells was accompanied by a near doubling of the paired-pulse ratio (PPR; 0.37 ± 0.02 vs 0.70 ± 0.07), suggesting a presynaptic change in probability of release. The plasticity onto PV^+ cells is constrained to the critical period. Deprivations prior to critical period onset (<P18) or in GAD65 knockout mice (Hensch et al. 1998), neither produce a shift of visual responsiveness in vivo, nor caused a change in EPSC amplitude or PPR in PV+ cells. Anatomical quantification of TC synapses around PV^+ cells agreed with the reduction in TC innervation.

Chapter 7

Discussion

Parvalbumin Positive Interneurons

Since Eccles' seminal work (1964), it has been accepted that there are two different classes of neuron in the brain: excitatory and inhibitory neurons. It has increasingly become appreciated that inhibitory interneurons are specialized not only by anatomical or physiological classification (Petilla Interneuron Nomenclature Group 2008) but also by their different functions in circuit processing and plasticity. Different types of interneurons have distinct receptive field properties (Hirsch et al. 2003), shaping either the receptive field or controlling the output of target cells (Bagnall et al. 2011) and respond to experience-dependent plasticity differently (Mainardi et al. 2011). We set out to characterize one class of interneuron, the fast-spiking parvalbumin positive (PV^+) large basket cells in layer 4 of mouse visual cortex by asking: How do they get there? How do they develop functionally? Who talks to them? And, how do they respond to altered experience?

We found that interactions between layer 5 pyramidal cells and migrating immature inhibitory cells is required for correct laminar placement of PV^+ cells and subsequent circuit function (Chapter 3). PV^+ cells undergo a dramatic postnatal, sensory development to become fast-spiking cells able to quickly follow sensory input (Chapter 5). We found strong thalamocortical (TC) connections onto PV^+ cells that undergo experience-dependent changes after monocular deprivation (Chapters 5 & 6). Since previous work has detailed the importance of GABA signaling and PV^+ cells in the

initiation of critical periods (Hensch 2005), the specific plasticity onto the PV^+ cells is particularly intriguing.

Critical Periods

Critical periods are brief windows in development when experience can permanently alter behavior, performance and/or neuronal circuits. In insects, worms and other animals with simpler neuroanatomy the neuro-circuitry is almost entirely genetically determined. In the model organism *C. elegans* all of the neurons and most of the synapses are stereotyped and pre-programmed (White et al. 1986, Riddle et al. 1997). The evolution of critical periods allows for post-natal modification of neuronal circuits in response to experience and the environment to fine tune and optimize neuronal processing.

Limiting critical periods to just certain periods allows for a stabilization of the neuronal circuits optimized early in life. This provides greater adaptability early with stable, efficient neural circuitry in adulthood (Bavelier et al. 2010). Additionally, plasticity is a cause of pathology as much as it is the mechanism for development and learning (Pascual-Leone et al. 2005). The stable excitatory/inhibitory balance present after the close of the critical period is consistent with a healthy adult brain. The excitatory/ inhibitory inbalance present in autism and schizophrenia may be a result of failure to close critical periods (Rubenstein & Merzenich 2003, Morishita & Hensch 2008, LeBlanc & Fagiolini 2011)

Although critical periods and ocular dominance plasticity have been studied for nearly 50 years now (Hubel & Wiesel 1965), many of the specifics remain unclear. We

cannot say what specific role inhibition plays, nor which specific synaptic plasticity events drive the large and long-term anatomic rearrangements. We know a threshold level of inhibition is required (Hensch et al. 1998), as well as signaling through particular $GABA_A$ receptors (Fagiolini et al. 2004), to begin the plasticity process. We have indications that GABA signaling, through the PV^+ cell specific maintenance of Otx2 (Beurdeley et al. 2012), along with other molecular brakes, eventually limits the critical period.

Inhibitory neurons which shape and modify the cortical output may be ideally placed within the neural circuitry to control plasticity. PV^+ cells contact hundreds of cells. In experiments by Packer and Yuste (2011) some PV^+ cells contacted every local pyramidal cell tested. Thus having inhibitory PV^+ cells control plasticity would be a convenient method for shaping the response in much of the cortex. The critical period initiation coincides with maturation of PV^+ cell intrinsic properties and TC input.

Surveying all synaptic input onto layer 4 cells, we found that short-term monocular deprivation (STMD) decreased the amplitude of miniature excitatory post-synaptic currents (mEPSCs) onto pyramidal and PV^+ cells. Yet, the experience-dependent change in mEPSC amplitude was larger on PV^+ cells and accompanied by a reduction in event frequency only there. While both pyramidal and PV^+ cells are targeted by TC fibers, we saw a PV^+ specific decrease in TC synaptic strength. Given only the modest decrease we saw in mEPSC amplitude onto pyramidal cells, the TC synapse may also be plastic but significantly weaker and within the noise. It could also be possible that after STMD entire fibers were eliminated, although we saw no change in stimulating strength required to activate a single fiber (Data not shown). Previous *in*

vivo and anatomical tests of TC synapses never examined PV^+ cells as a target (Coleman et al. 2010, Khibnik et al. 2010, Iurilli et al. 2011). Thus, their dramatic plasticity onto PV^+ cells has not been appreciated before this.

PV^+ cells of mouse primary visual cortex are more binocular than pyramidal cells (Yazaki-Sugiyama 2009, Kameyama et al. 2010). They respond equally well to stimulation of each eye, while pyramidal cells are biased towards the contralateral eye. Likewise, large-basket PV+ cells are not tuned for stimulus orientation (Sohya et al 2007, Liu et al. 2007, Kerlin et al 2010, Runyan et al. 2010). These broad receptive field properties may be of computational importance, as the microcircuit architecture for PV+ interneurons, and probably neocortical inhibition in general, is an unspecific, densely homogenous matrix covering all nearby pyramidal cells (Packer & Yuste 2011).

Surprisingly, results *in vivo* have shown that STMD initially shifts the response paradoxically toward the closed eye in fast-spiking (PV^+) cells (Yazaki-Sugiyama 2009). This unexpected bias is reversed with longer deprivations, making the inhibitory cells eventually more responsive to the open eye. Our finding of PV^+ cell-specific plasticity is consistent with this finding. STMD weakens the TC synapse onto PV^+ cells. It is highly likely that fibers from the open, ipsilateral eye are mediating this depression, as we targeted the stimulating electrode to the ipsilateral patch within the LGN. This result will require further confirmation by optogenetic tagging of just the open eye input (see below).

Weakening the TC synapse from the open, ipsilateral eye while leaving the synapse from the deprived, contralateral fibers intact could shift the response of PV^+ cells in favor of the deprived eye. This in turn may help to drive downstream plasticity in

the circuit. A reduction in feed-forward inhibition by the open eye (ie. TC weakening onto PV^+ cells) combined with a decrease in the sensory driven feed-forward excitation from the deprived, contralateral eye would help to weaken the cortical pyramidal cell response of the closed contralateral eye. As pyramidal cells are normally biased toward the contralateral eye, perhaps an increase of synaptic input from the open, ipsilateral eye, is needed to drive competition, which may be required for the subsequent weakening and pruning of intracortical synaptic connections serving the deprived eye (Heynen et al. 2003, Mataga et al. 2004, Crozier et al. 2007).

For years, great efforts have been made to correlate synaptic plasticity *in vitro* with the shift in responsiveness *in vivo* toward the non-deprived eye after MD. Different forms of long-term synaptic plasticity can be induced in pyramidal cells *in vitro* across several layers of visual cortex, but not all forms seem to be required for ocular dominance plasticity (Daw el al., 2004). Indeed, several mechanisms for long-term potentiation (LTP) or long-term depression (LTD) can be doubly dissociated from plasticity *in vivo* (Hensch 2005). For example, conditional enhancement of calcineurin impairs ocular dominance plasticity but not LTD induced by low-frequency stimulation (Yang et al. 2005). Conversely, mGluR2 deletion disrupts LTD in layer 2/3 while ocular dominance plasticity remains intact (Renger et al., 2002).

It seems counterintuitive that the non-deprived fibers from the open, ipsilateral eye onto PV+ cells would become depressed after STMD, but there are unique forms of spike-timing depending plasticity in inhibitory neurons that could accomplish this. In the somatosensory cortex, Lu et al. (2007) found correlated presynaptic release and post-synaptic firing of FS (PV^+) cells induces LTD at intracortical synapses. It does not matter

whether the pre-synaptic release occurs before or after spiking of the FS cell; so long as the two events are temporally close, the synapse is depressed. This LTD is mediated by metabotropic glutamate receptors (mGluRs).

An STDP mechanism, similar to the one found in somatosensory cortex could produce LTD at TC synapses in layer 4, PV^+ cells. Monocular deprivation desynchronizes the activity between the two eyes. Sensory experience would drive the open eye fibers, while modest spontaneous activity would weakly and sporadically drive deprived eye fibers. STDP weakens active connections more than inactive ones and would initially produce a greater depression of the open eye input. Yazaki-Sugiyama et al. (2009) modeled the plasticity onto PV^+ cells using a similar rule. They found that the STDP rule above would explain the relative initial depression of open eye fibers, while subsequent homeostatic mechanisms to gradually increase the overall firing rate to re-scale all synapses would eventually yield the more conventional preferred response to the open eye over the deprived eye. Both the *in vivo* results and our mEPSC recordings in PV^+ cells report a decrease in spontaneous activity after STMD. Thus, in future studies it would be exciting to explore both STDP rules at the TC to PV^+ cell synapse and homeostatic scaling mechanisms within PV^+ cells during longer monocular deprivations to support this two-stage model.

With the advances in optogenetics and transneuronal labeling (Han & Boyden 2007, Callaway 2008, Kuhlman & Huang 2008, Hasenstaub & Callaway 2010, Deisseroth 2011), it may soon be possible to, optogenetically or otherwise, isolate the fibers coming from each eye. Combining selective stimulation of eye-specific fibers with the optimized TC slice to insure preservation of many TC connections, we could assess

the experience-dependent plasticity of TC fibers from the open or deprived eye definitively. Alternating stimulation of single fibers would also answer questions about the binocularity of TC input onto layer 4 cells. In higher mammals, ocular dominance maps suggest that layer 4 cells receive input from a single eye (Hubel et al. 1977). In the mouse, *in vivo* responses show layer 4 cells are binocularly driven (Gordon & Stryker, 1996, Yazaki-Sugiyama et al. 2009), but the relative contribution of the intracortical versus thalamocortical inputs remains unclear.

It would also be informative to see if the experience-dependent TC plasticity is truly constrained to the critical period. Testing this synapse for plasticity after the closure of the critical period by performing STMD after P35 (Espinosa & Stryker 2012) may be technically difficult, if not impossible, due to the decreased viability of *ex vivo* brain slices with age. However, by prematurely opening then closing the critical period with early diazepam injections (Fagiolini et al. 2004) it may be possible to limit plasticity at an amenable age then to check the TC synaptic plasticity.

If experience-dependent plasticity is constrained, there must be a mechanism that first allows for plasticity in the PV^+ cells as they mature, then the same or a different mechanism to limit plasticity a short period later. The transcription factor Otx2 is one obvious candidate. The time-course of expression of Otx2 within PV^+ cells creates a model where a low threshold of Otx2 internalization is reached for the initiation of plasticity, then a higher threshold of Otx2 expression in the PV^+ cells limits plasticity (Beurdeley et al 2012). We have shown that continued translocation of Otx2 is required for the maturation and maintenance of the high firing rates and mEPSCs in PV^+ cells (Chapter 5).

Furthermore as a transcription factor with multiple genetic targets, Otx2 may be capable of modulating the expression of LTP/LTD related molecules within the PV^+ cells (eg TrkB; Aicardi er al. 2004; Jiang et al. 2003; Sermasi et al. 2000; Cellerino et al. 1996). Even if the TC plasticity is not constrained to the critical period, Otx2 may be acting to limit ocular dominance plasticity through other mechanisms specific to the PV^+ cells. Just as we found that Otx2 changes the synaptic input onto PV^+ cells, it would be useful to check how Otx2 affects the synaptic output of PV^+ cells, either through paired-cell recordings or miniature inhibitory post-synaptic currents (mIPSCs) in neighboring pyramidal cells. There may also be interactions between Otx2 and other critical period brakes (Bavelier et al 2010), such as Lynx1 or the Nogo receptor. It is possible that this one transcription factor controls both the onset and closure of the critical period.

Recently it has been shown that monocular deprivation after the end of the critical period produces a potentiation of response of cortical neurons toward the open eye, although the magnitude is weaker and time-course is longer than for critical period plasticity (Sawtell et al. 2003, Fischer et al. 2007, reviewed by Hofer et al. 2006, Morishita & Hensch 2008). Inhibitory neurons play an important role in adult plasticity as well as critical period plasticity. Post-critical period monocular deprivations may induce a shift in the distribution of inhibitory synapses on dendritic spines (Chen et al. 2012). It remains to be seen if post-critical period plasticity also changes the input onto inhibitory cells or just their output.

Here, we have shown that PV^+ cell development and maturation is required for proper cortical circuit function and plasticity. We have identified a possible first site of synaptic plasticity that drives ocular dominance plasticity. We have also established a

system for examining the TC synapse in the mouse visual system. This preparation may also be useful for examining disease models. For example we revealed an unexpected PV^+ cell hyper-connectivity in the visual cortex of the Mecp2 mutant mice (Chapter 3), which corresponds with their loss of spontaneous activity and acuity *in vivo* (Durand et al. 2012). Testing the TC synapse in these animals and perhaps adjusting their Otx2 delivery using RK peptides as we show in Chapter 5, could decrease the activity of the PV^+ cell network specifically, and may rescue the visual phenotype. Thus the present foundational work opens many novel directions for future research.

References

Agmon, A., and Connors, B.W. (1991). Thalamocortical responses of mouse somatosensory (barrel) cortex in vitro. Neuroscience 41, 365-379.

Agmon, A., and O'Dowd, D.K. (1992). NMDA receptor-mediated currents are prominent in the thalamocortical synaptic response before maturation of inhibition. Journal of neurophysiology 68, 345-349.

Ahmed, B., Anderson, J.C., Martin, K.A.C., and Nelson, J.C. (1997). Map of the synapses onto layer 4 basket cells of the primary visual cortex of the cat. The Journal of comparative neurology 380, 230-242.

Aicardi, G., Argilli, E., Cappello, S., Santi, S., Riccio, M., Thoenen, H., and Canossa, M. (2004). Induction of long-term potentiation and depression is reflected by corresponding changes in secretion of endogenous brain-derived neurotrophic factor. Proceedings of the National Academy of Sciences of the United States of America 101, 15788-15792.

Antonini, A., Fagiolini, M., and Stryker, M.P. (1999). Anatomical correlates of functional plasticity in mouse visual cortex. The Journal of neuroscience : the official journal of the Society for Neuroscience 19, 4388-4406.

Asada, H., Kawamura, Y., Maruyama, K., Kume, H., Ding, R., Ji, F.Y., Kanbara, N., Kuzume, H., Sanbo, M., Yagi, T., et al. (1996). Mice lacking the 65 kDa isoform of glutamic acid decarboxylase (GAD65) maintain normal levels of GAD67 and GABA in their brains but are susceptible to seizures. Biochem Biophys Res Commun 229, 891-895.

Atallah, B.V., Bruns, W., Carandini, M., and Scanziani, M. (2012). Parvalbumin-Expressing Interneurons Linearly Transform Cortical Responses to Visual Stimuli. Neuron 73, 159-170.

Auladell, C., Perez-Sust, P., Super, H., and Soriano, E. (2000). The early development of thalamocortical and corticothalamic projections in the mouse. Anat Embryol (Berl) 201, 169-179.

Bagnall, M.W., Hull, C., Bushong, E.A., Ellisman, M.H., and Scanziani, M. (2011). Multiple clusters of release sites formed by individual thalamic afferents onto cortical interneurons ensure reliable transmission. Neuron 71, 180-194.

Bannister, N.J., Nelson, J.C., and Jack, J.J. (2002). Excitatory inputs to spiny cells in layers 4 and 6 of cat striate cortex. Philosophical transactions of the Royal Society of London Series B, Biological sciences 357, 1793-1808.

Barkat, T.R., Polley, D.B., and Hensch, T.K. (2011). A critical period for auditory thalamocortical connectivity. Nat Neurosci 14, 1189-1194.

Baroncelli, L., Braschi, C., Spolidoro, M., Begenisic, T., Maffei, L., and Sale, A. (2011). Brain Plasticity and Disease: A Matter of Inhibition. Neural Plasticity 2011.

Barth, A.L., Gerkin, R.C., and Dean, K.L. (2004). Alteration of neuronal firing properties after in vivo experience in a FosGFP transgenic mouse. The Journal of neuroscience : the official journal of the Society for Neuroscience 24, 6466-6475.

Bartos, M., Vida, I., and Jonas, P. (2007). Synaptic mechanisms of synchronized gamma oscillations in inhibitory interneuron networks. Nat Rev Neurosci 8, 45-56.

Batista-Brito, R., and Fishell, G. (2009). Chapter 3 The Developmental Integration of Cortical Interneurons into a Functional Network. In Current Topics in Developmental Biology, H. Oliver, ed. (Academic Press), pp. 81-118.

Bavelier, D., Levi, D.M., Li, R.W., Dan, Y., and Hensch, T.K. (2010). Removing brakes on adult brain plasticity: from molecular to behavioral interventions. The Journal of neuroscience : the official journal of the Society for Neuroscience 30, 14964-14971.

Behrendt, R.P. (2003). Hallucinations: synchronisation of thalamocortical gamma oscillations underconstrained by sensory input. Conscious Cogn 12, 413-451.

Beierlein, M., Gibson, J.R., and Connors, B.W. (2000). A network of electrically coupled interneurons drives synchronized inhibition in neocortex. Nature neuroscience *3*, 904-910.

Beierlein, M., Gibson, J.R., and Connors, B.W. (2003). Two dynamically distinct inhibitory networks in layer 4 of the neocortex. Journal of neurophysiology 90, 2987-3000.

Berardi, N., Pizzorusso, T., and Maffei, L. (2004). Extracellular matrix and visual cortical plasticity: freeing the synapse. Neuron 44, 905-908.

Beurdeley, M., Spatazza, J., Lee, H.H., Sugiyama, S., Bernard, C., Di Nardo, A.A., Hensch, T.K., and Prochiantz, A. (2012). Otx2 binding to perineuronal nets persistently regulates plasticity in the mature visual cortex. The Journal of neuroscience : the official journal of the Society for Neuroscience 32, 9429-9437.

Boudreau, C.E., and Ferster, D. (2005). Short-term depression in thalamocortical synapses of cat primary visual cortex. The Journal of neuroscience : the official journal of the Society for Neuroscience 25, 7179-7190.

Butt, S.J., Fuccillo, M., Nery, S., Noctor, S., Kriegstein, A., Corbin, J.G., and Fishell, G. (2005). The temporal and spatial origins of cortical interneurons predict their physiological subtype. Neuron 48, 591-604.

Callaway, E.M. (2008). Transneuronal circuit tracing with neurotropic viruses. Current opinion in neurobiology 18, 617-623.

Cardin, J.A., Carlen, M., Meletis, K., Knoblich, U., Zhang, F., Deisseroth, K., Tsai, L.-H., and Moore, C.I. (2009). Driving fast-spiking cells induces gamma rhythm and controls sensory responses. Nature 459, 663-667.

Cellerino, A., Maffei, L., and Domenici, L. (1996). The distribution of brain-derived neurotrophic factor and its receptor trkB in parvalbumin-containing neurons of the rat visual cortex. Eur J Neurosci 8, 1190-1197.

Chahrour, M., and Zoghbi, H.Y. (2007). The Story of Rett Syndrome: From Clinic to Neurobiology. Neuron 56, 422-437.

Chao, H.-T., Chen, H., Samaco, R.C., Xue, M., Chahrour, M., Yoo, J., Neul, J.L., Gong, S., Lu, H.-C., Heintz, N., et al. (2010). Dysfunction in GABA signalling mediates autism-like stereotypies and Rett syndrome phenotypes. Nature 468, 263-269.

Chen, B., Schaevitz, L.R., and McConnell, S.K. (2005). Fezl regulates the differentiation and axon targeting of layer 5 subcortical projection neurons in cerebral cortex. Proceedings of the National Academy of Sciences of the United States of America 102, 17184-17189.

Chen, J.L., Villa, K.L., Cha, J.W., So, P.T.C., Kubota, Y., and Nedivi, E. (2012). Clustered Dynamics of Inhibitory Synapses and Dendritic Spines in the Adult Neocortex. Neuron 74, 361-373.

Chuang, N., Mori, S., Yamamoto, A., Jiang, H., Ye, X., Xu, X., Richards, L.J., Nathans, J., Miller, M.I., Toga, A.W., et al. (2011). An MRI-based atlas and database of the developing mouse brain. Neuroimage 54, 80-89.

Cobos, I., Long, J.E., Thwin, M.T., and Rubenstein, J.L. (2006). Cellular patterns of transcription factor expression in developing cortical interneurons. Cerebral Cortex 16 Suppl 1, i82-88.

Coleman, J.E., Nahmani, M., Gavornik, J.P., Haslinger, R., Heynen, A.J., Erisir, A., and Bear, M.F. (2010). Rapid structural remodeling of thalamocortical synapses parallels experience-dependent functional plasticity in mouse primary visual cortex. The Journal of neuroscience : the official journal of the Society for Neuroscience 30, 9670-9682.

Crair, M.C., Gillespie, D.C., and Stryker, M.P. (1998). The role of visual experience in the development of columns in cat visual cortex. Science 279, 566-570.

Crozier, R.A., Wang, Y., Liu, C.H., and Bear, M.F. (2007). Deprivation-induced synaptic depression by distinct mechanisms in different layers of mouse visual cortex. Proceedings of the National Academy of Sciences of the United States of America 104, 1383-1388.

Cruikshank, S.J., Lewis, T.J., and Connors, B.W. (2007). Synaptic basis for intense thalamocortical activation of feedforward inhibitory cells in neocortex. Nat Neurosci 10, 462-468.

Cruikshank, S.J., Rose, H.J., and Metherate, R. (2002). Auditory thalamocortical synaptic transmission in vitro. Journal of neurophysiology 87, 361-384.

Curley, A.A., Arion, D., Volk, D.W., Asafu-Adjei, J.K., Sampson, A.R., Fish, K.N., and Lewis, D.A. (2011). Cortical deficits of glutamic acid decarboxylase 67 expression in

schizophrenia: clinical, protein, and cell type-specific features. Am J Psychiatry 168, 921-929.

Daw, M.I., Ashby, M.C., and Isaac, J.T. (2007). Coordinated developmental recruitment of latent fast spiking interneurons in layer IV barrel cortex. Nat Neurosci 10, 453-461.

de Villers-Sidani, E., Chang, E.F., Bao, S., and Merzenich, M.M. (2007). Critical period window for spectral tuning defined in the primary auditory cortex (A1) in the rat. The Journal of neuroscience : the official journal of the Society for Neuroscience 27, 180-189.

de Villers-Sidani, E., Simpson, K.L., Lu, Y.F., Lin, R.C., and Merzenich, M.M. (2008). Manipulating critical period closure across different sectors of the primary auditory cortex. Nat Neurosci 11, 957-965.

Deisseroth, K. (2011). Optogenetics. Nat Methods 8, 26-29.

del Rio, J.A., de Lecea, L., Ferrer, I., and Soriano, E. (1994). The development of parvalbumin-immunoreactivity in the neocortex of the mouse. Brain Res Dev Brain Res 81, 247-259.

Dhossche, D.M., Song, Y., and Liu, Y. (2005). Is There A Connection Between Autism, Prader-Willi Syndrome, Catatonia, And GABA? In International Review of Neurobiology, M.D. Dirk, ed. (Academic Press), pp. 189-216.

Doischer, D., Hosp, J.A., Yanagawa, Y., Obata, K., Jonas, P., Vida, I., and Bartos, M. (2008). Postnatal differentiation of basket cells from slow to fast signaling devices. The Journal of neuroscience : the official journal of the Society for Neuroscience 28, 12956-12968.

Durand, S., Patrizi, A., Quast, K.B., Hachigian, L., Pavlyuk, R., Saxena, A., Carninci, P., Hensch, T.K., and Fagiolini, M. (2012). NMDA Receptor Regulation Prevents Regression of Visual Cortical Function in the Absence of Mecp2. Neuron *76*, 1078-1090.

Eccles, J.C. (1964). IONIC MECHANISM OF POSTSYNAPTIC INHIBITION. Science 145, 1140-1147.

Espinosa, J.S., and Stryker, M.P. (2012). Development and plasticity of the primary visual cortex. Neuron 75, 230-249.

Fagiolini, M., Fritschy, J.M., Low, K., Mohler, H., Rudolph, U., and Hensch, T.K. (2004). Specific GABAA circuits for visual cortical plasticity. Science 303, 1681-1683.

Fagiolini, M., and Hensch, T.K. (2000). Inhibitory threshold for critical-period activation in primary visual cortex. Nature 404, 183-186.

Fagiolini, M., Katagiri, H., Miyamoto, H., Mori, H., Grant, S.G., Mishina, M., and Hensch, T.K. (2003). Separable features of visual cortical plasticity revealed by N-methyl-D-aspartate receptor 2A signaling. Proceedings of the National Academy of Sciences of the United States of America 100, 2854-2859.

Fairen, A., Cobas, A., and Fonseca, M. (1986). Times of generation of glutamic acid decarboxylase immunoreactive neurons in mouse somatosensory cortex. The Journal of comparative neurology 251, 67-83.

Feldman, D.E. (2000). Inhibition and plasticity. Nature neuroscience 3, 303-304.

Feldman, D.E., Nicoll, R.A., and Malenka, R.C. (1999). - Synaptic plasticity at thalamocortical synapses in developing rat somatosensory cortex: LTP, LTD, and silent synapses. - 41, - 101.

Ferezou, I., Bolea, S., and Petersen, C.C. (2006). Visualizing the cortical representation of whisker touch: voltage-sensitive dye imaging in freely moving mice. Neuron 50, 617-629.

Fischer, Q.S., Aleem, S., Zhou, H., and Pham, T.A. (2007). Adult visual experience promotes recovery of primary visual cortex from long-term monocular deprivation. Learn Mem 14, 573-580.

Fogarty, M., Grist, M., Gelman, D., Marin, O., Pachnis, V., and Kessaris, N. (2007). Spatial genetic patterning of the embryonic neuroepithelium generates GABAergic interneuron diversity in the adult cortex. The Journal of neuroscience : the official journal of the Society for Neuroscience 27, 10935-10946.

Frenkel, M.Y., and Bear, M.F. (2004). How monocular deprivation shifts ocular dominance in visual cortex of young mice. Neuron 44, 917-923.

Freund, T.F. (2003). Interneuron Diversity series: Rhythm and mood in perisomatic inhibition. Trends Neurosci 26, 489-495.

Gabernet, L., Jadhav, S.P., Feldman, D.E., Carandini, M., and Scanziani, M. (2005). Somatosensory integration controlled by dynamic thalamocortical feed-forward inhibition. Neuron 48, 315-327.

Galarreta, M., and Hestrin, S. (1999). A network of fast-spiking cells in the neocortex connected by electrical synapses. Nature *402*, 72-75.

Galarreta, M., and Hestrin, S. (2001). Electrical synapses between GABA-releasing interneurons. Nature reviews Neuroscience 2, 425-433.

Galarreta, M., and Hestrin, S. (2001). Spike transmission and synchrony detection in networks of GABAergic interneurons. Science *292*, 2295-2299.

Galtrey, C.M., and Fawcett, J.W. (2007). The role of chondroitin sulfate proteoglycans in regeneration and plasticity in the central nervous system. Brain Research Reviews 54, 1-18.

Gandhi, S.P., Yanagawa, Y., and Stryker, M.P. (2008). Delayed plasticity of inhibitory neurons in developing visual cortex. Proceedings of the National Academy of Sciences of the United States of America 105, 16797-16802.

Geiger, J.R.P., Melcher, T., Koh, D.S., Sakmann, B., Seeburg, P.H., Jonas, P., and Monyer, H. (1995). Relative abundance of subunit mRNAs determines gating and Ca2+ permeability of AMPA receptors in principal neurons and interneurons in rat CNS. Neuron 15, 193-204.

Gibson, J.R., Beierlein, M., and Connors, B.W. (1999). Two networks of electrically coupled inhibitory neurons in neocortex. Nature *402*, 75-79.

Gil, Z., Connors, B.W., and Amitai, Y. (1997). Differential regulation of neocortical synapses by neuromodulators and activity. Neuron 19, 679-686.

Gil, Z., Connors, B.W., and Amitai, Y. (1999). Efficacy of thalamocortical and intracortical synaptic connections: quanta, innervation, and reliability. Neuron 23, 385-397.

Gogolla, N., Caroni, P., Luthi, A., and Herry, C. (2009). Perineuronal nets protect fear memories from erasure. Science 325, 1258-1261.

Gogolla, N., Leblanc, J.J., Quast, K.B., Sudhof, T.C., Fagiolini, M., and Hensch, T.K. (2009b). Common circuit defect of excitatory-inhibitory balance in mouse models of autism. J Neurodev Disord 1, 172-181.

Gonchar, Y., Wang, Q., and Burkhalter, A. (2007). Multiple distinct subtypes of GABAergic neurons in mouse visual cortex identified by triple immunostaining. Front Neuroanat 1, 3.

Gordon, J.A., and Stryker, M.P. (1996). Experience-dependent plasticity of binocular responses in the primary visual cortex of the mouse. The Journal of neuroscience : the official journal of the Society for Neuroscience 16, 3274-3286.

Grabert, J., and Wahle, P. (2009). Visual experience regulates Kv3.1b and Kv3.2 expression in developing rat visual cortex. Neuroscience 158, 654-664.

Grinvald, A., and Hildesheim, R. (2004). VSDI: a new era in functional imaging of cortical dynamics. Nat Rev Neurosci 5, 874-885.

Guy, J., Hendrich, B., Holmes, M., Martin, J.E., and Bird, A. (2001). A mouse Mecp2-null mutation causes neurological symptoms that mimic Rett syndrome. Nat Genet 27, 322-326.

Han, Y.K., Kover, H., Insanally, M.N., Semerdjian, J.H., and Bao, S. (2007). Early experience impairs perceptual discrimination. Nat Neurosci 10, 1191-1197.

Hartig, W., Derouiche, A., Welt, K., Brauer, K., Grosche, J., Mader, M., Reichenbach, A., and Bruckner, G. (1999). Cortical neurons immunoreactive for the potassium channel Kv3.1b subunit are predominantly surrounded by perineuronal nets presumed as a buffering system for cations. Brain research 842, 15-29.

Hasenstaub, A.R., and Callaway, E.M. (2010). Paint it black (or red, or green): optical and genetic tools illuminate inhibitory contributions to cortical circuit function. Neuron 67, 681-684.

Hashimoto, K., Fukushima, T., Shimizu, E., Komatsu, N., Watanabe, H., Shinoda, N., Nakazato, M., Kumakiri, C., Okada, S., Hasegawa, H., et al. (2003). Decreased serum levels of D-serine in patients with schizophrenia: evidence in support of the N-methyl-D-aspartate receptor hypofunction hypothesis of schizophrenia. Arch Gen Psychiatry 60, 572-576.

Heimel, J.A., Versendaal, D.v., and Levelt, C.N. (2011). The Role of GABAergic Inhibition in Ocular Dominance Plasticity. Neural Plasticity 2011.

Hensch, T.K. (2004). Critical period regulation. Annual review of neuroscience 27, 549-579.

Hensch, T.K. (2005). Critical period plasticity in local cortical circuits. Nat Rev Neurosci 6, 877-888.

Hensch, T.K., Fagiolini, M., Mataga, N., Stryker, M.P., Baekkeskov, S., and Kash, S.F. (1998). Local GABA circuit control of experience-dependent plasticity in developing visual cortex. Science 282, 1504-1508.

Hensch, T.K., and Stryker, M.P. (2004). Columnar architecture sculpted by GABA circuits in developing cat visual cortex. Science 303, 1678-1681.

Hevner, R.F., Daza, R.A., Englund, C., Kohtz, J., and Fink, A. (2004). Postnatal shifts of interneuron position in the neocortex of normal and reeler mice: evidence for inward radial migration. Neuroscience 124, 605-618.

Heynen, A.J., Yoon, B.J., Liu, C.H., Chung, H.J., Huganir, R.L., and Bear, M.F. (2003). Molecular mechanism for loss of visual cortical responsiveness following brief monocular deprivation. Nature neuroscience 6, 854-862.

Hirsch, J.A., Martinez, L.M., Pillai, C., Alonso, J.M., Wang, Q., and Sommer, F.T. (2003). Functionally distinct inhibitory neurons at the first stage of visual cortical processing. Nat Neurosci 6, 1300-1308.

Hofer, S.B., Ko, H., Pichler, B., Vogelstein, J., Ros, H., Zeng, H., Lein, E., Lesica, N.A., and Mrsic-Flogel, T.D. (2011). Differential connectivity and response dynamics of excitatory and inhibitory neurons in visual cortex. Nat Neurosci 14, 1045-1052.

Homma, R., Baker, B.J., Jin, L., Garaschuk, O., Konnerth, A., Cohen, L.B., Bleau, C.X., Canepari, M., Djurisic, M., and Zecevic, D. (2009). Wide-field and two-photon imaging of brain activity with voltage- and calcium-sensitive dyes. Methods Mol Biol 489, 43-79.

Hong, Y.K., and Chen, C. (2011). Wiring and rewiring of the retinogeniculate synapse. Current opinion in neurobiology 21, 228-237.

Hooks, B.M., and Chen, C. (2006). Distinct roles for spontaneous and visual activity in remodeling of the retinogeniculate synapse. Neuron 52, 281-291.

Huang, Z.J., Kirkwood, A., Pizzorusso, T., Porciatti, V., Morales, B., Bear, M.F., Maffei, L., and Tonegawa, S. (1999). BDNF Regulates the Maturation of Inhibition and the Critical Period of Plasticity in Mouse Visual Cortex. Cell 98, 739-755.

Hubel, D.H., and Wiesel, T.N. (1963). Receptive Fields of Cells in Striate Cortex of Very Young, Visually Inexperienced Kittens. Journal of neurophysiology 26, 994-1002.

Hubel, D.H., and Wiesel, T.N. (1965). Binocular interaction in striate cortex of kittens reared with artificial squint. Journal of neurophysiology 28, 1041-1059.

Hubel, D.H., and Wiesel, T.N. (1970). The period of susceptibility to the physiological effects of unilateral eye closure in kittens. The Journal of physiology 206, 419-436.

Hubel, D.H., Wiesel, T.N., and LeVay, S. (1977). Plasticity of ocular dominance columns in monkey striate cortex. Philosophical transactions of the Royal Society of London Series B, Biological sciences 278, 377-409.

Hubener, M. (2003). Mouse visual cortex. Current opinion in neurobiology 13, 413-420.

Huberman, A.D. (2007). Mechanisms of eye-specific visual circuit development. Current opinion in neurobiology 17, 73-80.

Huberman, A.D., Feller, M.B., and Chapman, B. (2008). Mechanisms underlying development of visual maps and receptive fields. Annual review of neuroscience 31, 479-509.

Hull, C., Isaacson, J.S., and Scanziani, M. (2009). Postsynaptic mechanisms govern the differential excitation of cortical neurons by thalamic inputs. The Journal of neuroscience : the official journal of the Society for Neuroscience 29, 9127-9136.

Isaac, J.T.R., Ashby, M.C., and McBain, C.J. (2007). The Role of the GluR2 Subunit in AMPA Receptor Function and Synaptic Plasticity. Neuron 54, 859-871.

Iurilli, G., Benfenati, F., and Medini, P. (2012). Loss of visually driven synaptic responses in layer 4 regular-spiking neurons of rat visual cortex in absence of competing inputs. Cerebral Cortex 22, 2171-2181.

Iwai, Y., Fagiolini, M., Obata, K., and Hensch, T.K. (2003). Rapid critical period induction by tonic inhibition in visual cortex. The Journal of neuroscience : the official journal of the Society for Neuroscience 23, 6695-6702.

Jaubert-Miazza, L., Green, E., Lo, F.S., Bui, K., Mills, J., and Guido, W. (2005). Structural and functional composition of the developing retinogeniculate pathway in the mouse. Vis Neurosci 22, 661-676.

Jiang, B., Akaneya, Y., Hata, Y., and Tsumoto, T. (2003). Long-term depression is not induced by low-frequency stimulation in rat visual cortex in vivo: a possible preventing role of endogenous brain-derived neurotrophic factor. The Journal of neuroscience : the official journal of the Society for Neuroscience 23, 3761-3770.

Jonas, P., Bischofberger, J., Fricker, D., and Miles, R. (2004). Interneuron Diversity series: Fast in, fast out ‚Äì temporal and spatial signal processing in hippocampal interneurons. Trends Neurosci 27, 30-40.

Kameyama, K., Sohya, K., Ebina, T., Fukuda, A., Yanagawa, Y., and Tsumoto, T. (2010). Difference in Binocularity and Ocular Dominance Plasticity between GABAergic and Excitatory Cortical Neurons. The Journal of Neuroscience 30, 1551-1559.

Kaneko, M., Stellwagen, D., Malenka, R.C., and Stryker, M.P. (2008). Tumor Necrosis Factor-Œ± Mediates One Component of Competitive, Experience-Dependent Plasticity in Developing Visual Cortex. Neuron 58, 673-680.

Katagiri, H., Fagiolini, M., and Hensch, T.K. (2007). Optimization of somatic inhibition at critical period onset in mouse visual cortex. Neuron 53, 805-812.

Kawaguchi, Y. (1995). Physiological subgroups of nonpyramidal cells with specific morphological characteristics in layer II/III of rat frontal cortex. The Journal of Neuroscience 15, 2638-2655.

Kawaguchi, Y., and Kubota, Y. (1993). Correlation of physiological subgroupings of nonpyramidal cells with parvalbumin- and calbindinD28k-immunoreactive neurons in layer V of rat frontal cortex. Journal of neurophysiology 70, 387-396.

Kerlin, A.M., Andermann, M.L., Berezovskii, V.K., and Reid, R.C. (2010). Broadly tuned response properties of diverse inhibitory neuron subtypes in mouse visual cortex. Neuron 67, 858-871.

Khibnik, L.A., Cho, K.K.A., and Bear, M.F. (2010). Relative Contribution of Feedforward Excitatory Connections to Expression of Ocular Dominance Plasticity in Layer 4 of Visual Cortex. Neuron 66, 493-500.

Kruglikov, I., and Rudy, B. (2008). Perisomatic GABA release and thalamocortical integration onto neocortical excitatory cells are regulated by neuromodulators. Neuron 58, 911-924.

Kuhlman, S.J., and Huang, Z.J. (2008). High-resolution labeling and functional manipulation of specific neuron types in mouse brain by Cre-activated viral gene expression. PLoS ONE 3, e2005.

Kwan, K.Y., Sestan, N., and Anton, E.S. (2012). Transcriptional co-regulation of neuronal migration and laminar identity in the neocortex. Development 139, 1535-1546.

Lamsa, K.P., Heeroma, J.H., Somogyi, P., Rusakov, D.A., and Kullmann, D.M. (2007). Anti-Hebbian long-term potentiation in the hippocampal feedback inhibitory circuit. Science 315, 1262-1266.

LeBlanc, J.J., and Fagiolini, M. (2011). Autism: a "critical period" disorder? Neural Plasticity *2011*, 921680.

Lee, C.C., and Sherman, S.M. (2008). Synaptic properties of thalamic and intracortical inputs to layer 4 of the first- and higher-order cortical areas in the auditory and somatosensory systems. Journal of neurophysiology 100, 317-326.

Lendvai, B., Stern, E.A., Chen, B., and Svoboda, K. (2000). Experience-dependent plasticity of dendritic spines in the developing rat barrel cortex in vivo. Nature 404, 876-881.

Lenneberg, E.H. (1967). Biological foundations of language.

Lewis, D.A., Hashimoto, T., and Volk, D.W. (2005). Cortical inhibitory neurons and schizophrenia. Nat Rev Neurosci 6, 312-324.

Linden, M.L., Heynen, A.J., Haslinger, R.H., and Bear, M.F. (2009). Thalamic activity that drives visual cortical plasticity. Nat Neurosci 12, 390-392.

Liu, B.H., Li, P., Li, Y.T., Sun, Y.J., Yanagawa, Y., Obata, K., Zhang, L.I., and Tao, H.W. (2009). Visual receptive field structure of cortical inhibitory neurons revealed by two-photon imaging guided recording. The Journal of neuroscience : the official journal of the Society for Neuroscience 29, 10520-10532.

Lodato, S., Rouaux, C., Quast, K.B., Jantrachotechatchawan, C., Studer, M.I., Hensch, T.K., and Arlotta, P. (2011). Excitatory Projection Neuron Subtypes Control the Distribution of Local Inhibitory Interneurons in the Cerebral Cortex. Neuron 69, 763-779.

Lu, J.T., Li, C.Y., Zhao, J.P., Poo, M.M., and Zhang, X.H. (2007). Spike-timing-dependent plasticity of neocortical excitatory synapses on inhibitory interneurons depends on target cell type. The Journal of neuroscience : the official journal of the Society for Neuroscience 27, 9711-9720.

MacLean, J.N., Fenstermaker, V., Watson, B.O., and Yuste, R. (2006). A visual thalamocortical slice. Nat Methods 3, 129-134.

Maffei, A., Lambo, M.E., and Turrigiano, G.G. (2010). Critical period for inhibitory plasticity in rodent binocular V1. The Journal of neuroscience : the official journal of the Society for Neuroscience 30, 3304-3309.

Maffei, A., Nataraj, K., Nelson, S.B., and Turrigiano, G.G. (2006). Potentiation of cortical inhibition by visual deprivation. Nature 443, 81-84.

Maffei, A., Nelson, S.B., and Turrigiano, G.G. (2004). Selective reconfiguration of layer 4 visual cortical circuitry by visual deprivation. Nat Neurosci 7, 1353-1359.

Mainardi, M., Landi, S., Berardi, N., Maffei, L., and Pizzorusso, T. (2009). Reduced Responsiveness to Long-Term Monocular Deprivation of Parvalbumin Neurons Assessed by c-Fos Staining in Rat Visual Cortex. PLoS ONE 4, e4342.

Marin, O. (2012). Interneuron dysfunction in psychiatric disorders. Nature reviews Neuroscience 13, 107-120.

Markram, H., Toledo-Rodriguez, M., Wang, Y., Gupta, A., Silberberg, G., and Wu, C. (2004). Interneurons of the neocortical inhibitory system. Nat Rev Neurosci 5, 793-807.

Mataga, N., Mizuguchi, Y., and Hensch, T.K. (2004). Experience-dependent pruning of dendritic spines in visual cortex by tissue plasminogen activator. Neuron 44, 1031-1041.

McBain, C.J., and Fisahn, A. (2001). Interneurons unbound. Nat Rev Neurosci 2, 11-23.

McGee, A.W., Yang, Y., Fischer, Q.S., Daw, N.W., and Strittmatter, S.M. (2005). Experience-driven plasticity of visual cortex limited by myelin and Nogo receptor. Science 309, 2222-2226.

McLaughlin, T., and O'Leary, D.D. (2005). Molecular gradients and development of retinotopic maps. Annual review of neuroscience 28, 327-355.

Metherate, R., and Aramakis, V.B. (1999). Intrinsic electrophysiology of neurons in thalamorecipient layers of developing rat auditory cortex. Brain Res Dev Brain Res 115, 131-144.

Metherate, R., and Cruikshank, S.J. (1999). Thalamocortical inputs trigger a propagating envelope of gamma-band activity in auditory cortex in vitro. Exp Brain Res 126, 160-174.

Meyer, A.H., Katona, I., Blatow, M., Rozov, A., and Monyer, H. (2002). In vivo labeling of parvalbumin-positive interneurons and analysis of electrical coupling in identified neurons. The Journal of neuroscience : the official journal of the Society for Neuroscience 22, 7055-7064.

Miyata, S., Komatsu, Y., Yoshimura, Y., Taya, C., and Kitagawa, H. (2012). Persistent cortical plasticity by upregulation of chondroitin 6-sulfation. Nat Neurosci 15, 414-422.

Miyoshi, G., Butt, S.J.B., Takebayashi, H., and Fishell, G. (2007). Physiologically Distinct Temporal Cohorts of Cortical Interneurons Arise from Telencephalic Olig2-Expressing Precursors. The Journal of Neuroscience 27, 7786-7798.

Miyoshi, G., and Fishell, G. (2011). GABAergic interneuron lineages selectively sort into specific cortical layers during early postnatal development. Cerebral Cortex 21, 845-852.

Molnar, Z., and Blakemore, C. (1995). How do thalamic axons find their way to the cortex? Trends Neurosci 18, 389-397.

Molyneaux, B.J., Arlotta, P., Hirata, T., Hibi, M., and Macklis, J.D. (2005). Fezl is required for the birth and specification of corticospinal motor neurons. Neuron 47, 817-831.

Morales, B., Choi, S.Y., and Kirkwood, A. (2002). Dark rearing alters the development of GABAergic transmission in visual cortex. The Journal of neuroscience : the official journal of the Society for Neuroscience 22, 8084-8090.

Morishita, H., and Hensch, T.K. (2008). Critical period revisited: impact on vision. Current opinion in neurobiology 18, 101-107.

Morishita, H., Miwa, J.M., Heintz, N., and Hensch, T.K. (2010). Lynx1, a cholinergic brake, limits plasticity in adult visual cortex. Science 330, 1238-1240.

Mrsic-Flogel, T.D., Hofer, S.B., Ohki, K., Reid, R.C., Bonhoeffer, T., and H√ºbener, M. (2007). Homeostatic Regulation of Eye-Specific Responses in Visual Cortex during Ocular Dominance Plasticity. Neuron 54, 961-972.

Murthy, V.N., Schikorski, T., Stevens, C.F., and Zhu, Y. (2001). Inactivity produces increases in neurotransmitter release and synapse size. Neuron *32*, 673-682.

Nakamura, K., Watakabe, A., Hioki, H., Fujiyama, F., Tanaka, Y., Yamamori, T., and Kaneko, T. (2007). Transiently increased colocalization of vesicular glutamate transporters 1 and 2 at single axon terminals during postnatal development of mouse neocortex: a quantitative analysis with correlation coefficient. European Journal of Neuroscience 26, 3054-3067.

Nery, S., Fishell, G., and Corbin, J.G. (2002). The caudal ganglionic eminence is a source of distinct cortical and subcortical cell populations. Nature neuroscience 5, 1279-1287.

O'Leary, D.D., Ruff, N.L., and Dyck, R.H. (1994). Development, critical period plasticity, and adult reorganizations of mammalian somatosensory systems. Current opinion in neurobiology 4, 535-544.

Packer, A.M., and Yuste, R. (2011). Dense, unspecific connectivity of neocortical parvalbumin-positive interneurons: a canonical microcircuit for inhibition? The Journal of neuroscience : the official journal of the Society for Neuroscience 31, 13260-13271.

Pascual-Leone, A., Amedi, A., Fregni, F., and Merabet, L.B. (2005). The plastic human brain cortex. Annual review of neuroscience *28*, 377-401.

Paxinos, G., and Franklin, K.B.J. (2001). The mouse brain in stereotaxic coordinates, 2nd edn (San Diego, Academic Press).

Petilla Interneuron Nomenclature Group, P. (2008). Petilla terminology: nomenclature of features of GABAergic interneurons of the cerebral cortex. Nat Rev Neurosci 9, 557-568.

Pinto, D.J., Brumberg, J.C., and Simons, D.J. (2000). Circuit Dynamics and Coding Strategies in Rodent Somatosensory Cortex. Journal of neurophysiology 83, 1158-1166.

Pizzarelli, R., and Cherubini, E. (2011). Alterations of GABAergic Signaling in Autism Spectrum Disorders. Neural Plasticity 2011.

Pizzorusso, T., Medini, P., Berardi, N., Chierzi, S., Fawcett, J.W., and Maffei, L. (2002). Reactivation of ocular dominance plasticity in the adult visual cortex. Science 298, 1248-1251.

Plotkin, J.L., Wu, N., Chesselet, M.F., and Levine, M.S. (2005). Functional and molecular development of striatal fast-spiking GABAergic interneurons and their cortical inputs. Eur J Neurosci 22, 1097-1108.

Pouille, F.d.r., and Scanziani, M. (2001). Enforcement of Temporal Fidelity in Pyramidal Cells by Somatic Feed-Forward Inhibition. Science 293, 1159-1163.

Renger, J.J., Hartman, K.N., Tsuchimoto, Y., Yokoi, M., Nakanishi, S., and Hensch, T.K. (2002). Experience-dependent plasticity without long-term depression by type 2 metabotropic glutamate receptors in developing visual cortex. Proceedings of the National Academy of Sciences of the United States of America 99, 1041-1046.

Richardson, R.J., Blundon, J.A., Bayazitov, I.T., and Zakharenko, S.S. (2009). Connectivity Patterns Revealed by Mapping of Active Inputs on Dendrites of Thalamorecipient Neurons in the Auditory Cortex. The Journal of Neuroscience 29, 6406-6417.

Riddle DL, Blumenthal T, Meyer BJ, et al., editors. C. elegans II. 2nd edition. Cold Spring Harbor (NY): Cold Spring Harbor Laboratory Press; 1997.

Rose, H.J., and Metherate, R. (2005). Auditory thalamocortical transmission is reliable and temporally precise. Journal of neurophysiology 94, 2019-2030.

Rubenstein, J.L., and Merzenich, M.M. (2003). Model of autism: increased ratio of excitation/inhibition in key neural systems. Genes Brain Behav *2*, 255-267.

Runyan, C.A., Schummers, J., Van Wart, A., Kuhlman, S.J., Wilson, N.R., Huang, Z.J., and Sur, M. (2010). Response features of parvalbumin-expressing interneurons suggest precise roles for subtypes of inhibition in visual cortex. Neuron 67, 847-857.

Sarihi, A., Jiang, B., Komaki, A., Sohya, K., Yanagawa, Y., and Tsumoto, T. (2008). Metabotropic glutamate receptor type 5-dependent long-term potentiation of excitatory synapses on fast-spiking GABAergic neurons in mouse visual cortex. The Journal of neuroscience : the official journal of the Society for Neuroscience 28, 1224-1235.

Sawtell, N.B., Frenkel, M.Y., Philpot, B.D., Nakazawa, K., Tonegawa, S., and Bear, M.F. (2003). NMDA receptor-dependent ocular dominance plasticity in adult visual cortex. Neuron 38, 977-985.

Sermasi, E., Margotti, E., Cattaneo, A., and Domenici, L. (2000). Trk B signalling controls LTP but not LTD expression in the developing rat visual cortex. Eur J Neurosci 12, 1411-1419.

Shatz, C.J., and Stryker, M.P. (1978). Ocular dominance in layer IV of the cat's visual cortex and the effects of monocular deprivation. The Journal of physiology 281, 267-283.

Smith, G.B., Heynen, A.J., and Bear, M.F. (2009). Bidirectional synaptic mechanisms of ocular dominance plasticity in visual cortex. Philosophical transactions of the Royal Society of London Series B, Biological sciences 364, 357-367.

Sohal, V.S., Zhang, F., Yizhar, O., and Deisseroth, K. (2009). Parvalbumin neurons and gamma rhythms enhance cortical circuit performance. Nature 459, 698-702.

Sohya, K., Kameyama, K., Yanagawa, Y., Obata, K., and Tsumoto, T. (2007). GABAergic neurons are less selective to stimulus orientation than excitatory neurons in layer II/III of visual cortex, as revealed by in vivo functional Ca2+ imaging in transgenic mice. The Journal of neuroscience : the official journal of the Society for Neuroscience 27, 2145-2149.

Spencer, K.M., Nestor, P.G., Niznikiewicz, M.A., Salisbury, D.F., Shenton, M.E., and McCarley, R.W. (2003). Abnormal Neural Synchrony in Schizophrenia. The Journal of Neuroscience 23, 7407-7411.

Spolidoro, M., Sale, A., Berardi, N., and Maffei, L. (2009). Plasticity in the adult brain: lessons from the visual system. Experimental Brain Research 192, 335-341.

Sugiyama, S., Di Nardo, A.A., Aizawa, S., Matsuo, I., Volovitch, M., Prochiantz, A., and Hensch, T.K. (2008). Experience-dependent transfer of Otx2 homeoprotein into the visual cortex activates postnatal plasticity. Cell 134, 508-520.

Tallon-Baudry, C., Bertrand, O., Peronnet, F., and Pernier, J. (1998). Induced gamma-band activity during the delay of a visual short-term memory task in humans. The Journal of neuroscience : the official journal of the Society for Neuroscience 18, 4244-4254.

Wagor, E., Mangini, N.J., and Pearlman, A.L. (1980). Retinotopic organization of striate and extrastriate visual cortex in the mouse. The Journal of comparative neurology 193, 187-202.

Wang, H.-X., and Gao, W.-J. (2010). Development of calcium-permeable AMPA receptors and their correlation with NMDA receptors in fast-spiking interneurons of rat prefrontal cortex. The Journal of physiology 588, 2823-2838.

Werker, J.F., Byers-Heinlein, K., and Fennell, C.T. (2009). Bilingual beginnings to learning words. Philosophical transactions of the Royal Society of London Series B, Biological sciences 364, 3649-3663.

White, J.G., Southgate, E., Thomson, J.N., and Brenner, S. (1986). The structure of the nervous system of the nematode Caenorhabditis elegans. Philosophical transactions of the Royal Society of London Series B, Biological sciences *314*, 1-340.

Wonders, C.P., and Anderson, S.A. (2006). The origin and specification of cortical interneurons. Nat Rev Neurosci 7, 687-696.

Xu, Q., Cobos, I., De La Cruz, E., Rubenstein, J.L., and Anderson, S.A. (2004). Origins of Cortical Interneuron Subtypes. The Journal of Neuroscience 24, 2612-2622.

Yazaki-Sugiyama, Y., Kang, S., Cateau, H., Fukai, T., and Hensch, T.K. (2009). Bidirectional plasticity in fast-spiking GABA circuits by visual experience. Nature 462, 218-221.

Zhang, L.I., Bao, S., and Merzenich, M.M. (2002). Disruption of primary auditory cortex by synchronous auditory inputs during a critical period. Proceedings of the National Academy of Sciences of the United States of America 99, 2309-2314.